



<https://theses.gla.ac.uk/>

Theses Digitisation:

<https://www.gla.ac.uk/myglasgow/research/enlighten/theses/digitisation/>

This is a digitised version of the original print thesis.

Copyright and moral rights for this work are retained by the author

A copy can be downloaded for personal non-commercial research or study,
without prior permission or charge

This work cannot be reproduced or quoted extensively from without first
obtaining permission in writing from the author

The content must not be changed in any way or sold commercially in any
format or medium without the formal permission of the author

When referring to this work, full bibliographic details including the author,
title, awarding institution and date of the thesis must be given

Enlighten: Theses

<https://theses.gla.ac.uk/>
research-enlighten@glasgow.ac.uk

Integrated Semiconductor Ring Lasers

A thesis for the degree of

Doctor of Philosophy, (Ph.D.)

submitted to the Faculty of Engineering,

Glasgow University

by

Thomas Krauss

May 1992

©

1992

ProQuest Number: 11011474

All rights reserved

INFORMATION TO ALL USERS

The quality of this reproduction is dependent upon the quality of the copy submitted.

In the unlikely event that the author did not send a complete manuscript and there are missing pages, these will be noted. Also, if material had to be removed, a note will indicate the deletion.



ProQuest 11011474

Published by ProQuest LLC (2018). Copyright of the Dissertation is held by the Author.

All rights reserved.

This work is protected against unauthorized copying under Title 17, United States Code
Microform Edition © ProQuest LLC.

ProQuest LLC.
789 East Eisenhower Parkway
P.O. Box 1346
Ann Arbor, MI 48106 – 1346

Stages

As every flower fades and as all youth
Departs, so life at every stage,
So every virtue, so our grasp of truth,
Blooms in its day and may not last forever.
Since life may summon us at every age
Be ready, heart, for parting, new endeavour,
Be ready bravely and without remorse
To find new light that old ties cannot give.
In all beginnings dwells a magic force
For guarding us and helping us to live.

Serenly let us move to distant places
And let no sentiments of home detain us.
The Cosmic spirit seeks not to restrain us
But lifts us stage by stage to wider spaces.
If we accept a home of our own making,
Familiar habit makes for indolence.
We must prepare for parting and leave-taking
Or else remain the slaves of permanence.

Even the hour of our death may send
Us speeding on to fresh and newer spaces,
And life may summon us to newer races.
So be it, heart: bid farewell without end.

(Hermann Hesse)

Acknowledgement

I wish to acknowledge the following people and organizations that were essential to the development of the project.

The late John Lamb for making the department the thriving place that it is, with some of the best facilities and technical support available in the country. My supervisor Peter Laybourn for accepting me as a research student, always having an open door when I needed it, guiding and encouraging me throughout, and ensuring that the project became successful and enjoyable.

Steve Beaumont and the Nanoelectronics group for the use of their facilities, the technical staff for their support and effort to keep up the morale not only in times of difficulty. Chris Wilkinson for the usage of the dry etching facility and the technical staff for their support and patience in dealing with my sometimes extensive requests.

John Roberts and Chris Button from the SERC III-V semiconductor growth facility at Sheffield University for the superb material they grew and supplied within less than two weeks of my request.

Iain Thayne for proof-reading many of my literary offerings, the stimulating discussions and telling me all I needed to know about field-effect transistors. Richard de la Rue for encouraging and helpful discussions and successful attempts to organize the optics group. Kathy the cleaner for shouting at me in the morning and waking me up for the day.

The Comission of the European Comunity, Directorate-General for Science, Research and Technology in Brussels for providing a generous grant during the first two years that helped me to enjoy my general existence and to concentrate most of my energy on the project. The SERC for supporting the general idea of the ring laser. Digital Equipment Corporation in Galway, Ireland, particularly Jim McLay, John Curran and Toby Joyce for showing serious interest in the work, which is a morale booster on its own, and the financial support in the later part of the project. Their commercial interest directed some of the work towards practical issues such as process consistency and packaging and supported the development of the optoelectronic integrated circuit.

The University for providing a stimulating campus and maintaining the Stevenson building, the scene of many refreshing exercise sessions. The Scottish hills for being there and the Glasgow University Mountaineering Club for providing the related entertainment.

Finally, my parents and Heidi for their invaluable moral support.

Abstract

The concept of a semiconductor laser with a circular resonator, its advantages and particular problems are discussed. The pillbox resonator is introduced and its operation on whispering gallery modes is illustrated using a computer model. The experimental evidence of the guiding mechanism is shown, leading to the first demonstration of continuous wave operation in a semiconductor ring laser with a threshold current of 24mA. The parameters of the GaAs/AlGaAs material that are relevant for the low threshold current operation are presented and all aspects of the fabrication procedure are covered, emphasizing the processes that led to smooth sidewalls and the low loss circular cavity. A further reduction of the threshold current to 12.5mA is shown, which is owing to a coating of silicon nitride that suppresses the non-radiative recombination current and reduces the scattering loss. The excess bending loss is calculated to be 3dB/360° and found to be independent of the radius between 30 μ m and 145 μ m. The influence of the Y-junction on the operation characteristic is studied and shown to cause kinks in the L-I curve; it is also held responsible for the relatively low differential quantum efficiency (0.02-0.04) of the devices. Strip-loaded guiding is demonstrated for radii between 300 μ m and 600 μ m and proposed as a solution for the problem of degradation that is caused by etching through the active layer.

The integration capability of the structure is demonstrated by the successful operation of a circuit comprising of a ring laser, a low-loss waveguide and a detector, and an optoelectronic integrated circuit featuring a ring laser and a field-effect transistor. The material parameters that are involved in performing these complicated functions are discussed and modeled numerically.

Contents

1. Introduction	1
1.1 The ring laser	2
1.1.1 Development of the ring laser	1.1.1 The pillbox ring laser
1.2 Photonic integration	5
1.3 Optoelectronic integration	5
1.4 Development and highlights of the integrated ring laser project	7
1.4.1 Semicircular devices, "U's"	1.4.2 The Pillbox
1.4.3 Polyimide insulation	1.4.4 Scattering
1.4.5 Cw operation	1.4.6 Silicon nitride
1.4.7 Integrated detector	1.4.8 Strip-loaded ring lasers
1.4.9 Integrated transistor	
1.5 Outline	12
2. Design considerations for ring lasers	13
2.1 Conformal transformation	13
2.2 Computer modelling	14
2.3 Modelling results	16
2.3.1 Pillbox ring lasers	2.3.2 Strip-loaded ring lasers
3. Ring laser material	19
3.1 Material parameters	20
3.1.1 Size and number of quantum wells	3.1.2 Barriers between quantum wells
3.1.3 Waveguide design	3.1.4 Sellmayer's equation
3.1.5 Cladding thickness	3.1.6 Doping concentration of the cladding layers
3.2 Improved material design	25
3.3 Comparison and characterisation of different material structures	26
3.3.1 Theory	3.3.2 Experimental
3.3.3 Results and Discussion	
4. Fabrication	30
4.1 Sample preparation	31
4.2 Lithography	31
4.2.1 Pattern Generation	4.2.2 Electron-beam exposure
4.2.3 Electron-beam resist	4.2.4 Alternative approaches
4.2.5 Alignment marks	4.2.6 Dry etching mask
4.3 Etching	38
4.3.1 Required etch depth	4.3.2 Dry Etching
4.3.3 Wet etching	

4.4	<i>Deposition of silicon nitride</i>	41
4.5	<i>Polyimide bridges</i>	42
4.6	<i>Contact metallization</i>	44
4.6.1	Cleaning before contact deposition	
4.6.2	Ohmic contacts, p-type	
4.6.3	Schottky contact, p-side	
4.6.4	Ohmic contacts, n-type	
4.7	<i>Bonding and Packaging</i>	46
4.7.1	Cleaving	
4.7.2	Bonding	
4.7.3	Packaging	
4.8	<i>Performance of an array comprising of 8 ring lasers</i>	49
5.	<i>Measurements</i>	50
5.1	<i>Laser pumping sources</i>	50
5.2	<i>Optical system</i>	52
5.3	<i>Signal detection</i>	54
5.4	<i>Typical results</i>	54
6.	<i>Devices</i>	56
6.1	<i>Strip-loaded stripe laser</i>	56
6.2	<i>Properties of ring lasers</i>	57
6.2.1	Spectral output - the longitudinal mode spacing	
6.2.2	Spectral output - the transverse mode spacing	
6.2.3	Current spreading in the pillbox resonator	
6.2.4	Scattering loss	
6.2.5	Radius	
6.2.6	Y-junction and L-I curve	
6.2.7	Temperature in a ring laser	
6.2.8	Degradation and device lifetime	
6.2.9	Polarization	
6.3	<i>Different device geometries</i>	71
6.3.1	Racetrack and polygon	
6.3.2	Two coupled ring resonators	
6.3.3	Output waveguide	
6.3.4	Ring lasers with a reverse-biased section	
6.4	<i>Strip-loaded ring laser</i>	75
7.	<i>Integration</i>	77
7.1	<i>Photonic Integrated Circuit (PIC)</i>	77
7.1.1	Modelling the passive properties of the PIC-material	
7.1.2	Refractive index in an active medium	
7.1.3	The solution of the coupled-mode equation for the PIC material	
7.1.4	Ring lasers in double-waveguide material	
7.1.5	Integrated modulator	
7.1.6	Integrated detector	

7.2 Optoelectronic integrated circuit (OEIC)	86
7.2.1 Circuit design 7.2.2 Material design 7.2.3 Fabrication 7.2.4 Broad area lasers 7.2.5 Field effect transistors 7.2.6 Ring laser OEIC	
8. Conclusion	94
8.1 Ring laser	94
8.1.1 Fabrication issues 8.1.2 Output coupling 8.1.3 The next generation 8.1.4 Conclusion on ring lasers	
8.2 Integration	96
8.2.1 Photonic integration 8.2.2 Optoelectronic integration	
8.3 Outlook	97
9. References	98
9.1 Publications and conference contributions arising from this work	98
9.2 Alphabetical list of references	98

1. Introduction

The ever increasing quest for information has created the need for systems that are capable of transmitting vast amounts of data over long distances. Copper cables, used since Samuel Morse's days, have finally reached their technological limit and are increasingly being replaced by fibre optic systems.

Semiconductor lasers are ideal sources for such systems. They provide coherent radiation at wavelengths suitable for low-loss fibre transmission, they are small, efficient and mass-producible.

Most semiconductor lasers manufactured today are used in CD-players and are based on GaAs, the most developed semiconductor for photonic applications. The emission wavelength can be tuned between 650nm and 900nm by replacing a fraction of gallium by aluminium, i.e. by growing a ternary $Al_xGa_{1-x}As$ crystal layer. This is possible because AlGaAs is very nearly lattice-matched to GaAs over the whole range $0 < x < 1$. The first window of low absorption for optical fibres is at the wavelength of 850nm, well within that range. GaAs lasers thus find a wide range of applications in systems such as short-haul local area networks. For long-haul transmission, though, it is necessary to change the material system to an Indium based ternary or quaternary, such as $In_xGa_{1-x}As$ or $In_xGa_{1-x}P_yAs_{1-y}$, which can be tuned between $1.0\mu\text{m}$ and $1.7\mu\text{m}$ and match the two windows for lowest absorption in fibres at $1.3\mu\text{m}$ and $1.55\mu\text{m}$. Because long haul transmission systems were not envisaged as an application and a more mature material system is beneficial to studying a particular device, GaAs was chosen for the development of ring lasers.

Apart from lasers, other photonic, electro-optic and electronic devices are of interest in an optical communication system. Waveguides and junctions are needed to direct, split or combine the light, modulators to generate optical signals, transistors to provide the driving circuitry, amplifiers at regular intervals to compensate for fibre losses, and detectors at the other end of the system to convert the information back into electrical signals.

It is a particular challenge to combine most of these components into an integrated circuit. Most commercial systems consist of discrete components realized in different materials and butt-coupled to each other, which is a substantial effort in alignment and packaging. An integrated solution is potentially superior, because it offers the possibility of having a single fabrication process, a higher density of components and easier packaging. Alignment is more accurate because it is performed by lithography rather than micromanipulation.

As is often the case, integration brings problems as well as advantages:

1. Lasers need a resonating cavity, which is usually produced by cleaving the end-facets. Cleaving reduces the substrate size to a few $100\mu\text{m}$ and makes it impossible to combine other elements along the optical axis. Therefore, new ways of providing feedback are required.
2. Laser action usually occurs just above the material band edge, which means that the material is highly absorbing at its own lasing wavelength. This makes it very difficult to combine lasers and low-loss waveguides on the same substrate.
3. The material structure for lasers and transistors is generally not compatible, which turns optoelectronic integration into a very complicated affair.

Furthermore, the properties of the integrated circuit need to be optimized as a whole. Improving the devices individually is only of limited use, since they influence each other optically and electrically.

The aim of this work is to propose solutions to these problems. The emphasis is on the development of a rather exotic device, a circular laser, to solve the laser resonator problem.

1.1 The ring laser

The vast majority of semiconductor lasers rely on a Fabry-Perot cavity formed by two cleaved facets. However, when the laser is to be integrated monolithically with other optical or electronic components, the need for cleaved facets constitutes a severe constraint, so that alternative methods of providing feedback are required. The following methods have been reported concerning stripe-geometry lasers:

1. A grating used as a feedback element in distributed feedback (DFB) and distributed Bragg reflector (DBR) lasers overcomes the need for one or both cleaved facets. Such lasers, however, involve a cumbersome fabrication process and the structure requires overgrowth.
2. Dry etching has been demonstrated¹ as a suitable technique for fabricating facets nearly as smooth as cleaved ones. The use of a faceted laser in an optoelectronic integrated circuit, however, introduces additional losses when coupling into subsequent components of the system.
3. Microcleaving², i.e. etching a cantilever which breaks off under ultrasonic impact leaving a cleaved facet, has the further disadvantage of requiring very high mesas, which is undesirable for multi-level lithography.

An alternative to the above techniques of forming a Fabry-Perot cavity is to use a circular waveguide resonator, an approach which completely eliminates the need for a facet as a feedback element. The idea of a ring laser is rather old, but the device has received little attention, despite its potential. Instead, most workers in the field concentrate on DFB lasers, because of their very good mode selection, linewidth and tunability. However, for applications such as local area networks (LAN) or the local end of digital television systems, the requirements are not necessarily as stringent as in long-distance data transmission, so a simpler and more economic solution is preferable. Integrated optoelectronic circuits employing ring laser sources might offer an interesting alternative for those applications.

Another application is to use ring resonators in a coherent communication system that operates with trains of short pulses. The circular geometry lends itself to colliding pulse mode locked operation, where an absorber is introduced into the cavity that only saturates when both the clockwise and the anticlockwise travelling pulses collide. Assuming that enough gain is provided for the two pulses to saturate the absorber, mode locked operation is expected to establish automatically. Ring lasers offer a great advantage over stripe lasers for this application, because the position of the absorber with respect to the output coupler is determined accurately by lithography. Using stripe lasers, placing the absorber exactly halfway between the two cleaved facets is a serious problem, because cleaving with μm -accuracy is very difficult. Also, the pulse repetition rate depends on the cavity length, which, for a ring laser, is again determined by lithography. Mode locked operation

¹ A.Behfar-Rad, S.S.Wong, J.M.Ballantyne, B.A.Soltz, and C.M.Harding, "Rectangular and L-shaped GaAs/AlGaAs lasers with very high quality etched facets", Applied Physics Letters, Vol.54, pp.493-495, 1989.

² H.Blauvelt, N.Bar-Chaim, D.Fekete, S.Margalit, and A.Yariv, "AlGaAs lasers with micro-cleaved mirrors suitable for monolithic integration", Applied Physics Letters, Vol.40, pp.289-291, 1982.

has not been attempted in this project, but the results described in the following suggest that ring laser devices have now been developed sufficiently for consideration in such advanced applications.

1.1.1 Development of the ring laser

The first discussion of waveguiding along a curved boundary dates back to 1912, when Lord Rayleigh first observed the 'whispering gallery'³ guiding effect in St. Paul's cathedral. The first applications for curved waveguides were found in microwave technology in the 1930's and 1940's. In 1962, lasing action was demonstrated in semiconductors^{4, 5} and, towards the end of the decade, curved waveguides were considered for optical applications⁶, essentially scaled down versions of their microwave counterparts.

A half-ring semiconductor laser was first realized in 1970⁷ in a zinc-diffused GaAs homojunction laser. Later, in 1976, the same geometry was used in a GaAs/AlGaAs heterostructure to create an optically pumped laser⁸. A fully circular semiconductor laser, electrically pumped, but without an output waveguide, was first demonstrated in 1977⁹ where the operation was monitored from the scattered light off the sidewalls.

The first circular laser involving a Y-junction was recorded in 1980¹⁰ with a threshold current around 300mA for a 200 μ m diameter device. Despite this demonstration of a full-ring resonator, the concept of half- or quarter-ring resonators was further pursued¹¹, to avoid the complications arising from outcoupling via the Y-junction. A few years later, a more detailed investigation of

³ Lord Rayleigh, "The problem of the whispering gallery", Scientific Papers, Cambridge University, Vol.5, pp.617-620, 1912.

⁴ R.N.Hall, G.E.Fenner, J.D.Kingsley, T.J.Soltys, and R.O.Carlson, "Coherent light emission from GaAs p-n junctions", Physical Review Letters, Vol.9, pp.366-368, 1962.

⁵ M.I.Nathan, W.P.Dumke, G.Burns, F.H.Dill, and G.J.Lasher, "Stimulated emission of radiation from GaAs p-n junctions", Applied Physics Letters, Vol.1, pp.62-64, 1962.

⁶ E.A.J.Marcattili, "Bends in optical dielectric guides", Bell Systems Technical Journal, Vol.48, pp.2103-2132, 1969.

⁷ J.A.Carra, L.A.D'Asaro, J.C.Dyment, G.J.Herskowitz, "GaAs Lasers utilizing light propagation along curved junctions", IEEE Journal of Quantum Electronics, Vol.6, pp.367-371, 1970.

⁸ D.Botez, L.Figueroa, and S.Wang, "Optically pumped GaAs - Ga_{1-x}Al_xAs half-ring laser fabricated by liquid-phase epitaxy over chemically etched channels", Applied Physics Letters, Vol.29, pp.502-504, 1976.

⁹ N.Matsumoto and K.Kumabe, Japanese Journal of Applied Physics, Vol.16, p.1395, 1977.

¹⁰ A.S-H.Liao and S.Wang, "Semiconductor injection lasers with a circular resonator", Applied Physics Letters, Vol.36, pp.801-803, 1980.

¹¹ I.Ury, S.Margalit, N.Bar-Chaim, M.Yust, D.Wilt, and A.Yariv, "Whispering-gallery lasers on semi-insulating GaAs substrates", Applied Physics Letters, Vol.36, pp.629-631, 1980.

different ring laser geometries and fabrication issues was published¹². However, ring lasers were still regarded impractical due to their high threshold current ($> 100\text{mA}$) and the consequently arising requirement of pulsed operation. As materials and technology improved further, this barrier was finally broken in 1990, when cw operation was demonstrated in an etched full ring¹³, in a half-ring geometry¹⁴, and, a year later, in square-shaped ring lasers¹⁵.

1.1.2 The pillbox ring laser

The present work has been concentrating on a 'pillbox'-type structure, which was the first to show that continuous wave (cw) operation of semiconductor ring lasers is possible. This made ring lasers a real alternative to the device geometries discussed previously. The pillbox design uses the 'whispering gallery' effect as a guiding mechanism. The whispering gallery modes undergo total internal reflections at the outer GaAs-air interface without requiring an inner boundary as long as the angle of incidence is shallow.

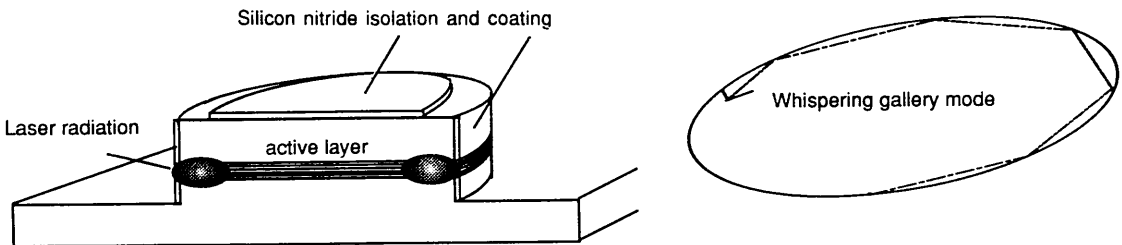


Figure 1. Cross section of a pillbox ring laser and ray model for the propagation of a whispering gallery mode.

The omission of the inner boundary reduces the scattering losses and facilitates heat dissipation into the substrate. To reduce the pumping current, the inside of the pillbox is electrically isolated by a layer of silicon nitride, so only an outer annulus of $4\mu\text{m}$ is pumped. The best devices to date have a cw threshold current of 12.5mA , which is a 5-fold decrease since the first devices were fabricated at the beginning of the project. The description of the work leading to this successful result forms the major part of this thesis. The emphasis is on achieving low threshold currents, in contrast to the previous project on the same subject¹⁶, which was aimed towards single-mode operation. The philosophy is that a multimode room temperature cw device is more useful than a single-mode device operated pulsed or at liquid nitrogen temperatures.

¹² A.F.Jeziarski and P.J.R.Laybourn, "Integrated semiconductor ring lasers", IEE Proceedings, Vol.135, Pt.J, pp.17-24, 1988.

¹³ T.Krauss, P.J.R.Laybourn, and J.Roberts, "Cw operation of semiconductor ring lasers", Electronics Letters, Vol.26, pp.2095-2097, 1990.

¹⁴ N.Bar-Chaim, K.Y.Lau, M.A.Mazed, M.Mittelstein, Se Oh, J.E.Ungar, and I.Ury, "Half-ring geometry quantum well GaAlAs lasers", Applied Physics Letters, Vol.57, pp.966-967, 1990.

¹⁵ S.Oku, M.Okayasu, and M.Ikeda, "Low-threshold cw operation of square-shaped semiconductor ring lasers (orbiter lasers)", IEEE Photonics Technology Letters, Vol.3, pp.588-590, 1991.

¹⁶ A.F.Jeziarski, "Semiconductor ring lasers", Ph.D. Thesis, Glasgow University, 1990.

1.2 Photonic integration

The problem of high material absorption at the lasing wavelength is usually overcome by overgrowing the partially processed wafer (figure 2a). Layers of different composition are used that are transparent at the lasing wavelength, an elegant, but technologically very demanding process.

Impurity induced disordering (IID) is another technique to alter the material properties locally (figure 2b). It makes use of the fact that the absorption-edge in a quantum well material is different than in material with the same average composition. This technique involves interdiffusing the lattice with dopants such as zinc or silicon, or ion implantation and subsequent annealing¹⁷. IID is currently an active area of research in the department.

Since one of the philosophies of this project is to propose simple alternatives, neither overgrowth nor IID were considered.

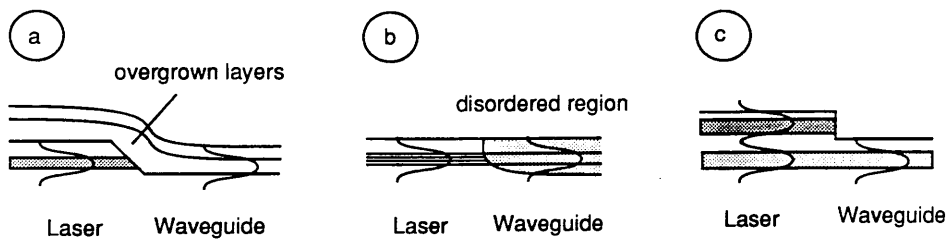


Figure 2. Three alternative schemes for combining an active (laser) and passive (waveguide) component on the same substrate.

An easier solution is to combine two waveguides vertically (figure 2c), which only requires a single epitaxial growth process. This is possibly not the best way of solving the problem, but in some respects the simplest. The top waveguide, where the lasing occurs, is designed with a smaller bandgap than the bottom one. The waveguides are directionally coupled, so the laser light is transferred to the bottom layer where it can travel with low loss.

One of the main advantages of integrating a passive waveguide with active components on the same circuit is that the coupling is entirely determined by the lithographic process and the material design, i.e. it can be well controlled and optimized. For comparison, the alignment in a hybrid circuit is a major problem, because the required accuracy is in the order of $\pm 0.1\mu\text{m}$, which is difficult to achieve.

1.3 Optoelectronic Integration

"In one of its rare moments of cooperative spirit, nature has endowed the III-V semiconductors based on GaAs/AlGaAs and InP/GaInAsP with a double gift. These are ... the materials of choice for semiconductor lasers but in addition it is possible to use them, especially GaAs/GaAlAs, as base materials for electronic circuits in a manner similar to that in silicon. ... The main reason for an accelerating drive towards an integrated optical circuit technology derives from the reduction of parasitic reactances that are always associated with conventional wire interconnections, plus the

¹⁷ D.G.Deppe and N.Holonyak,Jr., "Atom diffusion and impurity induced layer disordering in quantum-well semiconductor heterostructures", Journal of Applied Physics, Vol.64, pp.R93-R113, 1988.

compatibility with the integrated electronic circuit technology that makes it possible to apply the advanced techniques of the latter to this new class of devices.”¹⁸

Using a less poetic description, the following advantages arise from optoelectronic integration:

1. The speed that can be obtained in an extended circuit is unachievable with hybrid devices, which is not obvious when comparing the highest modulation speeds obtained to date ($\approx 20\text{GHz}$ for both hybrid and integrated systems)¹⁹. However, these results have been obtained for single optimized devices. In practical applications, when using arrays or whole circuits, interconnections become increasingly difficult without a compromise in speed. Integrated circuitry then offers better performance than hybrid solutions.
2. The packing density is increased by orders of magnitude, similar to the performance leap in electronics when discrete components were replaced by integrated circuits.
3. The packaging is much simpler and cheaper since it involves fewer elements.
4. Another economical reason is that an all-in-one process is much more attractive to the manufacturer, because only a single production line with one integrated circuit is required rather than multiple lines with individual devices.

To take advantage of these benefits, the following problems have to be addressed:

1. Fabrication compatibility.
 - a. In the epitaxial process (MBE), optical layers tend to be grown at higher temperatures than electronic ones. If the electronic layer is grown first, there is the danger of impurity interdiffusion during the growth of the optical layer.
 - b. The fabrication sequence is also critical, layers that involve elevated temperatures (annealing of ohmic contacts or implanted regions, deposition of dielectric films etc.) must be processed accordingly.
 - c. Planarity of the chip is another consideration. If a mesa has been etched, e.g. to form a laser, focussing (different focal plane for the alignment marks and features to be exposed) and resist properties (build-up at the mesa step) are affected in subsequent lithographic steps. This is less critical when using e-beam lithography, but an important issue when using optical techniques.
2. Individual devices can interfere with each other, either thermally, due to a local heatup, or electrically, if the isolation between two devices is not sufficient.
3. Input/output connections, both electrical and optical, must be properly designed to allow access and minimize interference.

¹⁸ A.Yariv, "Optical Electronics" 4th ed., pp.585-587, HRW Sanders, 1991.

¹⁹ I.K.Uomi, Hitachi Ltd, "Ultrahigh speed DFB lasers", CLEO 90, Paper CThA1 (17GHz).
2.Y.H.Lo, P.Grabbe, R.Bhat, J.L.Gimlett, P.S.D.Lin, A.S.Grozd, M.A. Koza, and T.P.Lee, Bellcore, "Very high speed 1.5 μm DFB OEIC transmitter", CLEO 90, Paper WWM1 (19GHz).

The above considerations indicate that the optimization of individual devices is limited and compromises are necessary, it is thus possible that the benefits of integration are reduced by inferior device quality.

1.4 Development and highlights of the integrated ring laser project

The project started off as a continuation of previous work on the same subject²⁰, where the feasibility of circular semiconductor lasers with very small radii ($R < 20\mu\text{m}$) had been demonstrated. To achieve single-mode operation, very thin structures with waveguides as small as $1\mu\text{m}$ had been etched. Despite the good spectral characteristics of these devices, they were of limited practical use, because threshold currents were well above 100mA. Continuous wave operation at room temperature would have been difficult to achieve without a change in design, which led to the development of the pillbox structure.

1.4.1 Semicircular devices, "U's"

Having modelled the field distribution in a circular waveguide without an inner boundary (section 2.2), it remained to be seen if such a device would work in practice. Therefore, semicircular lasers with a straight waveguide in the shape of a filled "U" were fabricated. To some respect, they allow the observation of laser action inside the ring resonator, because the light distribution does not change considerably beyond the curved part. The straight section was added to ensure reliable microprobing, but it was kept short to distort the observation as little as possible.

When such a device is operated below lasing threshold, the output face looks like a uniformly luminescing bar. With increasing pumping current, the light intensity shifts to the outside, which indicates that a resonator is formed along the outer annulus of the semicircle.

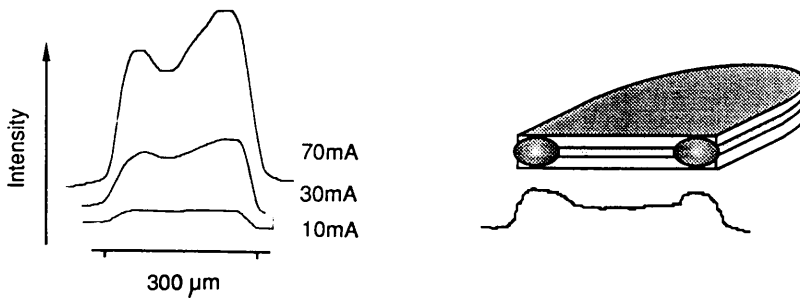


Figure 3. The whispering-gallery effect demonstrated with a 'U'- shape laser

The graph has been obtained by scanning a small photodetector across the image of the front face of the "U". The last scan has been made with reduced detector sensitivity to show that the ratio between the sidelobes and the centre has increased, not just the overall intensity.

1.4.2 The Pillbox

After this encouraging observation, pillbox-type ring lasers with no isolation or any other confinement mechanism at the inside of the ring, simply a pillbox with a tangential waveguide, were fabricated and produced the following spectrum. The tangential waveguide was chosen because it seemed the most straightforward solution.

²⁰ A.F.Jeziarski, "Semiconductor ring lasers", Ph.D. Thesis, Glasgow University, 1990.

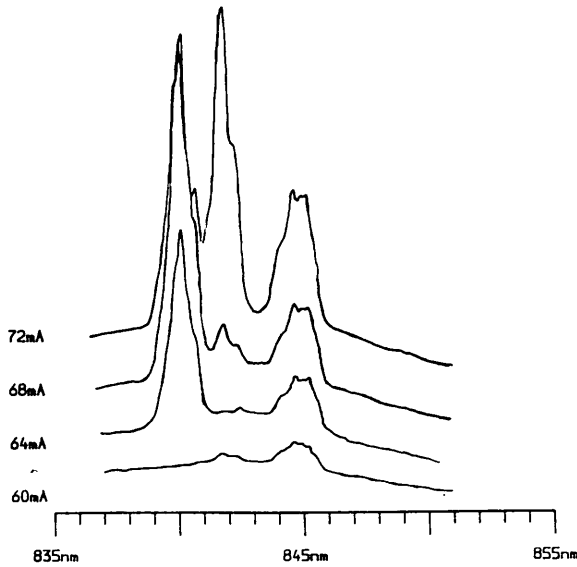


Figure 4. Spectrum of a pillbox ring laser with no isolation in the centre.

The lasing threshold is at 60 mA, a low value considering the size of $84\mu\text{m}$ diameter, which translates into a threshold current density of about $1100\text{A}/\text{cm}^2$. For comparison, stripe lasers of comparable length in the same single-quantum well material have shown lasing at a threshold of $300\text{A}/\text{cm}^2$.

Only fragments of that material were left at the time, so the subsequent experiments were conducted with double heterostructure material of inferior quality. However, most effects could be studied equally well, only the threshold currents obtained were higher.

1.4.3 Polyimide insulation

The next step was to introduce an electrical isolation pad for the central part of the ring. The size of this pad has an important influence on the threshold current, because it restricts the pumped area to the outer annulus. Polyimide was chosen for this purpose because it is easy to use (spin-on process) and acts as its own negative resist (section 4.5) for e-beam exposure, i.e. it was compatible with the current process. $94\mu\text{m}$ diameter devices with polyimide pads varying between 50 and $92\mu\text{m}$ were fabricated, so the smallest pumped annulus created was only $1\mu\text{m}$ wide.

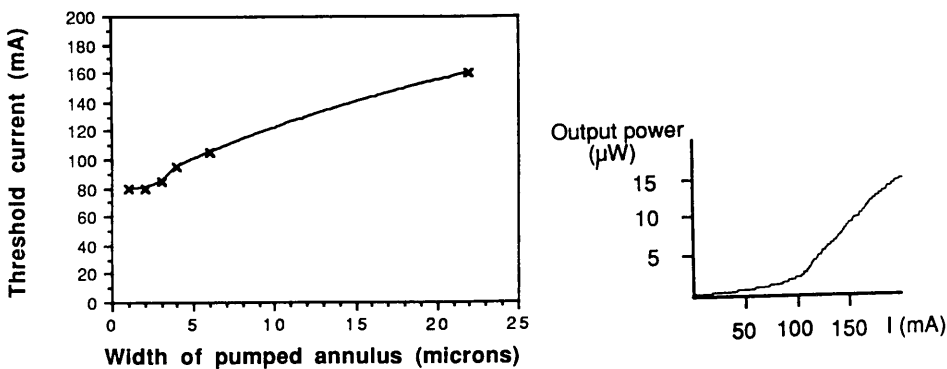


Figure 5. Threshold current vs. width of the pumped annulus and L-I curve of an early device.

It is interesting to note that the threshold current does not decrease significantly with decreasing width of the annulus. This shows that the effect of current spreading is quite strong, i.e. carriers drifting towards the inside of the pillbox. The effect becomes stronger the smaller the pumped annulus and nearly compensates the reduction in threshold current below a width of $3\text{-}4\mu\text{m}$. Therefore, it is unnecessary to reduce the pumped filament to below that value, which allows for more fabrication tolerance.

1.4.4 Scattering

At that stage, the fabrication technique was not sufficiently developed to produce rings with very smooth sidewalls, so scattering was a serious problem. Scattering manifests itself as bright luminescence of the sidewalls, part of which can be collected with the collimating microscope objective. The following figure illustrates this effect, where a spectrum was taken a) only from the output of the waveguide and b) collecting the emission of the whole device. Figure 6c) illustrates how the ring laser radiation manifests itself as a "bar" and a "dot" in the projected image.

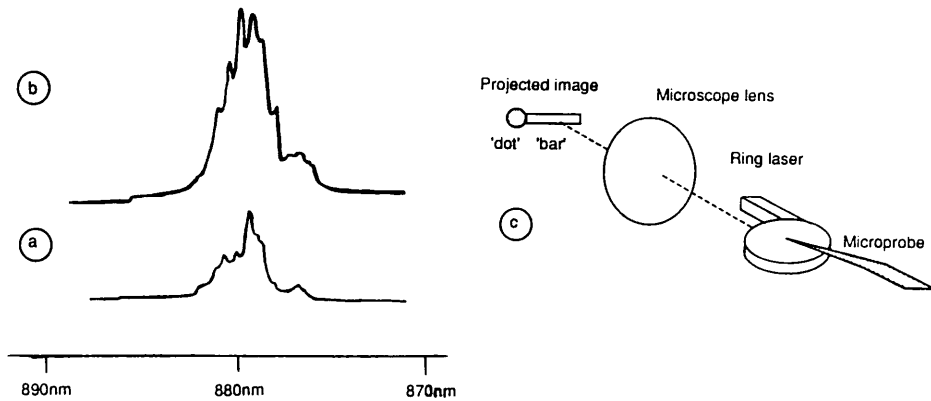


Figure 6. Comparison of waveguide output and scattered emission.

Although only a part of the scattered light can be collected by the lens, the signal is stronger than that from the output of the waveguide alone. This shows that only a fraction of the power is coupled into the waveguide and the major part is dissipated by scattering. The two spectra are similar in shape, which indicates that the luminescence really is scattered light rather than spontaneous emission.

The scattering problem was solved by improving the fabrication and producing smoother sidewalls. Additionally, better material was obtained, a single quantum well structure grown by MOCVD. The next generation of pillbox ring lasers thus evolved, the first devices that could operate continuously.

1.4.5 Cw operation

A room-temperature cw threshold of 24mA was achieved. One of the devices that produced this much improved result is shown together with its spectrum, that, for the first time, clearly correlates to the free spectral range of the cavity.

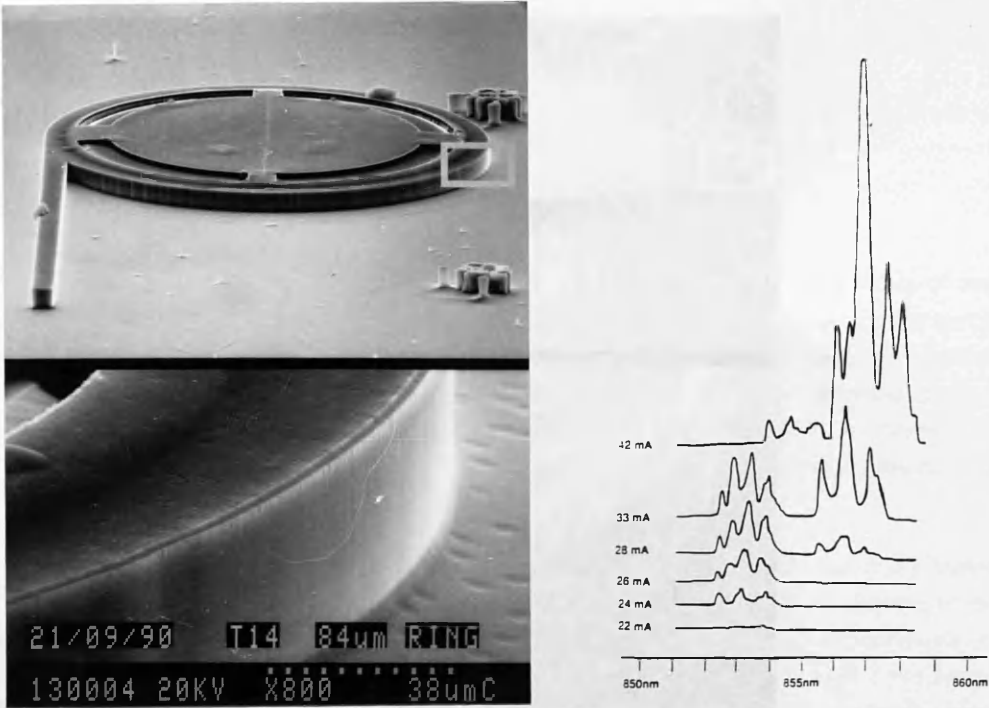


Figure 7. Micrograph and spectrum of the first device that operated cw, emphasizing the smoothness of the walls.

The output was mostly confined to the waveguide, a further sign of improvement.

1.4.6 Silicon nitride

The next change, coating the devices with silicon nitride and using it for isolation instead of polyimide, resulted in the suppression of the non-radiative recombination current, a further reduction of the scattering loss and the ability to wire-bond. The resulting threshold current was 15mA, which was further reduced to 12.5mA by etching the inside of the ring to increase the current confinement. Using this data, it was possible to calculate the spreading current and derive the effective threshold current and the excess bending loss of the device (5mA and 3dB/360°, respectively). These low values clearly show that the concept of whispering gallery modes in a pillbox resonator is viable.

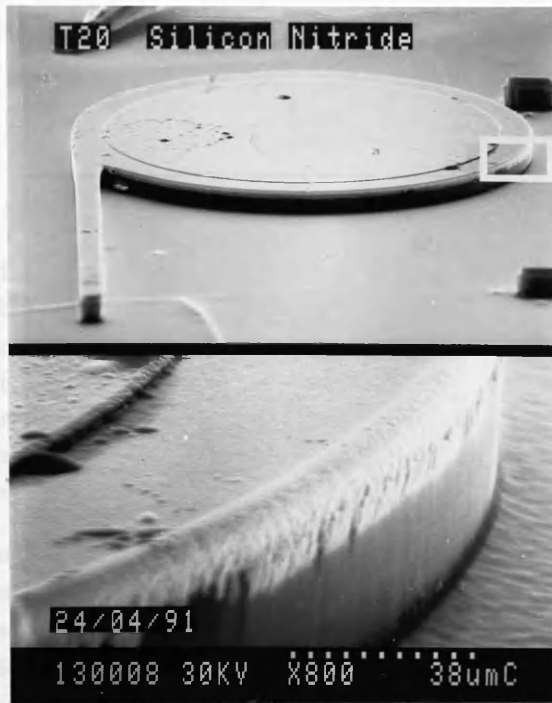


Figure 8. Micrograph of the first silicon nitride coated ring laser.

1.4.7 Integrated detector

Using double-waveguide material, an integrated ring laser - waveguide - detector circuit was realized, the first photonic integrated circuit comprising a ring laser.

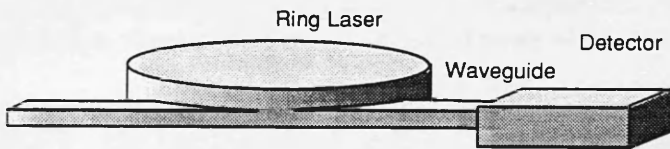


Figure 9. Sketch of an integrated laser - waveguide - detector circuit based on double-waveguide material.

The detector current was shown to be decoupled from the laser current, so it was suitable for monitoring purposes.

1.4.8 Strip-loaded ring lasers

One of the major problems of ring lasers, degeneration, derives from the necessity of etching through the active layer to achieve optical confinement for the small radii used. Bigger radii, in the order of $500\mu\text{m}$, allow the use of strip-loading as a guiding mechanism. Strip-loading leaves the junction buried, so the degradation is reduced if not eliminated. Threshold currents between 38mA ($600\mu\text{m}$) and 47mA ($300\mu\text{m}$) and a differential quantum efficiency $\eta_d \geq 0.10\text{W/A}$ were obtained for $5\mu\text{m}$ wide quarter-ring lasers.

1.4.9 Integrated transistor

The successful demonstration of a field-effect transistor controlling a ring laser gave the final touch to the project. Hence, the basic elements of an extended optoelectronic circuit, i.e. a waveguide, a

detector, and a transistor had been combined with a ring laser. The only missing element, a modulator, was also attempted, but did not operate successfully.

1.5 Outline

This thesis is organized as follows:

The next chapter introduces the whispering-gallery guiding effect, which is the basis of operation of a pillbox ring laser. Ring laser material, which is the most important prerequisite for turning this concept into practice, is discussed in the third chapter. The underlying theory of quantum-well materials is presented and the performance of several structures that were obtained in the course of the project is compared. The fourth chapter covers the procedures that are involved in fabricating the devices, emphasizing the ones that were particularly important for ring lasers. The fifth chapter describes the measurement setup and its limitations.

After having laid the foundation for the understanding of the results in the previous chapters, the core of the work is presented in chapters 6 and 7. Chapter 6 shows the results of the ring laser work, discusses the parameters that influence the performance of the devices and describes various geometrical aspects. Chapter 7 goes one step further by showing the efforts that have been made towards integrating the ring laser device with other optical and electronic elements. Modelling constitutes a significant part of this chapter because it is important to evaluate the properties of the more complex materials that are required to perform the desired multitude of tasks. The eighth chapter concludes the work, discussing the problems that have been solved and those that have not, and suggests further activities that are made possible through the results presented here.

In addition to the footnotes, the references are compiled in an alphabetical list at the end of the thesis.

2. Design considerations for ring lasers

Most of the ring laser geometries developed in the past relied on some sort of confinement mechanism for the inner boundary, such as stress-induced refractive index changes²¹ or etching²². The former approach causes adhesion problems due to different thermal expansion coefficients, the latter is not ideal either:

1. High loss of the structure because of scattering at two interfaces.
2. High non-radiative recombination current due to surface states because the pn junction is exposed on both sides.
3. High thermal resistance because the heat generated at the junction can only escape in one direction, an effect which has been modelled and demonstrated²³.

In order to solve these problems, the pillbox structure was developed. Its operation can be visualized with the ray model²⁴, shown in figure 1, or by using the conformal transformation technique²⁵, to transform the curved structure into a straight one. This transformation results in an apparent rise of the refractive index towards the outer edge that eliminates the necessity of forming an inner boundary to support the low-order modes, and they can propagate as 'whispering-gallery' modes. Based on this model, a computer program was developed to simulate the waveguiding properties and study the modal distribution of the structure.

2.1 Conformal transformation

Conformal transformation²⁶ is a method of transforming an area from one complex plane into another. It is mostly used to transform complicated field distributions into ones that can be solved analytically. To demonstrate the method, a torus segment is transformed into a rectangle (figure 10).

Let

$$W = R_2 \ln \frac{Z}{R_2} \quad [2.1]$$

be a function of the two complex variables W and Z

$$W = u + jv \quad Z = x + jy \quad [2.2]$$

²¹ A.F.Jeziarski and P.J.R.Laybourn, "Integrated semiconductor ring lasers", IEE Proceedings, Vol.135, Pt.J, pp.17-24, 1988.

²² A.F.Jeziarski and P.J.R.Laybourn, "Polyimide embedded semiconductor ring lasers", Proceedings SPIE No. 1141, pp.7-11, 1989.

²³ W.Chen, "Thermal problems in semiconductor ring lasers", M.Sc. thesis, Glasgow University, 1989.

²⁴ S.Sheem and J.R.Whinnery, "Guiding by single curved boundaries in integrated optics", Wave Electronics, Vol.1, pp.61-68, 1974.

²⁵ M.Heiblum and J.H.Harris, "Analysis of Curved Optical Waveguides by Conformal Transformation", IEEE Journal of Quantum Electronics, Vol.11, pp.75-83, 1975.

²⁶ W.J.Gibbs, "Conformal transformations", The British Thomson-Houston Co. Ltd, 1958.

2.Design considerations for ring lasers

In this example, it is advantageous to put Z into polar coordinates, so

$$Z = re^{j\phi} \quad [2.3]$$

Substituting [2.2] and [2.3] into [2.1] and separating the real and imaginary parts yields

$$u + jv = R_2 \ln \frac{re^{j\phi}}{R_2} \quad [2.4]$$

$$u = R_2 \ln\left(\frac{r}{R_2}\right) \quad v = R_2\phi \quad [2.5]$$

The following figure illustrates the procedure.

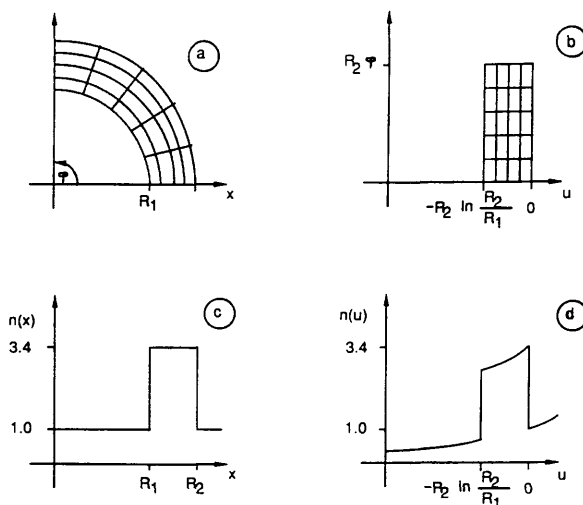


Figure 10. Transformation of a torus in the x - y (R - ϕ) plane into a rectangle in the u - v plane and change of the refractive index.

The transformed refractive index is calculated using the modulus of the change of Z with W from [2.1].

$$n(u) = n(x) \left| \frac{dZ}{dW} \right| \quad [2.6]$$

$$n(u) = n(x) e^{\frac{u}{R_2}} \quad [2.7]$$

The result of this operation is shown in fig.10d), where the values of $n(x)$ in fig.10c) have been multiplied by $\exp(u/R_2)$.

2.2 Computer modelling

The starting point for the modelling is a program²⁷ that was originally designed to calculate the effective index and the mode distribution of straight waveguides. The program can be applied to ring structures by conformally transforming them into straight waveguides, i.e. by replacing the refractive index values according to [2.7].

The calculation is based on finite differences, where the scalar wave equation is transformed into a numerically soluble version. The wave equation for TE modes is

²⁷ MRS Taylor, Department of Electronics and Electrical Engineering, University of Glasgow.

2.Design considerations for ring lasers

$$\frac{\delta^2 E_x}{\delta x^2} + \frac{\delta^2 E_y}{\delta y^2} + k^2(n_{ij}^2 - n_{eff}^2)E_x = 0 \quad [2.8]$$

The waveguide cross-section is covered with a mesh of the size Δ . The function $E_x(x,y)$ is replaced by discrete values at the mesh points and the partial derivatives by the expressions

$$\frac{\delta^2 E_x}{\delta x^2} = \frac{E_{i+1j} + E_{i-1j} - 2E_{ij}}{\Delta^2} \quad [2.9a]$$

$$\frac{\delta^2 E_y}{\delta y^2} = \frac{E_{ij+1} + E_{ij-1} - 2E_{ij}}{\Delta^2} \quad [2.9b]$$

at the point $(i\Delta, j\Delta)$. The values are calculated over and over again until the difference from one loop to the next is smaller than a predetermined value. The program had been very efficiently designed to allow for vector processing. Therefore, it takes less than a minute to calculate arrays of the size 50 x 50 data points.

The first of the following two graphs illustrates the modelling frame, showing the cross-section of a pillbox ring laser device. The second one is the result of the modelling and shows the mode distribution for the fundamental mode as well as the corresponding waveguide structure. Note that in figure 12, the refractive index n is in the third dimension, to show the influence of the conformal transformation. It has been cut off at a value of 2.5 in order to emphasize on the area of interest.

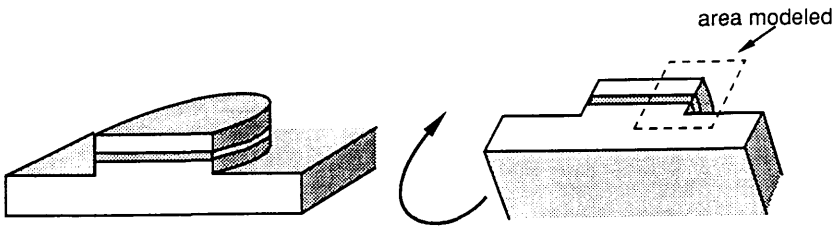


Figure 11. Cross-section of a pillbox ring laser and a rotated version to illustrate the orientation of the graph below.

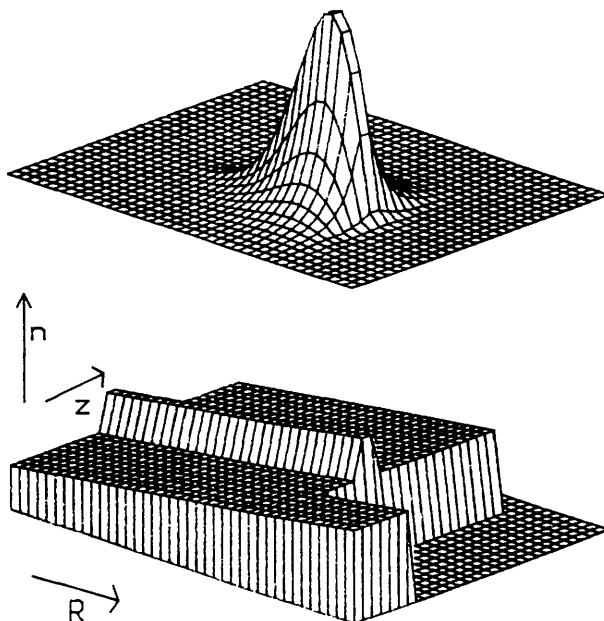


Figure 12. The mode distribution in a pillbox ring laser. Each contour line represents 0.1 micrometers.

2.3 Modelling results

2.3.1 Pillbox ring lasers

The program allows one to vary the geometry of the device and to calculate the corresponding mode profile. A particular design can be assessed in terms of its capability to confine a mode or to allow leakage into the substrate. Studying various parameters led to the following conclusions:

1. The model demonstrates that the whispering-gallery modes are reasonably well confined towards the inside of the pillbox.
2. It shows that rings smaller than $10\mu\text{m}$ radius can guide modes due to the strong confinement of the GaAs-air interface.
3. The knowledge of the mode width, as shown in figure 4, is important for the design of the pumping geometry.

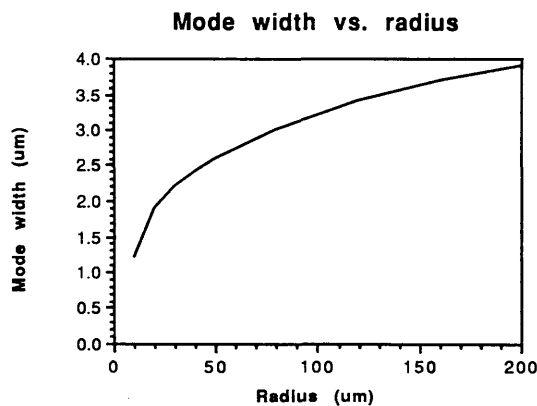


Figure 13. Width of the whispering-gallery mode vs. radius of the pillbox.

The width has been taken between the two points where the intensity is $\frac{1}{10000}$ of the maximum value. Since higher-order modes extend further into the pillbox, they can be suppressed by providing gain only to a thin outer annulus, thus not providing sufficient gain to the mode tails. However, this mechanism is not very selective because of current spreading (section 6.2.3).

If an inner boundary was introduced, it would not have an effect as long as the width of the waveguide was bigger than the mode width. This assumption is supported by experimental evidence²⁸ that shows an increase in loss for $150\mu\text{m}$ radius curved waveguides when the waveguide width is decreased below $4\mu\text{m}$. The loss increases as the inner boundary starts interacting with the mode, since the corresponding mode width from figure 13 is $3.5\mu\text{m}$.

4. The mode position in the resonator is a function of the refractive index, because the index profile is asymmetrical. This is most evident for waveguides of different radii, where the steeper index distribution for smaller radii forces the mode closer to the wall. However, physical effects such as refractive index changes due to gain and temperature can have similar effects on the mode position, as discussed in section 6.2.6.

²⁸ J.P.Hohimer, D.C.Craft, G.R.Hadley, and G.A.Vawter, "Cw room-temperature operation of Y-junction semiconductor ring lasers", *Electronics Letters*, Vol.28, pp.374-375, 1992.

2.Design considerations for ring lasers

5. If different ways of obtaining a refractive-index contrast on the outside of the pillbox can be found (e.g. by disordering or proton implantation), a change of $\Delta n \approx 0.2$ is required for a $50\mu\text{m}$ radius device.
6. The knowledge of the mode position enables one to design an intersection between curved and straight waveguide sections such that the position of the field maxima are matched and the coupling loss is minimized²⁹.

The limited validity of the model was experienced in a later experiment: The model suggests that for $50\mu\text{m}$ diameter devices, the interface between the active layer and the lower cladding can be on the same level as the substrate, i.e. the whole of the lower cladding can be buried. The experiment (section 4.3.1) showed that a space of at least $0.4\mu\text{m}$ is required to prevent the mode tail from leaking into the substrate. This misrepresentation emphasizes that the results of this simplified model have to be treated with care. Thus, the benefit of the model is more in providing qualitative insights rather than quantitative design parameters.

2.3.2 Strip-loaded ring lasers

If the radius is increased considerably, the model suggests that strip-loading can be used for guiding. The following graphs represent a similar view to the one shown before, except that the frame has been rotated by 90° .

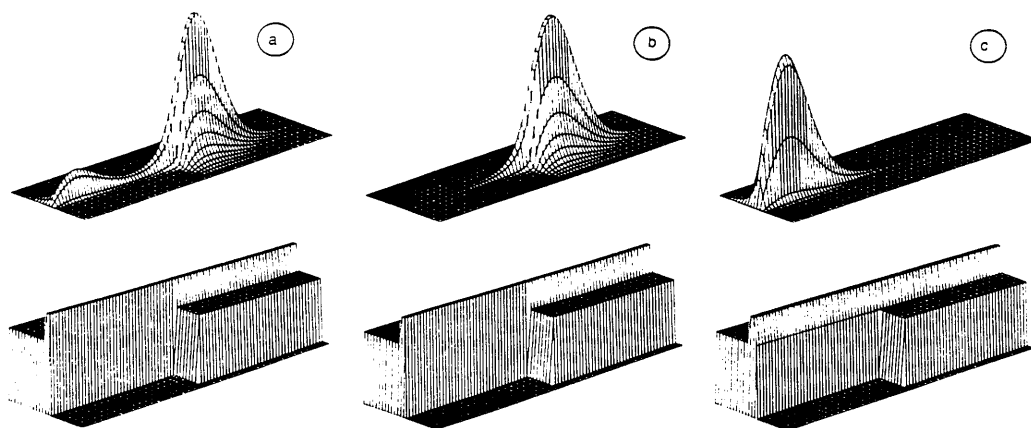


Figure 14. Guiding of a strip-loaded curved waveguide.

The first graph shows the limit of guiding at $320\mu\text{m}$ radius and a considerable fraction of the mode leaking into the substrate. The second graph displays a fully confined mode for a radius of $400\mu\text{m}$, which suggests that such a device should operate successfully. The third graph points out the importance of removing the entire cladding, i.e. etching down to the active layer. Using the same radius as before ($400\mu\text{m}$), but leaving $0.1\mu\text{m}$ of the cladding layer, the mode is not confined at all. This has important implications for the fabrication of such a structure, since the standard etching process using SiCl_4 is not selective nor sufficiently controllable to be terminated accurately at the interface between the cladding and the active layer. Thus, a different etchant and/or a two-stage etching process is required to realize a ring laser using strip-loading.

²⁹ E.G.Neumann, "Curved dielectric optical waveguides with reduced transition losses", IEE Proceedings, Vol.129, Pt.H, pp.278-280, 1982.

2.Design considerations for ring lasers

As mentioned before, the data thus obtained can only give a rough indication of the results to be expected, because the influence of carriers and gain is neglected in this model. However, the results shown in figure 14 led to the successful demonstration of strip-loaded guiding for curved lasers down to a radius of $300\mu\text{m}$ (section 6.4).

3. Ring laser material

To enable stimulated emission in a laser medium, more electrons are required in a higher energetic level than in the corresponding lower one, i.e. the carrier distribution that exists at thermal equilibrium has to be inverted. Inversion is achieved in a semiconductor by joining two heavily doped regions and applying a forward bias. In thermal equilibrium, carriers diffuse from the n-type into the p-type region and form a depletion layer which acts as a barrier. Under sufficient forward bias, electrons can overcome this barrier, and fill up the conduction band to the quasi-Fermi level E_{fc} , whereas the valence band is left with empty states down to the quasi-Fermi level for holes E_{fv} . The levels are called 'quasi-Fermi' because they only exist when a forward bias is applied.

Having been excited into the conduction band, the electrons relax back into the valence band within a few nanoseconds, thereby dissipating their excess energy as a photon. The photons, as they travel through the crystal, can induce the transition of another electron which in turn produces another photon. The second photon is in phase with the first one, the whole process being called 'stimulated emission'. The process keeps repeating until the rate of induced transitions equals the rate of pumped electrons, and the gain saturates.

Stimulated emission can only occur in direct-gap semiconductors, where the transition does not require a change of momentum of the electron. Indirect-gap semiconductors are not suitable because the electron requires a change in both energy and momentum to undergo a transition, whereas the transition inducing photon, with its negligibly small momentum, can only induce a change in energy. This is why silicon, which would be the most attractive semiconductor for photonics applications due to its wide use in electronics, cannot be used. Silicon is an indirect bandgap semiconductor.

If the photons thus created are bound within an optical resonator, only the ones of or very close to the wavelength which is an integer multiple of the resonator length are amplified. All the other ones cancel out by destructive interference. In case of double heterostructure lasers, the active layer is embedded between the p-type and the n-type region. It is usually left undoped and is made of lower bandgap material to confine the electrons and holes. Double heterostructure lasers were the first to find real applications because room-temperature cw operation was achieved.

To determine the thickness of the active layer, one has to consider two parameters, the current density and the optical energy density, both being determined by the active layer.

1. The gain is proportional to the carrier density, so the active layer should be as thin as possible from the electrical point of view.
2. The gain is also proportional to the photon density, which has an optimum value at a certain waveguide thickness. If the active layer gets thinner, the light spreads out into the adjacent layers and the photon density is reduced. This optimum value is given by³⁰

$$t = \frac{0.227 \lambda}{\sqrt{n_g^2 - n_c^2}} \quad [3.1]$$

t being the guide thickness, λ the wavelength, n_g the refractive index of the guide and n_c the refractive index of the cladding, respectively. In a typical AlGaAs/GaAs laser, this thickness is $0.15\mu\text{m} - 0.2\mu\text{m}$ (compare to figure 19).

³⁰ H.G.Unger, "Optische Nachrichtentechnik 2", Course of the FernUni Hagen (equivalent to the Open University), p.372, 1984.

3. Ring laser material

Because both requirements cannot be met by a single layer, it is necessary to introduce more layers which optimize each condition independently. Consequently, lasers with separate optical and carrier confinement were introduced³¹, which reduce the threshold current at room temperature to around $500 A/cm^2$. This is quite an achievement considering that the threshold current for initial structures was above $10000 A/cm^2$.^{32,33}

Quantum-well material takes this idea one step further: The active layer is reduced to $\approx 10nm$, which is in the order of the de-Broglie wavelength of electrons. Therefore, they are confined in a potential well where only certain discrete energy levels are allowed. The density of states is transformed into a step-like function which has a much higher concentration of carriers for the fundamental transition than a parabolic density of states. This in turn reduces the threshold current density considerably; values of $55 A/cm^2$ have been reported³⁴. Additionally, the threshold current is less temperature dependent so room temperature operation is easier to achieve.

3.1 Material parameters

The material is designed to optimize both the electrical and optical efficiency, i.e. the aim is to maximize the internal current-light conversion efficiency η_i and the optical confinement factor per well Γ_w . The first of the following figures (15a) illustrates the parameters involved in designing a quantum well laser, while the second (15b) shows a typical single quantum well laser, the material that has been used for most of the experiments.

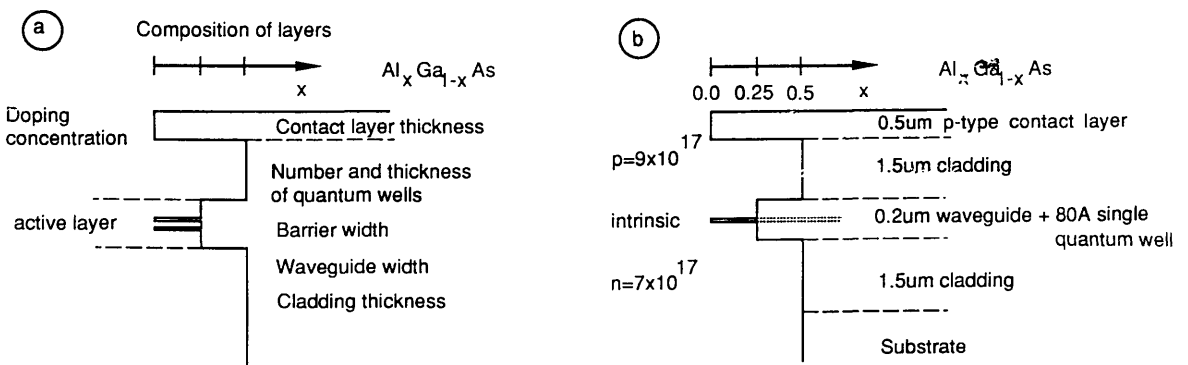


Figure 15. The parameters involved in designing a quantum well laser (a) and typical material design (b), CB387.

³¹ G.H.B.Thompson and P.A.Kirkby, "(GaAl)As lasers with a heterostructure for optical confinement and additional heterojunctions for extreme carrier confinement". IEEE Journal of Quantum Electronics, Vol.9, pp.311-318, 1973.

³² R.N.Hall, G.E.Fenner, J.D.Kingsley, T.J.Soltys, and R.O.Carlson, "Coherent light emission from GaAs p-n junctions", Physical Review Letters, Vol.9, pp.366-368, 1962.

³³ M.I.Nathan, W.P.Dumke, G.Burns, F.H.Dill, and G.J.Lasher, "Stimulated emission of radiation from GaAs p-n junctions", Applied Physics Letters, Vol.1, pp.62-64, 1962.

³⁴ A.Yariv, "Optical Electronics", 4thed. , pp.603-606, HRW Sanders 1991.

3.1.1 Size and number of quantum wells

Since only discrete energy levels are allowed in a quantum well, the size of the wells influences the lasing wavelength. Figure 16 shows this dependence, assuming that the transition takes place between an electron and a heavy hole with a ratio of 1:2 between the depth of the well in the valence band and the conduction band, respectively. The data has been obtained solving the one-dimensional Schrödinger equation.

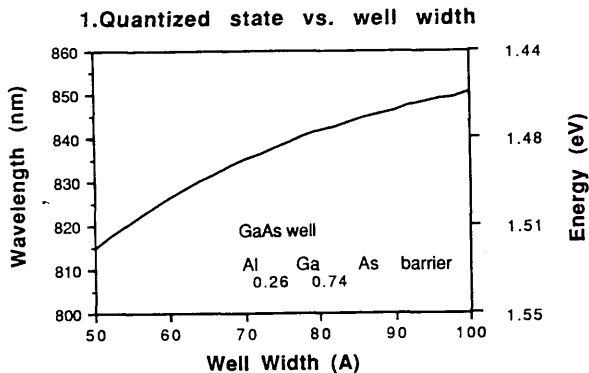


Figure 16. The dependence of the lasing wavelength on the quantum well size.

Since the effect of free and injected carriers on the bandgap has not been taken into account, the calculated values deviate from the real ones; the lasing wavelength for a 80Å single quantum well structure is around 850nm rather than 840nm as shown above. However, the study gives a valuable insight into the change of emission wavelength with quantum well size.

The optimum number of wells is determined by the gain required to overcome the losses in the material, i.e. the following condition applies in a stripe laser at threshold^{35, 36}.

$$g = \alpha_i + \frac{1}{L} \ln \frac{1}{R} \quad [3.2]$$

The gain g in the material equals the sum of the losses, which are the internal loss or optical loss α_i and the mirror loss $L^{-1} \ln R^{-1}$, L being the length and R the reflection coefficient of the facets.

For a quantum well laser, [3.2] changes to

$$n_w \Gamma_w g_w = \alpha_{int} + \frac{1}{L} \ln \frac{1}{R} \quad [3.3]$$

which accounts for the fact that only the optical field that overlaps with the quantum well can induce stimulated emissions and provide gain; n_w being the number of wells and Γ_w the optical confinement factor per well. In order to express [3.3] in terms of pumping current, it is necessary to introduce the following gain-current relation:

$$\frac{g_w}{g_0} = \ln \frac{J_w}{J_0} + 1 \quad [3.4]$$

³⁵ A.Kurobe, H.Furuyama, S.Naritsuka, N.Sugiyama, Y.Kokubun, and N.Nakamura, "Effects of well number, cavity length, and facet reflectivity on the reduction of threshold current of GaAs/AlGaAs multi-quantum well lasers", IEEE Journal of Quantum Electronics, Vol.24, pp.635-639, 1988.

³⁶ P.McIlroy, A.Kurobe, and Y.Uematsu, "Analysis and application of theoretical gain curves to the design of multi-quantum-well lasers", IEEE Journal of Quantum Electronics, Vol.21, pp.1958-1963, 1985

where g_0 and J_0 are the saturation parameters for the gain and the current density, as defined in reference 36, and J_w is the threshold current density per well. This relation accounts for the fact that a material with more wells requires more current to initiate lasing but has a steeper gain curve once inversion is achieved. The following figure is an illustration of [3.4] and shows the gain-current relation for materials with different numbers of wells.

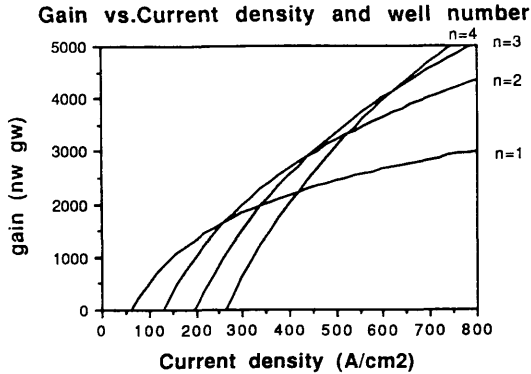


Figure 17. Gain vs current density for different numbers of wells at a given well size of 75 \AA .

The loss is determined by the size and type of laser as well as the quality of the material. For a typical stripe laser of $L = 200 \mu\text{m}$, $R = 0.3$ and $\alpha_i = 10 \text{ cm}^{-1}$, the total loss according to [3.3] is 70 cm^{-1} . The required gain for that laser is 2300 cm^{-1} , assuming a confinement factor of $\Gamma_w = 3.3\%$. According to figure 17, the corresponding threshold current density is 350 A/cm^2 and the optimum number of wells is two. If one well was to be used, the threshold current density would rise to 530 A/cm^2 , which is a significant increase.

This underlines how important it is to choose the number of wells according to the device application envisaged. For example, single quantum well material, which is the material of choice for many applications, only has a low threshold current density for low loss devices. If the devices are more lossy, the threshold current density rises quickly because the gain curve saturates. This was the case in earlier ring lasers that had high wall losses due to scattering. The threshold current of these devices was only slightly lower in single quantum well (SQW) material than in a double heterostructure (DH), indicating that the gain was well within saturation. On the other hand, the material was ideal to study the fabrication and design of the devices, because small improvements gave rise to big reductions in threshold current.

3.1.2 Barriers between quantum wells

In case of a multiple quantum well (MQW) structure, the barrier size is another important parameter. For a barrier height of $x = 0.2$ ($\text{Al}_{0.2}\text{Ga}_{0.8}\text{As}$), the width should exceed 35 \AA , otherwise the wavefunctions in the wells overlap and form energy bands rather than well-defined energy states³⁷. Increasing the barrier width much beyond that value results in a decrease of Γ_w because of increasing distance between the wells and the peak of the optical field. From the electronic point of view, it has been shown³⁸ that the electron capture time, which is directly proportional to the

³⁷ S.P.Cheng, F.Brillouet, and P.Correc, "Design of quantum well AlGaAs-GaAs stripe lasers for minimization of threshold current-application to ridge structures, IEEE Journal of Quantum Electronics, Vol.24, pp.2433-2440, 1988.

³⁸ P.W.M.Blom, J.E.M.Haverkort, and J.H.Wolter, "Optimization of barrier thickness for efficient carrier

threshold current, is minimized if the barrier states have a maximum overlap with the confined states in the well. The following figure shows the optimum barrier width as a function of the well width for a barrier composition of $x = 0.3$. The barrier width is small ($< 100\text{\AA}$), just before a new bound state is coupled into the well.

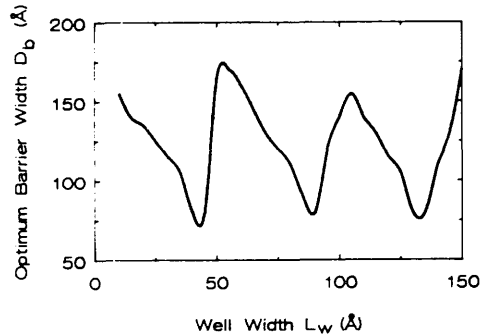


Figure 18. Optimum barrier width vs. well width for barrier height $x = 0.3$ taken from reference 38.

This theoretical result is supported by experimental evidence. A combination of 50\AA wells, a barrier composition of $x = 0.2$ and width of 40\AA gives both a very low capture time and threshold current³⁹.

3.1.3 Waveguide design

The aim of the waveguide design is to maximize the optical confinement factor in the quantum well, Γ_w . Since Γ_w is the fraction of the mode that travels within the quantum well, only this portion of the wave can induce stimulated emission. Γ_w is the fraction of the power within the well divided by the whole power carried by the laser mode, which can be calculated using a one-dimensional scalar finite difference program.

$$\Gamma_w = \frac{\int_{\text{well}} E_{(x)}^2 dx}{\int_{\text{waveguide}} E_{(x)}^2 dx} = \frac{\sum_{i=i_0}^{i=i_1} E_i^2 \Delta x}{\sum_{i=0}^n E_i^2 \Delta x} \quad [3.5]$$

A very small meshsize (10\AA) has been chosen to give a reasonable number of nodes within the well. Γ_w can be maximized by various combinations of waveguide width and composition, including linear and parabolic gradings. The following figures show its dependence on the waveguide width at various well widths (figure 19a) and at various compositions (figure 19b). The result agrees with [3.1], the optimum width being $0.2 \mu\text{m}$ for a refractive index step of $\Delta n = 0.2$ (= composition step $\Delta x = 0.4$). However, the confinement factor can be increased from 3%, using these parameters, to more than 4% by reducing the cladding index and the guide thickness appropriately.

capture in graded-index and separate-confinement multiple quantum well lasers", Applied Physics Letters, Vol. 58, pp.2767-2769, 1991.

³⁹ W.T.Tsang, "Extremely low threshold AlGaAs modified multi-quantum well heterostructure lasers grown by molecular beam epitaxy", Applied Physics Letters, Vol.39, pp.786-788, 1981.

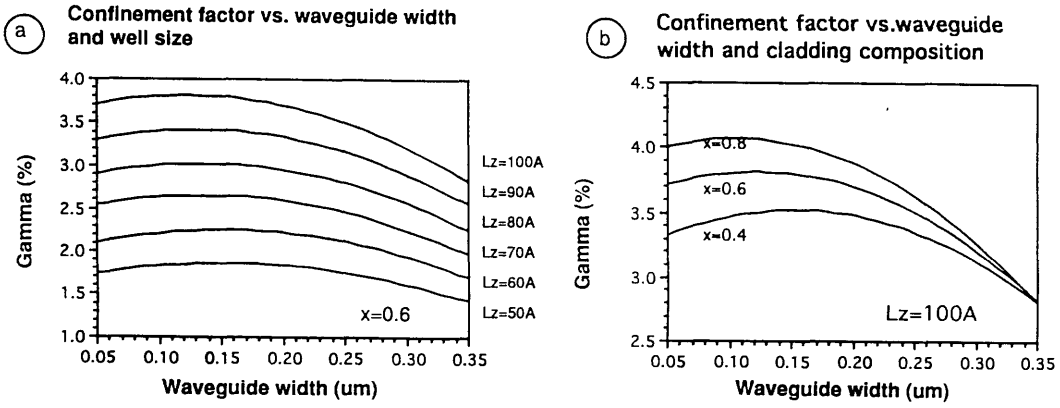


Figure 19. The dependence of the optical confinement factor on the well width, guide width and composition.

However, the cladding composition (figure 19b) is limited by practical considerations. For aluminum fractions greater than 0.5, the mismatch, although very small, between GaAs and AlGaAs becomes significant for a layer thickness in the μm -range, such as required for the laser cladding. It then becomes increasingly difficult to grow the structure without 'relaxation', i.e. the epitaxial layer relaxing into its inherent lattice rather than maintaining the dimensions of the seeding crystal⁴⁰. Relaxation is unwanted because the interface between the original and the relaxed crystal gives rise to defects that enhance the optical absorption.

3.1.4 Sellmayer's equation

The refractive indices of the different material compositions involved have been calculated using Sellmayer's equation⁴¹, to give precise values and to take the wavelength dispersion into account.

$$n^2 = A(x) + \frac{B}{\lambda_0^2 - C(x)} - D(x)\lambda_0^2 \quad [3.6]$$

with the following empirical constants

A	B	C	D
10.906-2.92x	0.97501	(0.52886 - 0.735 x) ² , x ≤ 0.36 0.30386-0.105 x) ² , x ≥ 0.36	[0.002467(1.41 x + 1)]

3.1.5 Cladding thickness

The purpose of the cladding is to provide a low-loss medium to carry the evanescent field and prevent the guided mode from coupling into the cladding layer. In a standard structure, the cladding is up to $2\mu\text{m}$ thick, but recent results⁴² suggest that this thickness can be reduced to as little as $0.45\mu\text{m}$, depending on the laser structure, without increasing the threshold current density.

⁴⁰ A.H.Kean, MBE group, Department of Electronics and Electrical Engineering, University of Glasgow.

⁴¹ For example in: R.G.Hunsperger, "Integrated Optics: Theory and Technology", 2nded., Series in Optical Sciences 33, p.61, Springer 1984.

⁴² A.Behfar-Rad, J.R.Shealy, S.R.Chinn, and S.S.Wong, "Effect of cladding layer thickness on the per-

3. Ring laser material

Experiments have been conducted to verify this result. Stripe lasers were fabricated with the cladding etched down to $1.6\mu\text{m}$, $0.9\mu\text{m}$ and $0.8\mu\text{m}$. This led to difficulties in forming the contact since the p^+ GaAs top contact layer had been removed and the exposed AlGaAs readily forms a much thicker oxide layer than the GaAs. However, for the devices that could be contacted, no difference in threshold current to the unetched monitor was measured. This confirms that the usual cladding depth of up to $2.0\mu\text{m}$ is excessive and can be reduced without compromising the performance. A thin cladding is very desirable, because it reduces the spreading current (section 6.2.3) and the required etch depth. Etching a shallower mesa is very advantageous for integration purposes, because it simplifies multi-level lithography.

3.1.6 Doping concentration of the cladding layers

The doping in a laser structure is relatively high in order to provide a good contact and reduce the parasitic resistance. However, since a significant fraction of the optical field travels within the cladding, very high doping, which leads to free-carrier absorption, must be avoided. Free-carrier absorption becomes significant⁴³ for doping concentrations of above $1 \times 10^{18}/\text{cm}^3$, so a doping level of $6-9 \times 10^{17}/\text{cm}^3$ is usually chosen as the best compromise.

3.2 Improved material design

The material structure shown in figure 15b) had been very useful for developing the ring laser, but the results achieved with the devices and the above considerations suggest that a further improvement is possible.

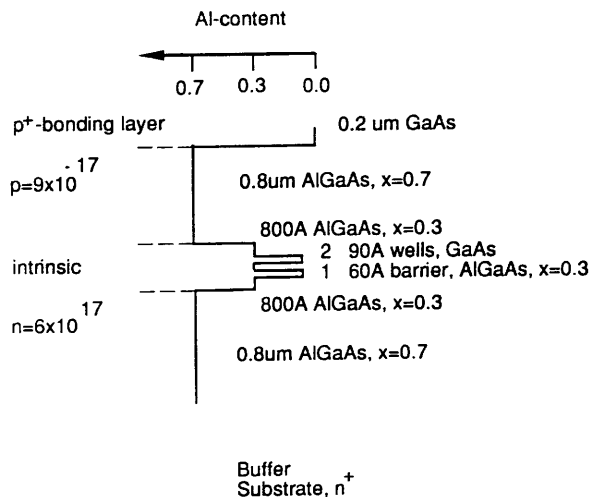


Figure 20. Improved ring laser material design.

Several design changes have been implemented:

1. The number of quantum wells has been increased from one to two. According to figure 17, this reduces the threshold current density for the required gain of 2500cm^{-1} (section 6.2.3) from $600\text{A}/\text{cm}^2$ to $400\text{A}/\text{cm}^2$. Also, the steeper gain curve for double quantum well material suggests that for a given variation in loss between similar lasers, the variation in threshold current is

formance of GaAs-AlGaAs graded index separate confinement heterostructure single quantum-well lasers', IEEE Journal of Quantum Electronics, Vol.26, pp.1476-1480, 1990.

⁴³ W.T.Tsang, "Extremely low threshold (AlGa)As graded-index separate-confinement heterostructure lasers grown by molecular beam epitaxy", Applied Physics Letters, Vol.40, pp.217-219, 1982.

3. Ring laser material

smaller than for a single quantum well. This addresses the problem of varying thresholds within an array as discussed in section 4.8.

2. The quantum well/barrier dimensions have been optimized according to section 3.1.2, using 90Å wells and 60Å barriers.
3. The width of the active layer and the cladding composition have been chosen to maximize Γ_w according to figure 19. This involved a reduction of the active layer thickness to 0.15 μm and an aluminium composition of $x=0.7$ in the cladding. A further increase of x would have been possible, but the structure would have been more difficult to grow due to relaxation (section 3.1.3). Also, fabrication becomes an issue, because the wet etch that is used to remove the NiCr etch mask (1:1 $\text{HCl}:\text{H}_2\text{O}$) also attacks AlGaAs with high aluminium fraction. The resulting confinement factor is $\Gamma_w = 3.4\%$. This corresponds to $\Gamma_w = 3.6\%$ for a single well, because the maximum of the field does not coincide with the position of the wells in the case of double quantum well material.
4. The cladding thickness has been decreased to reduce the current spreading effect as discussed in section 6.2.3.. A reduction of 50% in spreading current is expected with a reduction in cladding thickness from 2 μm to 1 μm .

A layer (CB524) incorporating the changes outlined above has been grown. The material characterisation suggests that the design enhancements have improved the performance (section 3.3.3), but it was not yet possible to fabricate devices successfully to verify the expected improvement of ring laser operation.

3.3 Comparison and characterisation of different material structures

During the course of the project, several laser structures have been obtained from Glasgow molecular beam epitaxy (MBE) and from Sheffield molecular vapour phase epitaxy (MOVPE). In order to get a better understanding of their properties and to evaluate their potential for ring laser fabrication, an assessment of their threshold current density J_{th} and internal optical absorption α_i has been made.

1. CB387 is the Sheffield-grown single quantum well (SQW) structure shown in figure 1b.
2. QT98 is the same structure as CB387, also Sheffield, except that a second waveguide has been added underneath the laser waveguide for integration purposes (figure 54).
3. CB524, Sheffield, is the double quantum well structure shown in figure 20.
4. A264 is a Glasgow grown laser incorporating four quantum wells and a graded index (GRIN) waveguide. At the time when it was designed, ring lasers were very lossy, so four wells were incorporated to provide more gain.

The threshold current density J_{th} can be obtained from a single device, but in order to get information about the internal loss, lasers of different length need to be evaluated.

3.3.1 Theory

In order to get an expression relating the two parameters that are accessible to measurement, threshold current and laser length, [3.3] and [3.4] are combined to obtain

$$\ln \frac{J_w}{J_0} + 1 = \frac{\alpha_{int} + \frac{1}{L} \ln \frac{1}{R}}{n_w \Gamma_w g_0} \quad [3.7]$$

Analyzing the threshold current density J_{th} in a quantum well laser yields

$$J_{th} = \frac{n_w J_w}{\eta_i} \quad [3.8]$$

where η_i is the internal quantum efficiency and J_w is the current density per well.

Substituting [3.6] into [3.5] and solving for J_{th} gives

$$\ln J_{th} = \frac{1}{L} \left(\frac{\ln \frac{1}{R}}{n_w \Gamma_w g_0} \right) + \left[\frac{\alpha_i}{n_w \Gamma_w g_0} + \ln \frac{J_0 n_w}{\eta_i} - 1 \right] \quad [3.9]$$

This equation is a straight line in a $1/L - \ln J_{th}$ graph, where the first term on the right side of [3.7] gives the slope and the second term the intersection with the y-axis. The slope yields g_0 , which is known from theory³⁶, so this value gives a good indication of the experimental accuracy. The second term, assuming the theoretical value of $J_0 = 180 \text{ A/cm}^2$ from reference 35 and $\eta_i = 0.8$, gives the optical loss α_{int} . The problem with this measurement is that η_i and α_i cannot be determined independently. If η_i deviates from the assumed value of 0.8, the difference will show in α_i , i.e. a material which is of high optical quality but has a low electrical conversion efficiency will appear to have a high absorption coefficient. Therefore, the values obtained for α_i should be taken as an overall measure of quality rather than a literal description of the optical performance.

3.3.2 Experimental

The materials were patterned into stripes of $40\mu\text{m}$ width and 3mm length. They were dry-etched to $4\mu\text{m}$ depth and cleaved into samples of different lengths between 0.3 and 1mm. On average, 4 lasers per length were measured to give 1 of the 4-5 points on the graphs shown. The lasers were operated pulsed ($\tau = 500\text{ns}$, $T = 50\mu\text{s}$) and the lasing threshold was determined from the current level where a mode spectrum can be distinguished.

The overall resistance through the structure, consisting of two Ohmic contacts, the epilayer and substrate (no thinning was performed) as well as the probes was measured to give an idea of the electrical behaviour.

3. Ring laser material

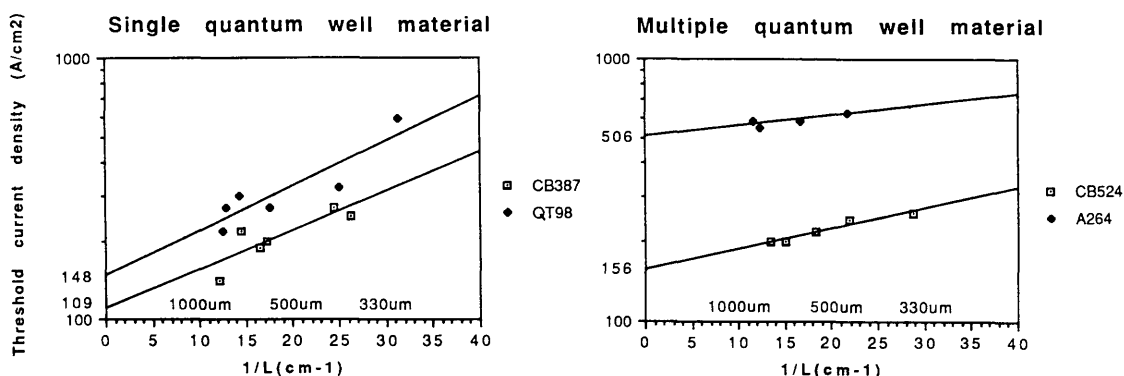


Figure 21. Threshold current density vs. inverse length for different materials to derive the internal loss coefficient.

The slope in the logarithmic plots is seen to depend mostly on the number of wells, since the two SQW structures display almost identical behaviour and the slope progressively decreases for two and four wells. The internal loss, however, is manifested as a vertical displacement of the curves, which is particularly obvious for the two MQW structures. The difference between CB387 and QT98 is caused by the optical confinement factor. It is interesting to note that the curves for CB387 and CB524 intersect at around $200 A/cm^2$, which is in the same order as the theoretical prediction ($250 A/cm^2$, figure 17).

3.3.3 Results and Discussion

In the table below, the values of g_0 , α_i and the threshold current density for a $600\mu m$ long laser $J_{th,600}$ have been derived from the graphs, the optical confinement factor per well Γ_w has been calculated using a finite-difference program (section 3.1.3) and the resistance has been measured directly on approximately $600\mu m$ long lasers.

Material ID	$J_{th,600}$	Γ_w	g_0	α_i	Resistance
CB387	$180 A/cm^2$	3.4%	$950 cm^{-1}$	$8.3 cm^{-1}$	12 Ω
QT98	$270 A/cm^2$	1.3%	$1204 cm^{-1}$	$8.6 cm^{-1}$	12 Ω
CB524	$200 A/cm^2$	3.4%	$1105 cm^{-1}$	$< 10 cm^{-1}$	14 Ω
A 264	$600 A/cm^2$	3.0%	$1450 cm^{-1}$	$70 cm^{-1}$	6 Ω

The following points may be noted:

1. The theoretical value for g_0^{36} of $1200 cm^{-1}$ is quite close to the values that have been obtained by the experiment, so the experimental accuracy is better than $\pm 20\%$, which is acceptable considering the amount of data.
2. The loss of the first three structures is very good, below $10 cm^{-1}$. The third structure, CB524, revealed the inaccuracy of the assumption that $\eta_i = 0.8$; using this value, the internal loss would have been negative in [3.9]. Therefore, the internal quantum efficiency has to be better than $\eta_i = 0.8$ and the internal loss has to be very low. These conclusions show that the design changes implemented in CB524 led to a substantial improvement of the material performance.
3. The double waveguide laser, QT 98, only has a higher threshold current because of the smaller optical confinement factor Γ_w , because its α_i is very close to the internal loss of its single-waveguide counterpart, CB387.

3. Ring laser material

4. The attempt to grow a parabolic graded index separate confinement heterostructure (GRIN SCH) was not very successful as indicated by the rather high loss of 70cm^{-1} . The low resistance is caused by the doping concentration in the active layer of $2 \times 10^{17}/\text{cm}^3$.

4. Fabrication

After the material has been obtained from the growth facility, the following fabrication sequence is employed to produce semiconductor ring laser devices:

1. Sample preparation

The wafer is cleaved into dice of suitable size and cleaned using various solvents.

2. Lithography

Electron-beam lithography is used exclusively for the pattern generation, a technique which is well established in the department. The ring laser pattern is transferred into a metal mask by evaporation and lift-off.

3. Dry etching

Reactive Ion Etching (RIE) with $SiCl_4$ is used to transfer the pattern into the material, thereby creating a mesa.

4. Silicon nitride

The deposition of silicon nitride serves the dual purpose of providing an electrical isolation for the centre of the ring and passivating the mesa sidewall. A contact window is opened by locally dry etching the nitride in C_2F_6 .

5. Polyimide

Polyimide is used to form a bridge between the mesa and the bottom surface. This is required to connect the device to a bonding pad.

6. Ohmic contacts and etch mask

After suitable surface preparation, the final step is the deposition and annealing of the ohmic contacts.

7. Packaging and wire-bonding

The sample is mounted in a ceramic package and wire-bonded.

4. Fabrication

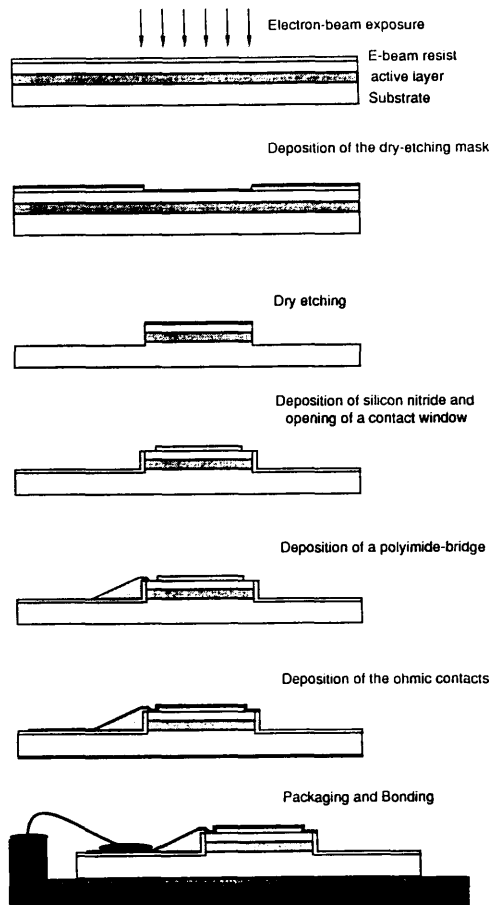


Figure 22. The basic fabrication steps

4.1 Sample preparation

An array of lasers is envisaged as the final result. This arrangement has been chosen because comparative measurements are much easier to perform than on individual devices. Therefore, the wafer is cleaved into dice of typically $4 \times 5 \text{ mm}^2$, 4mm being the maximum width that can be cleaved with the required accuracy of $\pm 50 \mu\text{m}$, considering the substrate thickness of $500 \mu\text{m}$. To achieve this accuracy, it is essential to cleave the wafer exactly along the crystal direction by only scribing a little mark at one end of it; scribing a full line across the wafer would result in cleavage along that line, even if misaligned to the crystal axis.

The dice are then prepared for lithography by cleaning in subsequent ultrasonic baths of trichlorethylene, methanol, acetone, isopropyl alcohol (IPA) and a final rinse of deionized (DI) water.

4.2 Lithography

Electron-beam lithography has been chosen because it has several advantages over optical lithography:

1. Flexibility

Creating a pattern takes only a few hours; so does the actual exposure. This compares favourably with the time required to fabricate an optical mask which is in the order of a week

or two. The flexibility in changing patterns is especially advantageous in the quest for the optimum geometry of ring lasers.

2. Resolution

The geometry of the devices can be defined very accurately, which is important for device properties such as coupling between the ring and the waveguide or the exact size of features.

3. Alignment accuracy

Since multi-layer lithography is necessary, the overlay accuracy becomes an important issue. An accuracy of 200-300nm can be obtained with the electron-beam system, but not using optical methods.

The drawback of the high resolution is that pixelation occurs: Due to the limited number of pixels that can be scanned, the stepwidth of the pattern generator can be larger than the resolution of the resist. Perfectly smooth curved structures are thus hard to obtain. It is very important to have smooth curvatures, because they are a necessary prerequisite for smooth sidewalls that result in low scattering loss of the ring resonator.

Comparing the results obtained by electron-beam lithography to those of other workers in the department that use optical lithography revealed that smooth curvatures are a problem, whatever technique is used. Optical lithography does not necessarily give better results without a similar effort.

For the same reason of limited pixel number, the field size that can be scanned is limited to the size of one or two devices. Larger fields, desirable for further integration, are possible but require an additional alignment effort which would not be necessary using optical masks.

4.2.1 Pattern Generation

The electron-beam machine (a modified Philips SEM 500 scanning electron microscope) scans rectangles in order to build up the pattern within a frame of 4096x4096 pixels. The software package that usually provides the coordinates does not include the possibility of designing circles with the necessary resolution.

Therefore, a specific program was developed. It generates 1 pixel (42nm @ 640x) wide rectangles, 1200 of which are required to create a 100 μ m diameter ring. Using that many rectangles reduces the influence of the step-like exposure significantly.

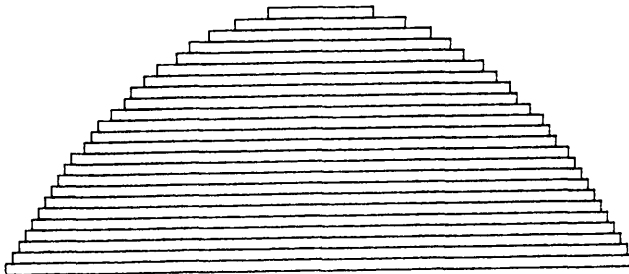


Figure 23. A segment of a circle approximated by rectangles. The circle is distorted due to the different pixel size in x and y.

4.2.2 Electron-beam exposure

In order to understand the influence of the parameters involved and to optimize them for the purpose of ring laser fabrication, a detailed study of the exposure process was carried out. Several parameters need to be balanced against each other to achieve the best results.

1. Magnification.

The magnification determines both the stepsize of the pattern generator (also referred to as "pixel size") and the size of the frame to be exposed, since the frame is limited to 4096x4096 pixels. The following table gives the magnifications most commonly used:

Magnification	Frame size x	Frame size y	Pixel size x	Pixel size y
640x	212 μ m	167 μ m	52nm	42nm
320x	436 μ m	332 μ m	106nm	81nm
160x	846 μ m	658 μ m	207nm	161nm

This table applies to the later part of the project after the scan coils had been slightly modified. In the earlier part, the sizes were smaller and so were the devices, e.g. a circle composed of 1200 pixels at 640x had a diameter of 84 μ m; after the change, the size of the same pattern was 100 μ m. The magnification also determines the alignment accuracy. The bigger the magnification, the smaller the pixel size and thus the absolute alignment error.

The magnification in x and y can be adjusted individually by adjusting the scan coil current, which is particularly important for alignment since fluctuations occur from day to day. The adjustment also facilitates the production of structures of any given size, such as gratings of a specific pitch. The available range covers nearly a full step in magnification.

2. Spotsize.

The spotsize is the physical size of the spot that is scanned across the sample and is independent from the stepsize of the pattern generator discussed above. However, both of them determine the resolution, whichever is bigger. The influence of the spotsize is shown in the following micrographs, where two rings have been exposed and etched under otherwise identical conditions.

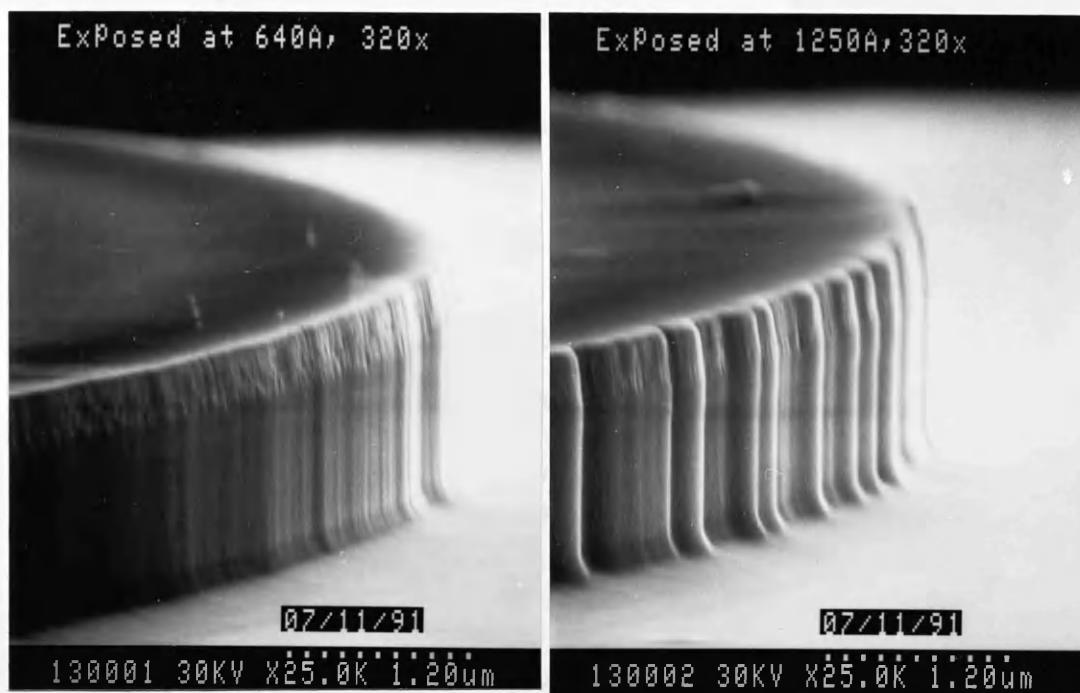


Figure 24. Two structures exposed with a 64nm and a 125nm spot, respectively, at a pixel size of 81nm.

The structure on the left shows nearly smooth sidewalls, with a residual roughness in the order of 10nm, i.e. $< \lambda/20^{44}$ and too small to have an effect on the scattering loss. The second micrograph clearly shows the effect of pixelation, the spotsize being bigger than the resolution limit of the resist.

The spotsize also determines the electron flux onto the sample; the bigger the spotsize, the more electrons are available and the shorter is the exposure time. In the interest of reasonable machine time, the spot size is therefore always chosen as big as possible, especially for structures where resolution is not an issue.

However, the exposure time cannot be indefinitely reduced. It is limited by the maximum speed of the scan generator, which is $2\mu\text{s}/\text{pixel}$. For high quality exposures, the scantime should be longer than $10\mu\text{s}$, because the beam blanking is not fast enough and generates exposure tails and distortions.

3. Acceleration voltage.

The Phillips SEM 500 is usually operated at 50kV for highest resolution and all parameters discussed so far apply to this voltage. Since in the particular case of ring lasers, high resolution is not desired, exposures were also performed using 25kV acceleration voltage. This had the effect of reduced pixelation and emission current. To counteract the reduced emission current and to avoid extensive exposure times, the spotsize was increased. This in turn increases the pixelation, so the same result as before was obtained, i.e. an exposure at 25kV and 125nm spotsize yields the same result as an exposure at 50kV and 64nm spotsize. Besides, since the electron penetration through the sample at 25kV is significantly reduced, there is the increased danger of charge accumulation in the sample. This leads to repulsion of the incident electrons

⁴⁴ Considering $\lambda = 850\text{nm}$, $n = 4$

which causes severe distortions of the pattern. Therefore, 50kV is exclusively used for the pattern generation.

Hence, the parameters to achieve the best results are:

Magnification	640x
Pixel size	42nm
Spotsize	64nm
Acceleration voltage	50kV
Exposure dose	500 μ C/cm ²

The beam current using these parameters is about 700pA and the scantime 16 μ s/pixel; the exposure time for a 100 μ m diameter circle is in the order of 1min. Equally good results are possible at 320x magnification (81nm pixel size) with all other parameters identical, enabling the creation of a small circuit in a single frame, with the penalty of reduced alignment accuracy.

4.2.3 Electron-beam resist

The two key properties of the resist after exposure and development are the profile and the resolution.

1. The resist profile is important for lift-off. An undercut is necessary, so the evaporated metal layer on top of the resist and the one on top of the substrate are not connected and the resist can be easily dissolved, allowing perfect pattern transfer. If the resist profile is overcut, the metal forms a continuous film which lifts off as a whole or not at all.
2. The resolution of the process determines the influence of the step-by-step exposure. If the stepsize is greater than the resolution, the exposure steps show up for features other than straight lines, such as rings. After the subsequent etching, these steps cause wall roughness, which leads to more scattering loss of the ring resonator. The resolution also determines how well other features can be defined, such as Y-junctions. Therefore, the optimum resolution should be in the order of 100nm, to avoid pixelation and yet define the pattern well.

The exposure mechanism is a combination of directly impinging electrons and backscattered ones, the former being highly resolved and the latter being scattered 2-3 μ m around the point of incidence⁴⁵. The ratio between the two is determined by the exposure dose. At low exposures, the amount of backscattered electrons is too small to have a noticeable impact, whereas their influence is more and more obvious at higher doses, an effect which is depicted in the following figure.

⁴⁵ This applies to exposure with a 50kV beam on GaAs substrate.

4. Fabrication

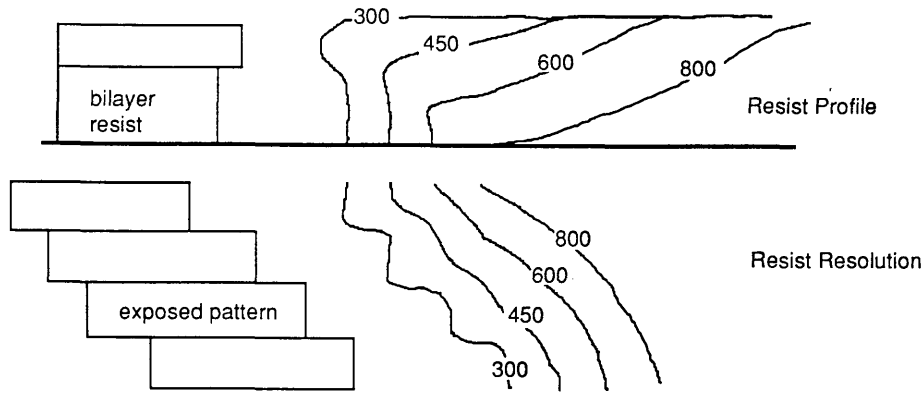


Figure 25. Influence of the exposure dose on the resist profile and resolution.

The top half of the sketch shows the resist profile after development, the ideal profile on the left and the real profile as a function of the exposure dose on the right. The lower half presents the pattern, again, ideal on the left and real on the right. The aim of the exposure is an undercut profile for reliable lift-off and a smooth curvature for a low-loss resonator.

1. For low exposure doses ($300\text{-}400 \mu\text{C}/\text{cm}^2$), the exposure is determined by the directly impinging electrons, resulting in high resolution and a very advantageous profile for lift-off. Such a profile is either achieved by using a bilayer resist, the upper layer being less sensitive than the lower one, or by using thick resist where the electrons suffer from scattering within the layer itself, thereby creating a small undercut.
2. As the exposure dose is increased ($500\text{-}600 \mu\text{C}/\text{cm}^2$), the influence of the backscattered electrons becomes increasingly obvious, decreasing the resolution (due to their large scattering radius) and the undercut; lift-off becomes more difficult. A higher exposure dose also increases the width of the exposed structure by about $1\mu\text{m}$ on either side, so a $3\mu\text{m}$ line is $5\mu\text{m}$ wide at $600\mu\text{C}/\text{cm}^2$.
3. At high exposure doses ($> 700 \mu\text{C}/\text{cm}^2$), the influence of the backscattered electrons dominates the exposure and the profile becomes completely overcut. Reliable lift-off is very difficult if not impossible.

Operating in the range of $500\text{-}600 \mu\text{C}/\text{cm}^2$ is the best compromise for ring lasers, because the resolution is bad enough to create smooth circular features and the resist profile still allows successful lift-off, especially when using thick resist. A bilayer resist is used, consisting of 18% BDH and 10% BDH dissolved in chlorobenzene. The resulting thickness is $2.5\mu\text{m}$, which is sufficient to allow pattern definition across the several microns high mesa. Spinning the resist any thicker would result in cracks after the development.

Baking the film for at least 2 hours is necessary to ensure its adhesion to the substrate, otherwise, it might peel off in an aqueous solution. A solution of 1:1 4-methylpentan 2-1 : IPA is used at 23°C for 30s to develop the resist. The following figure shows a ring laser pattern after e-beam exposure and development.

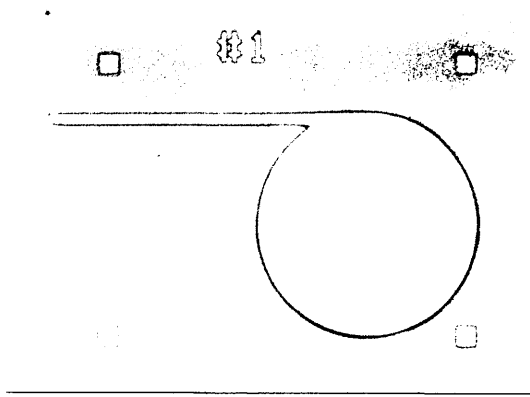


Figure 26. Ring laser pattern after exposure and development.

4.2.4 Alternative approaches

In order to find out if the process used was the best for the purpose, several different ways of creating or improving the pattern were examined.

1. Photoresist was tried as an alternative to electron-beam resist, because its resolution is expected to be poorer, which should result in smoother circular features. It is also known to be e-beam sensitive. However, the resulting curvature was very rough which showed that photoresist does not improve the smoothness.
2. Another idea was firstly to evaporate the metalization and then use polyimide as a negative resist. The metal was wet etched and the polyimide removed by oxygen ashing to get to the same stage as after lift-off. The advantage is that polyimide has a poor resolution ($\approx 1\mu\text{m}$), which makes it very suitable for producing smooth circular features. However, wet etching the metal was found to leave a rather granular edge, which is rougher than that due to pixelation in the e-beam resist. Therefore, this technique did not improve the process either.
3. A different approach was to post-process the e-beam resist after development. Postbaking the resist was investigated at different times and temperatures, but no conditions for a reliable process were found. Either there was no effect at all or the resist profile melted away, destroying the undercut.
4. Ashing the resist in an oxygen plasma after development proved to be very succesful at high plasma pressures (60-70mTorr), where the etching is isotropic, so it preferentially erodes exposed features such as edges. This smoothes out the pixelated resist pattern and produces ideal conditions for getting perfectly circular features without destroying the undercut too much. This method was initially used to produce smooth features, but controlling the exposure dose proved to be a more reliable way of getting equally good results.
5. Another procedure was to wet etch the device after dry etching, hoping that the wet etch would smooth the surface. Various etching solutions based on ammonia, hydrochloric or sulphuric acid were applied, none of which had the expected effect. They either increased the existing irregularities, discriminated between GaAs and AlGaAs, or etched preferentially in certain crystal directions, all of which are unacceptable for the circular structure. This experience also confirmed that dry etching is the best technique to create the ring laser mesa.

4.2.5 Alignment marks

The alignment marks for subsequent lithography levels (the squares in each corner in figure 26) are written at the same stage as the pattern, because the mesas that they form after dry-etching produce a sufficient contrast for the automatic alignment system. The alignment system finds a mark by scanning a line across it, recognizing the intensity distribution (bright across the mark, darker for the background) and moving the stage until the mark appears in the defined position. In a second, fine-alignment stage, the pattern is moved by software manipulation, because the accuracy of the stage movement is limited to one micron. This ensures alignment accuracy in the order of a few pixels, i.e. 100's of nm.

4.2.6 Dry etching mask

An alloy consisting of 90% nickel and 10% chromium (Ni-Cr) is evaporated onto the sample as a mask for the subsequent dry etching. Degassing the evaporation boat before use and evaporating at low pressure ($p < 6 \times 10^{-6} \text{ mbar}$) is beneficial to good adhesion. The evaporation rate should be 1-2nm/sec; lower rates cause overheating of the sample, especially when a thick layer is deposited, higher rates give non-uniform films. The selectivity of the dry etching process is better than 50:1, i.e. 20nm of NiCr are required for every $1 \mu\text{m}$ of GaAs etched. For simplicity, a gold film, such as the top layer of the ohmic contact, can be used as an etch mask. A 30-50nm thick layer erodes during a $3 \mu\text{m}$ deep etch, so the etch rate of gold is comparable to that of NiCr.

After evaporation, the metal is lifted off in warm acetone, followed by a rinse in IPA and DI Water. This final rinse is required because acetone leaves a residue that can cause micromasking ("grass") in the subsequent dry etching.

4.3 Etching

Etching defines the ring laser structure. It has to penetrate the active layer in order to provide the high dielectric contrast (GaAs-air) that is required to provide sufficient optical confinement for guiding around the tight bend. The two important properties of an etchant are its selectivity and isotropy. An etchant is selective if it discriminates between materials of different composition, such as GaAs and AlGaAs. Isotropy describes an etchant in terms of directional progression, i.e. the ratio between etching in all 3 spatial directions. Control of this property is particularly important, because it determines the verticality of the walls and the uniformity of etching in both lateral directions, i.e. if a circle is evenly etched or distorted. An etchant is called anisotropic if it only progresses in one direction.

Prior to an explanation of the various etching techniques employed, the requirements on the etch depth are discussed.

4.3.1 Required etch depth

The model developed in chapter 2 predicts that sufficient optical confinement is achieved for a $50 \mu\text{m}$ radius device if the structure has just been etched through the active layer, i.e. if the active layer and the top cladding are exposed and the bottom cladding is buried. However, since the model is a rather simplified one, it is questionable if this result applies in practice. Ring lasers were fabricated with various etch depths, ranging from just below the active layer (depth = $0 \mu\text{m}$) to $1.4 \mu\text{m}$ below it.

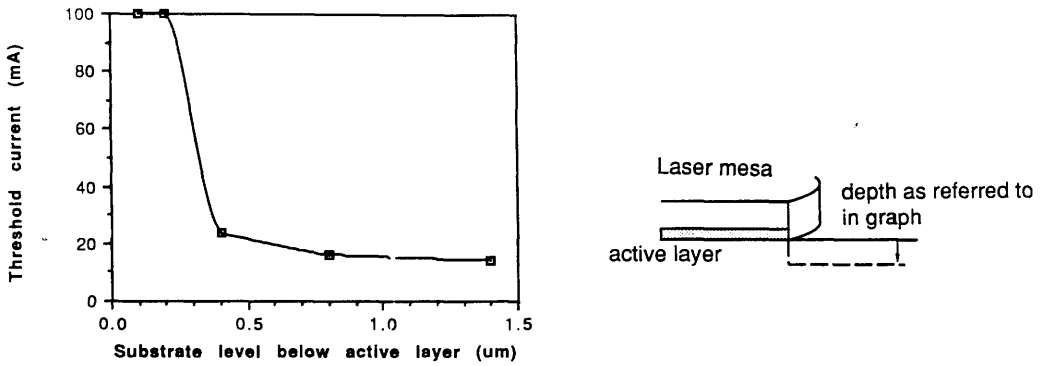
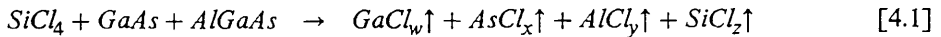


Figure 27. Threshold current vs. etch depth below the active layer and illustration of the experiment.

The result was a surprisingly sharp transition between devices that did not work at all (depth < 0.3 μm) and those that worked very well (depth > 0.4 μm). The field distribution offers an explanation, because a significant tail of the optical mode extends into the lower cladding. Due to the small radius (50 μm), the fraction of the mode that is not contained within the etched structure will readily leak into the substrate. Beyond 0.4 μm , the mode tail has dropped to a small fraction and the loss has become insignificant. However, the steepness of the transition between a confining and a leaky structure can not be fully explained.

4.3.2 Dry Etching

In order to achieve smooth, vertical sidewalls of optical quality, dry etching is preferable over wet etching. The dry etching technique employed is reactive ion etching (RIE) with silicon tetrachloride (SiCl_4). This process is very anisotropic and non-selective, i.e. it produces vertical sidewalls without discriminating between GaAs and AlGaAs. SiCl_4 forms volatile reaction products with both GaAs and AlGaAs.



The etch rate is in the range of 0.13-0.2 $\mu\text{m}/\text{min}$ and depends on 3 basic parameters: pressure, gas flow and power, the latter being usually held constant at 100W. The gas flow and the etch pressure are interrelated because the pump rate of the vacuum system is constant. Figure 28a) shows the etch depth vs. time for a 3x3mm² sample and 28b) the etch rate vs. gas flow and pressure for a 20x20mm² sample. The first diagram demonstrates the reproducibility that can be achieved since the points are all on or very close to the straight line. This enables etching as good as $\pm 100\text{nm}$ in 2.5 μm , as required for some structures. It also shows that the induction time (the time before etching starts) is reasonably short, in the order of 0.5min.

The second graph reveals a few facts about the etching process: At low pressure and flow, the plasma density is low, so the reaction is limited by the number of species that reach the sample. An increase in flow at that point results in an increase in etch rate, because more reactant is supplied. This continues until the reaction reaches a saturation point at a pressure/flow combination of 10mTorr/9sccm. If the flow is increased further, the etch rate does not increase any more, indicating that the reaction time limits the process rather than the amount of available reactant.

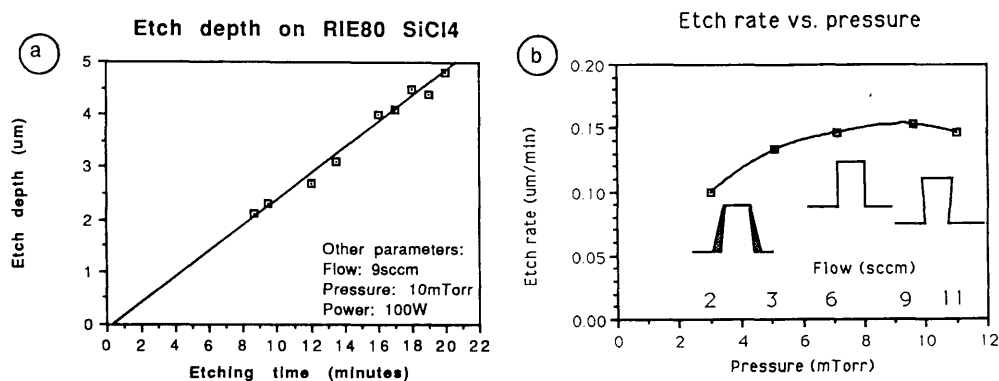


Figure 28. The dependence of the etching on time and flow/pressure.

Apart from determining the etch rate, the pressure also has an influence on the profile of the structure:

1. At very low pressures ($p < 5\text{mTorr}$), the gas flow is so low that it is very hard to control reliably, which increases the error margin of the results significantly. The profile is vertical or even undercut, because debris deposited on the sidewall can act as a mask for further etching. An unknown deposit is sometimes formed, which appears dark in the optical and transparent in the electron microscope (just like an organic material), but can be removed with dilute HCl.
2. At low pressures ($p = 5\text{-}8\text{mTorr}$), the profile is vertical, and the results are reproducible.
3. At pressures above 8mTorr , the profile becomes undercut, because the ions undergo more collisions with each other, thereby gaining a momentum perpendicular to the electric field. An undercut profile, i.e. a slanted sidewall, is unwanted for laser devices because vertical mirrors are essential to ensure complete backreflection into the waveguide.

Therefore, the etching pressure is usually regulated to 8mTorr . Dependence of the etch rate on the composition of the material or the doping concentration has not been observed.

A parameter which is often neglected is the loading factor, i.e. the dependence of the etch rate on the surface area of material to be etched. Comparing the two graphs above reveals its importance: figure 28a) has been obtained for $3\text{x}3\text{mm}^2$ samples, the resulting etch rate being $0.21\mu\text{m}/\text{min}$. The same conditions for $20\text{x}20\text{mm}^2$ samples in figure 28b) yield $0.14\mu\text{m}/\text{min}$. These different etch rates can be avoided by putting the samples onto a bigger plate of GaAs, which keeps the surface area constant and guarantees a consistent, although lower, etch rate. Apart from these controllable parameters, the rate also depends on the age and the state of the etching table, so 1 or 2 dummy runs are always advisable when accurate etching is required.

4.3.3 Wet etching

Wet etching is not used in the standard ring laser process. However, several wet etches have been investigated because they offer advantages over dry processes in certain cases.

1. A hydrofluoric acid (HF) based solution is selective and isotropic. Depending on the concentration, it discriminates between AlGaAs layers of different composition. A 1:10 HF:H₂O solution removes a layer of $\text{Al}_{0.7}\text{Ga}_{0.3}\text{As}$, but leaves $\text{Al}_{0.3}\text{Ga}_{0.7}\text{As}$. A 1:4 solution has been used to discriminate between $\text{Al}_{0.5}\text{Ga}_{0.5}\text{As}$ and $\text{Al}_{0.2}\text{Ga}_{0.8}\text{As}$. The removal of an AlGaAs layer can be well controlled, because layers of high Al-content readily form oxides, which is identified by the formation of interference fringes. Once the fringes have disappeared, a layer of low Al-

4.Fabrication

content has been reached. An HF-based wet etch applied after $SiCl_4$ dry etching is slightly inhibited by the dry etch residuals, so a higher concentration is required.

HF etches are used to fabricate strip-loaded ring lasers (section 6.4) or to remove the laser cladding from the FET-layers as required for the OEIC (section 7.2.3).

2. A sulphuric acid based etch, $H_2SO_4:H_2O_2:H_2O$ 4:1:100 is non-selective and isotropic with an etch rate of $100\mu\text{m}/\text{min}$ at room temperature. It has been used to remove the top surface of the contact layer where damage was suspected (section 4.6.1), and to remove the dry etch residuals from the mesa wall to see if they had any influence on the laser performance.

Another application is its use as an isolation etch in the OEIC process. The dry-etch residuals, as mentioned earlier, inhibit etching, so a higher concentration, such as 4:1:20, is required to penetrate the damaged surface layer. In order to control the reaction, the solution is cooled to 5°C , which results in an etch rate of $150\text{-}200\text{nm}/\text{min}$. Also, the degree of undercut for the highly concentrated solution is reduced from 10:1 (lateral to vertical etching) at room temperature to 2:1 at 5°C .

3. A hydrochloric acid based solution, $HCl:H_2O_2:H_2O$, 1:1:20, is a selective etch for AlGaAs which preferentially etches normal to the $\langle 110 \rangle$ crystal direction, i.e. it has a much higher etch rate laterally than vertically. This discrimination is very useful in evaluating the dry etch depth in respect to the layer structure, because the layers are easily identified without the etch depth being distorted. The lateral etch rate is $50\text{-}100\text{nm}$ in 20s.

4.4 Deposition of silicon nitride

A 2000\AA thick film of silicon nitride is deposited by Plasma Enhanced Chemical Vapour Deposition (PECVD), which is a low-temperature process thus minimizing the thermally imposed stress. The film serves the dual purpose of passivating the sidewalls and providing the insulation pad for the centre of the pillbox. The deposition is performed with an ammonia flow rate of 8sccm and a silane flow rate of 2sccm at a pressure of 250mTorr , using an Rf-power of 5W . The deposition is isotropic, yielding a comparable film thickness on the surface and the sidewalls of the etched mesa. The chemistry of the deposition process is difficult to describe because of the many species that are present in the plasma. The following formula is therefore to be taken as a rough approximation:⁴⁶



The formula shows that hydrogen is released during the process. Hydrogen is known⁴⁷ to deactivate both shallow acceptor and donor impurities to a thickness of a few 100nm , and to passivate the electrical activity of dangling or defective bonds. The resistance of the surface thus increases significantly, which reduces the non-radiative recombination current. The deposition temperature of 300°C is very suitable for the incorporation of hydrogen into the crystal and is close to the value of 250°C that is commonly used for the hydrogenation of GaAs. The experimental confirmation of the passivation effect is shown in the following table:

⁴⁶ S.M.Sze, "VLSI Technology", 2nd ed., p.263, McGraw-Hill, 1988.

⁴⁷ S.J.Pearnton, J.W.Corbett, and T.S.Shi, "Hydrogen in crystalline semiconductors", Applied Physics A, Vol.43, pp.153-195, 1987.

Coating	Pre-Clean	Threshold current
None	None	26mA
SiO_2	N_2	27mA
$SiNH$	N_2	22mA
$SiNH$	NH_3	19mA

These results were obtained with $5\mu\text{m}$ wide stripe lasers that had been etched through the active layer. The monitor (uncoated) and the SiO_2 coated device had similar threshold currents of 26mA and 27mA. The nitride coated samples had lower threshold currents of 22mA and 19mA, the effect being reinforced by an ammonia pre-clean, which again indicates the influence of hydrogen.

Another effect of the nitride coating is that the additional dielectric interface reduces the scattering loss, which is proportional to the refractive index steps at the interfaces ⁴⁸, $\alpha \propto \sum \Delta n^2$. The combined effect of passivation and improved index matching is manifested in an improvement of the threshold current from 24mA and 15mA for uncoated and coated ring laser devices.

To provide the pumping current to the outer annulus of the ring, a window is opened on the top of the mesa by another dry etching step with C_2F_6 using a NiCr mask.

4.5 Polyimide bridges

The devices are usually contacted by microprobing the centre of the pillbox. This technique is fast and reliable, but it limits the smallest possible device size to a minimum of $50\text{-}60\mu\text{m}$ diameter. Additionally, the physical impact of a probing needle scratching across the top of a laser can have a rather destructive effect. Wire bonding cannot be performed on top of the mesa due to the detrimental mechanical stress. Therefore, a separate bonding pad is required if the devices are to be used more than once. The problem of contacting across a $2\mu\text{m}$ high vertical mesa can be solved by various techniques using polyimide as illustrated in the following figure. One possible approach⁴⁹ is to cover the dry-etched structure with a layer of polyimide. Using the spin-on technique, a thinner film forms on top of the mesa than on the bottom, which is removed by subsequent oxygen-ashing thereby exposing the top of the mesa (fig.29a).

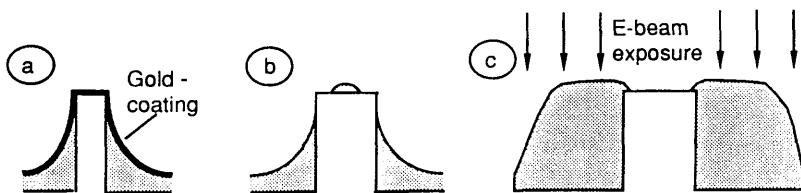


Figure 29. Using polyimide for contacting purposes.

Gold is then evaporated at various angles to produce a continuous film across the whole structure. This technique is well suited for devices that are to be separated by cleaving, but not if multiple devices are to be contacted individually on the same chip. Also, the technique only works on very narrow ribs; in the case of bigger structures, the effect illustrated in fig.29b) occurs: After ashing the

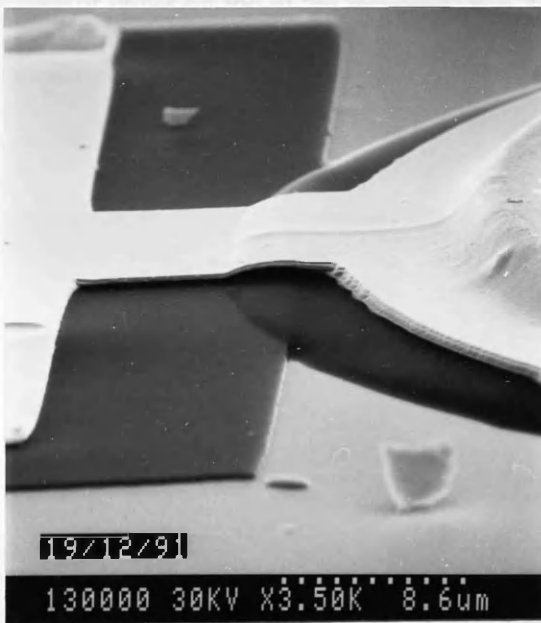
⁴⁸ M.S.Stern, P.C.Kendal, R.C.Hewson-Browne, P.N.Robson, and D.A.Quinney, "Scattering loss from rough sidewalls in semiconductor rib waveguides", Electronics Letters, Vol.25, pp.1231-1232, 1989.

⁴⁹ A.F.Jeziarski and P.J.R.Laybourn, "Polyimide embedded semiconductor ring lasers", Proceedings SPIE Vol.1141, pp.9-13, 1989.

4.Fabrication

sample for a certain period of time, the polyimide on the sidewalls has already receded from the corner; at the same time, the top surface has not completely cleared and polymer leftovers remain. This configuration makes it difficult to produce a continuous and uniform contact.

Fig.29c) shows an alternative which utilizes the sensitivity of polyimide to electron beams. A thick layer is spun onto the sample and e-beam exposed outside the structure. After development, the polyimide remains where exposed and, due to scattering, it extends 1-2 μ m into the non-exposed area. This technique is more elaborate, but it gives better results and is more controllable. Polyimide has been chosen for this application because it forms good and stable films. It also acts as a negative resist for electron-beam exposure⁵⁰ which facilitates the fabrication. Exposure at 1500-2000 μ C/cm² and development in acetophenone at 35°C for 5-8min yields strongly overcut sidewalls and bridges that are suitable for contacting across. The film thickness can be varied between 0.6 μ m and 5 μ m, depending on the concentration of the spin-on solution used and the height of the mesa that is contacted.



CROSS-SECTION OF THE BONDING ARRANGEMENT

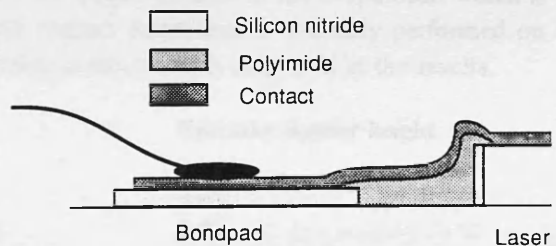


Figure 30. Sketch and micrograph of a finished device with a polyimide bridge to contact across the mesa step.

The problem with a technique involving polyimide is that it cannot be used as an insulator for a wire-bonding contact, because, due to its softness, it absorbs the ultrasonic pulse which is used to weld the wire to the contact. Therefore, it can only be only used to form a bridge between the top of the mesa and the substrate. The bonding pad itself must be isolated by silicon nitride.

After the electron-beam exposure and development, the polyimide-film is fully cured at 350° for 1 hour, otherwise, it is liable to cracking during the subsequent contact deposition and annealing. After annealing, it is exposed to an oxygen plasma in order to break the surface bonds and to improve the adhesion of the subsequent metalization. This combined curing and ashing process has shown to be very reliable and gives reproducible results.

⁵⁰ W.Patrick, W.S.Mackie, S.P.Beaumont, and C.D.W.Wilkinson, "Polyimide as a negative electron resist and its application in crossovers and metal on Polymer mask fabrication", Journal of Vacuum Science and Technology B, Vol.4, pp.390-393, 1986.

4.6 Contact metallization

If a metal is in close contact with a semiconductor, a barrier is formed at the interface. This effect can be understood most easily taking the p-type contact as an example, where the metal-semiconductor interface is taken as the junction of a p-n diode with the metal representing the n-type material. In such a configuration, the barrier width depends inversely on the doping concentration. To decrease the barrier width and allow the carriers to tunnel through the barrier, it is necessary to increase the doping locally. This is done by depositing and annealing an acceptor metal, which thus diffuses into the semiconductor. The barrier width also depends on the state of the surface, so careful cleaning is essential before depositing the contacts.

4.6.1 Cleaning before contact deposition

During the processing steps, especially the ones that involve heat, an oxide layer that acts as an insulator grows on top of the semiconductor. To remove this layer and prepare the surface for the contact, various processes can be employed. A comparison has been made to assess these different procedures by depositing $100\mu\text{m} \times 100\mu\text{m}$ Schottky contacts (Ti-Au) onto p^+ material. The samples were either cleaned with ammonia ($\text{NH}_4\text{OH}:\text{H}_2\text{O}$, 1:2, 60s), hydrochloric acid ($\text{HCl}:\text{H}_2\text{O}$, 1:2, 60s), or not at all. Most samples were sputter cleaned in the evaporator, which is a standard procedure. Since annealing improves the contact formation, it was only performed on one sample, so the influence of the surface preparation is more clearly displayed in the results.

Number	Treatment	Schottky barrier height
1	No treatment, sputter clean	3.2V
2	Ammonia etch, sputter clean	2.4V
3	Ammonia etch, no sputter clean	1.1V
4	Ammonia etch, sputter clean and anneal	0.1V
5	Hydrochloric acid etch, sputter clean	3.0V

1. The comparison of all etched samples with #1 shows that some treatment is definitely required.
2. The sputter clean, which is performed to improve the adhesion of the metallization, is detrimental to the formation of a good contact, as indicated by samples no.2 and no.3.
3. Ammonia etch leaves a better surface than hydrochloric acid etch (no.2 and no.5). This is in agreement with other investigations⁵¹, who found that etching the oxide with ammonia etch leaves a more stoichiometric surface than when hydrochloric acid etch is used. Therefore, the surface is less reactive, and it grows less oxide when exposed to air.
4. The major factor in producing good ohmic contacts is annealing, as illustrated by sample no.4. A sufficiently high temperature, such as 450°C for 30s, causes the contact metal to diffuse through the barrier and to create an ohmic contact.

As a result of this investigation, treatment no.3 with annealing was chosen.

A problem that occurs when the contacts are scaled down ($2\text{-}3\mu\text{m}$ wide) is non-uniform conduction. Some parts of the device conduct better than others, which leads to an increased threshold

⁵¹ C.C.Chang, P.H.Citrin, and B.Schwartz, "Chemical preparation of GaAs surfaces and their characterization by Auger electron and x-ray photoemission spectroscopies", Journal of Vacuum Science and Technology, Vol.14, pp.943-952, 1977.

current and non-uniformity of the red glow (section 5.1). Devices can be so badly affected that the contacts melt locally under current injection.

The non-uniform conduction is not caused by damage of the surface layer due to prior processing, because removing a thin (50 -100nm) layer by wet etching ($H_2SO_4:H_2O_2:H_2O$, 4:1:100, 30s) does not solve the problem. However, exposing the samples to an oxygen plasma for 1min after the deoxidation etch and immediately placing them in the evaporator results in uniform contacts and a more consistent device performance. This is believed to be related to the removal of remaining water vapour which inhibits the adhesion of the metalization and the formation of a good contact.

4.6.2 Ohmic contacts, p-type

The standard p-type contact for GaAs is a layer of zinc sandwiched between two layers of gold (Au, 300Å, Zn, 300Å, Au, 300Å). However, contacts fabricated using this recipe repeatedly showed adhesion problems.

Therefore, a contact composed of nickel and gold is generally used. Nickel was found suitable as a p-type dopant in GaAs and is known as an adhesion promotor for gold. Besides, the p-doping concentration in the contact layer of the laser structure is very high ($5 \times 10^{18}/cm^3$), which makes it relatively easy to achieve good contacts. The adhesion of the Ni-Au contact is superior to the adhesion of the Au-Zn-Au contact and the resistance is comparable for both recipes.

4.6.3 Schottky contact, p-side

As shown in the table above, Ti-Au forms a Schottky (diode) contact, unless it is annealed at an elevated temperature, such as 450°C for 30s. This requirement can be used advantageously to simplify the fabrication process, because the dopant does not diffuse in excess during the polyimide curing (350°, 1h), so the ohmic contact can also be used as an etch mask. Other contacts, such as Au-Zn-Au or Ni-Au, would desintegrate during such an extended heat treatment.

4.6.4 Ohmic contacts, n-type

A typical composition is Ni, 50Å, Au, 600Å, Ge, 400Å, Ni, 200Å, and Au, 1000Å, germanium being the dopant and nickel the diffusion promotor. This contact has been studied intensively⁵² and did not require any further investigation. The lowest resistance is achieved with annealing the contact at 325°C for 30s, but it can stand the increased annealing of Ti-Au contacts (450°C, 30s) without noticeable degradation.

⁵² Nanoelectronics group, Department of Electronics and Electrical Engineering, University of Glasgow

4.7 Bonding and Packaging

4.7.1 Cleaving

The devices are cleaved to gain access to the output waveguide. They are typically divided into dice of $1 \times 4 \text{ mm}^2$ that contain 8-10 devices in a row, which allows for a very high packing density; the devices in such arrays can be placed as close as $150 \mu\text{m}$ to each other, whereas a spacing of $500\text{-}600 \mu\text{m}$ is required for individually cleaved devices.

To enable cleaving, the samples are scribed on the surface, between the first device of the array and the sample edge. The cleaving is performed on a small apparatus, where the samples are attached to a flexible plastic foil and pressed onto a razor blade. This technique is very reliable and hardly any samples get damaged during this procedure. The minimal size that can be cleaved is 0.4 mm for a wafer thickness of 0.5 mm . The samples are not thinned because they are much easier to handle when thicker, although the thermal resistance of the devices (section 6.2.6) would improve with thinning.

4.7.2 Bonding

Microprobing is mostly used to contact the lasers. This is acceptable for research purposes, where most of the devices are only tested once or twice. However, for commercial applications, a way of bonding and packaging the devices had to be devised. Therefore, the lasers are connected to a separate bonding pad, which consists of a metal contact on top of a film of silicon nitride, and mounted in a ceramic package.

1. Bondpad isolation.

Polyimide cannot be used as an isolator underneath a contact for wire-bonding, because it absorbs the ultrasonic pulse that welds the wire to the contact. Therefore, the much harder silicon nitride is used. The adhesion of this bonding sandwich (substrate-nitride-contact) is an important issue, because the bonding wire produces a significant strain. Therefore, it is advisable to use plasma deposition for the silicon nitride film, because the low temperature of the process causes negligible thermal strain, so the films generally adhere very well. However, some samples showed adhesion problems, and the wire stuck well to the contact but lifted off parts of the bondpad, which is a phenomenon that is currently not well understood.

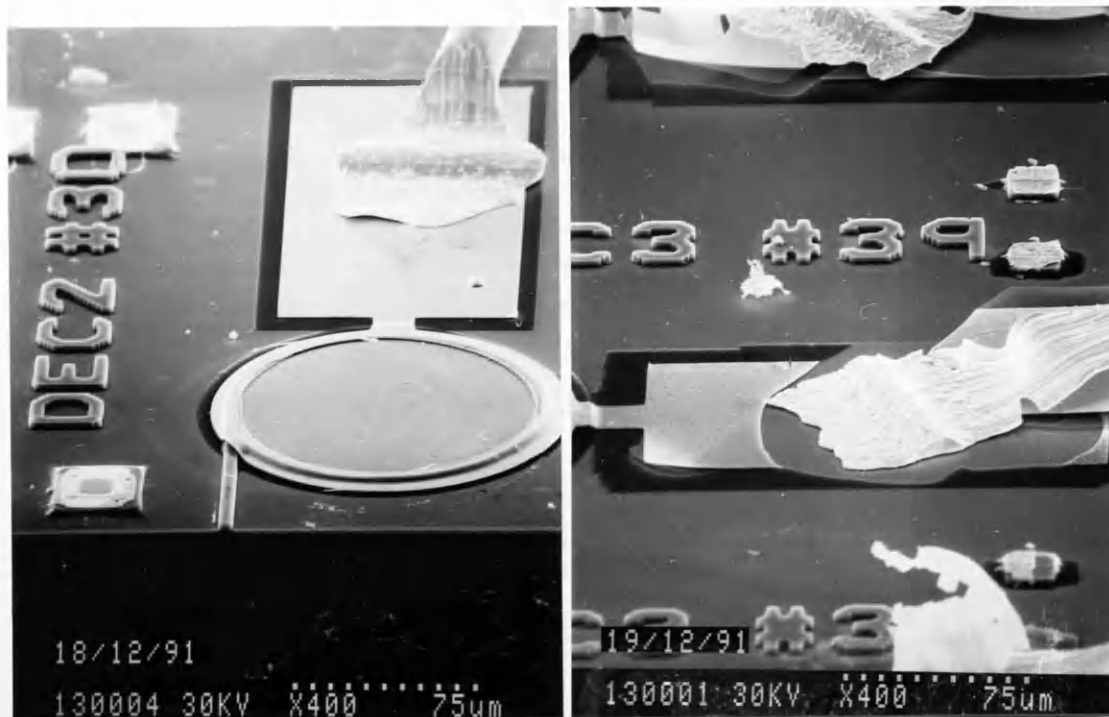


Figure 31. Example of good and bad adhesion of the bonding pad. Both samples had been processed identically.

2. Metallization for bonding.

The composition of the metal contact is critical. It mainly consists of a thick layer of gold with an adhesion promoting layer. Initially, nickel was used as adhesion promoter, but bonding was difficult and nickel seems to interfere with the wire-bonding process. Other groups in the department use NiCr-gold bonding pads which show excellent adhesion and bondability. However, it is desirable to deposit the top ohmic contact and the bonding pad simultaneously, which discards NiCr since it does not form a good ohmic contact.

Titanium does not create this problem and provides comparable adhesion. It can be used both for the p-type contact and the bonding pad, i.e. it is not necessary to introduce another lithography level. The recipe used is titanium (50nm) and gold (400nm), the thick layer of gold ensuring that bonding can be performed reliably. The annealing step that is required for the ohmic contact formation does not interfere with the ability to wire-bond.

3. Wire-bonding.

The actual bonding of the wire to the pad is performed by bringing the two in close contact and applying an ultrasonic pulse to the wedge that holds the wire. Both gold and aluminium wires can be used, the former giving better and more reliable results. Besides, it avoids the problems that occur on the long run with using aluminium, i.e. the formation of 'cold contacts' after thermal cycling, which are caused by the formation of a gold-aluminium alloy that leads to bad conduction and breaking of the wire at the interface. The gold wire used is very thin, in the order of $25\mu\text{m}$ in diameter.

4.7.3 Packaging

A rectangular ceramic package has been chosen to accommodate the devices. The material has a high thermal conductivity ($\sim 200 \text{ W/m K}$, compared to 400 W/m K for copper) and the package is

4.Fabrication

normally used for testing electronic devices at very low temperatures (4°K to 77°K). The samples are placed in a cavity where one side has been cut off to allow access to the output of the lasers. There are 11 connections that can be bonded to on the inside and soldered to a PCB or other circuitry on the outside. The laser array is mounted in the package using conductive epoxy, which does not impose any strain on the device and provides the ground connection for the bottom contact. The limited thermal conductivity of the epoxy is not a major problem for the present design since the heat resistance of the devices and the substrate (section 6.2.6) are responsible for the low heat flow and the high junction temperature. However, using indium solder is preferable once this thermal problem has been solved.

A completed package with an array of bonded lasers is shown in the following.

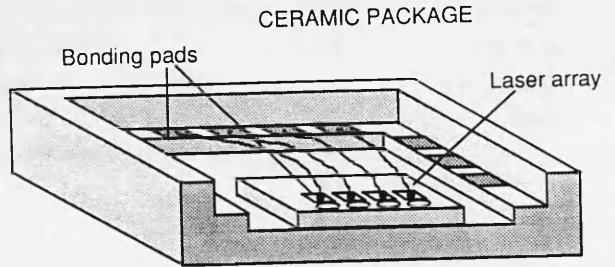


Figure 32. An array of packaged and bonded devices.

The package can be sealed for further protection if desired.

4.8 Performance of an array comprising of 8 ring lasers

A comparison of 8 ring lasers in a row was conducted to investigate the consistency of the fabrication process. Threshold currents were found to vary between 13mA and 21mA, and the output power at $1.5xI_{th}$ was in the range of 0.1mW to 0.2mW. The spectra were multimode consisting of three to six dominant longitudinal modes.

Number	I_{th}	Output($1.5xI_{th}$)	Longitudinal modes
33	15mA	0.16mW	6
34	17mA	0.12mW	4
35	17mA	0.11mW	3
36	15mA	0.08mW	4
37	21mA	0.10mW	4
38	17mA	0.10mW	4
39	13mA	0.16mW	6
40	13mA	0.08mW	3

The consistency of the results is as good as can be expected from the serial multi-lithography fabrication process used. As a comparison, the variation of the threshold current for commercial devices, between 6-9mA⁵³ within the same batch, is in the same order. Considering the low degree of process control that can be exercised in the research environment shows that the consistency achieved is very respectable. The reproducibility of the process is also adequate, since the threshold current of 13mA was obtained for identical devices in three out of five batches.

⁵³ Brian Garret, BNR Europe.

5. Measurements

The measurement setup is described and its accuracy and limitations are discussed. Properties that are used to characterise the devices are the light-current curve, the output spectrum and the threshold current (I_{th}).

1. The light-current curve is one of the most fundamental characteristics of a laser, since it relates input to output. It is most conveniently displayed by using a current ramp for pumping and observing the resulting emission and the driving signal in x-y mode on an oscilloscope. To obtain a printout, the curve can also be displayed on a chart recorder by selecting a very slow (10-20s period) signal.
2. The spectrum contains important information about the characteristics of a laser, such as the threshold current, the mode spacing and the temperature. It is obtained by feeding the collimated beam through a grating monochromator and scanning the grating with a stepper motor. The change in intensity is displayed on the oscilloscope and/or chart recorder.
3. The threshold current is the most important parameter characterising a laser, since it allows an overall assessment of the quality of the device; both the quality of the resonator and the gain of the material are taken into account. The threshold current can be derived from either the spectrum or the L-I curve. Using the L-I curve by detecting the sudden increase in output power when the device turns from luminescence to lasing, is a very convenient method. However, many, particularly poor devices, do not show a sharp turn-on because of a high degree of spontaneous emission, so the interpretation of the curve is very difficult. Spontaneous emission from the output waveguide of the ring laser also blurs the result. Therefore, another, more cumbersome method is preferred, whereby the lasing threshold is determined from the current level where a mode spectrum can be distinguished.

The arrangement shown below is used for the measurements. All optical elements are mounted on a board and fitted with micropositioners wherever necessary.

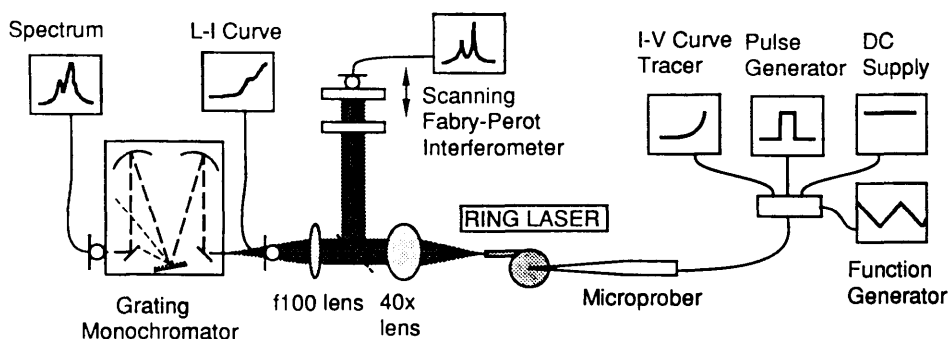


Figure 33. Experimental arrangement for laser testing

5.1 Laser pumping sources

The top contact is microprobed to supply the pumping current. This is the easiest method of contacting and sophisticated and time-consuming techniques of bonding and packaging are not necessary if the devices are only being tested for research purposes. Because the lasers are electrically isolated from each other, it is possible to address each one individually; which has the advantage that comparative measurements can be made without having to change the sample. The slight pressure imposed on the samples by the prober holds them in place.

5. Measurements

Most devices show a red glow under current injection, which is very useful for the evaluation of the device operation and the ohmic contact quality. Bad contacts produce a non-uniform glow which often results in increased threshold currents. The nature of the glow is not entirely understood, but is probably linked to luminescence of the $Al_{0.26}Ga_{0.74}As$ -cladding, the aluminum fraction of 0.26 corresponding to an emission wavelength of $\approx 700\text{nm}$. It was not possible, however, to detect a signal by investigating that wavelength range with the monochromator.

Four pumping sources are employed to drive the laser diodes:

1. The I-V curve tracer is primarily used to obtain the electrical characteristics of the device such as contact barrier height and resistance. Because of its low duty cycle (1:2), the resulting luminescence signal is quite strong, even below threshold, and is sufficient to align the output of the laser to the optical system.

For lasers that can operate cw (I_{th} in the order of 50mA or lower), the curve tracer can also be used for an approximate threshold current measurement since its output signal is a voltage ramp. Spectra obtained by driving the devices with the curve tracer are very similar to ones obtained using DC, which is very useful for rough assessments.

2. A pulse generator that can deliver pulses of up to 50V at 100ns (a rather ancient, but very powerful valve-instrument) is used to pump the devices without subjecting them to a temperature increase. It is required for devices with thresholds above 50mA, and very useful in general to allow measurements without heat-distortion. A resistor of 47Ω is put in series with the diode and the voltage across it yields the pumping current. Pulses used in practice are 200-500ns long with a duty cycle of 1:100. To monitor the electrical properties during operation, the pumping can be toggled between the pulse generator and the I-V curve tracer.
3. A ramp generator is used as described before to obtain the L-I curve. The ramp signal can be fed through a circuit⁵⁴ where the signal is gated by the pulse generator to create a pulsed ramp signal and eliminate heating effects.
4. A constant voltage supply is available for DC measurements. DC facilitates measurements with the Fabry-Perot spectrum analyser and those where 2 sources are required, e.g. for the integrated laser-detector circuit.

In order to illustrate the influence of the pulse length on the laser output, the following measurement was made. It shows the decay of the output power of a typical ring laser with time.

⁵⁴ Designed and built by John Weaver, Department of Electronics and Electrical Engineering, University of Glasgow.

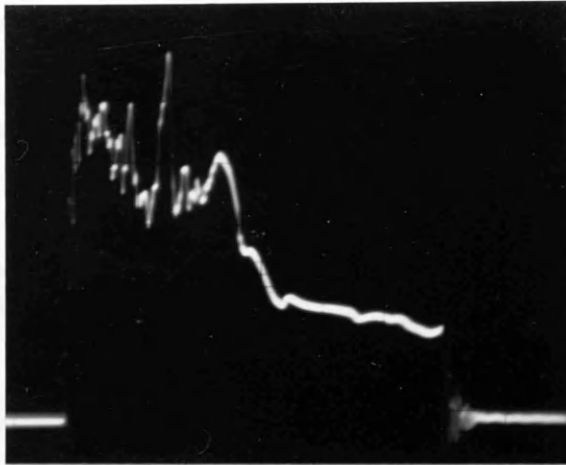


Figure 34. Output power of a ring laser during a $6\mu s$ long pulse. The maximum power is 2mW.

This trace underlines the importance of using short pulses, ($\tau < 1\mu s$), to avoid heating effects. Pulses longer than $3\text{-}4\mu s$ give similar results to DC measurements, because the temperature distribution has reached steady state. The noise at the beginning of the pulse is believed to be due to electrical backreflections.

5.2 Optical system

The lasers are placed on a brass block for testing, which acts both as a heat sink and an electrical contact. Because the samples are large enough, in the order of $1\text{x}4\text{mm}^2$, the surface area is sufficient to form a good electrical contact with the base, which is demonstrated by the low resistance that has been measured for some devices (section 3.3.3). It is thus not necessary to use conductive epoxy, which simplifies the measurement procedure significantly.

1. A small microscope fitted with a 100x lens-eyepiece system is mounted on top of the stage. The field of view is 1.25mm, which allows clear observation of the samples and good control of the positioning of the probing needle. The minimum stripewidth that can be contacted using microprobes is $10\mu m$.
2. The laser emission is collimated by a 40x/0.65 microscope lens. A second lens with a focal length of 100mm is used to match the aperture within the monochromator (given by the diameter of the mirrors and their focal length) to that of the incoming light. Matching the apertures is important for two reasons:
 - a. If the aperture is too big, the diameter of the beam becomes larger than the mirrors and not all of the light is fed through the optical system.
 - b. If the aperture is too small, the resolution of the monochromator is reduced, because it depends inversely on the aperture.

The lens sits on a magnetic mount to allow easy removal for the placement of a detector directly at the output of the laser.

3. The spectral measurements are performed using a grating monochromator. The resolution is in the order of 1\AA and is calculated as follows:

The grating diffracts the incoming radiation according to its wavelength, so different wavelengths travel as beams with different angles. The spherical mirror at the output end of the

5. Measurements

monochromator focusses these beams in its focal plane, the position of the spot depending on the angle of the incoming beam. Two spots are considered resolved if their distance equals the radius of their diffraction discs.

The angle of diffraction at a grating is given by

$$\sin \alpha = \frac{\lambda}{g} \quad [5.1]$$

where λ is the wavelength and g the pitch of the grating. The angle α is translated into the distance x in the focal plane of the spherical mirror,

$$x = f \tan \alpha \quad [5.2]$$

Because the angles are small, the error of equating sine and tangent can be tolerated, so

$$\frac{\lambda}{g} = \frac{x}{f} \quad [5.3]$$

Taking the difference between two wavelengths to get their lateral separation Δx ,

$$\Delta \lambda = \frac{g}{f} \Delta x \quad [5.4]$$

The radius of a diffraction disc, which is the minimum size for Δx , depends on the optical system and is given by $\rho = 0.61 \frac{\lambda}{nA}$ where nA is the aperture of the image-forming system. Because a spherical mirror introduces aberrations, a more realistic value to use is $\rho = \lambda/nA$. This distance is the minimum practical width of the output slit, $\rho = \Delta x$; closing the slit any further does not increase the resolution. The numerical aperture of the present monochromator is 0.1, so $\Delta x \simeq 10\mu\text{m}$. Since $g \simeq 2\mu\text{m}$ and $f = 500\text{mm}$, the value for $\Delta \lambda$ is

$$\Delta \lambda \simeq 0.4\text{\AA} \quad [5.5]$$

In practice, the slit is opened further than $10\mu\text{m}$ to increase the throughput, so a practical value for the maximum resolution is $\Delta \lambda = 1\text{\AA}$.

4. Alternatively, a scanning Fabry-Perot interferometer can be used to obtain the spectrum. However, this measurement was not performed because the spectral distribution of the laser emission (2-3nm) for the present ring laser devices is too wide. Also, the maximum resolution of a scanning Fabry-Perot spectrum analyzer can only be achieved with a highly collimated beam. Collimating the output of a semiconductor laser is a difficult task, because of the different divergence angle and mode spectrum in the x and y direction.

For an unequivocal measurement, the free spectral range of the interferometer $\Delta \lambda_{FP}$ must be larger than that of the signal $\Delta \lambda_s$, i.e.

$$\Delta \lambda_{FP} = \frac{\lambda^2}{2nl} > \Delta \lambda_s \quad [5.6]$$

This condition yields for the spacing l of the Fabry-Perot cavity

$$l < \frac{\lambda^2}{2n\Delta \lambda_s} \quad [5.7]$$

With $n = 1$ (air), $\lambda = 0.85$, and $\Delta \lambda_s = 3\text{nm}$, l is calculated to $< 120\mu\text{m}$, which is very difficult to adjust. Besides, the resolution of the apparatus is determined by the finesse of the Fabry-Perot resonator. The finesse depends on the reflectivity of the mirrors and is related to the number of roundtrips of an average photon before it leaves the cavity. It is given by

5. Measurements

$$F = \frac{\pi\sqrt{R}}{1-R} \quad [5.8]$$

And the resolution of the interferometer by

$$\Delta\lambda_{FP} = \frac{\Delta\lambda_s}{F} \quad [5.9]$$

In the given case, $F = 150$, so $\Delta\lambda_{FP} = 0.2\text{\AA}$, an order of magnitude better than the grating interferometer. However, it was not yet possible to obtain this resolution, because it requires very good alignment and collimation. The resolution will be easier to reach with devices that have a lower spectral width, i.e. that operate on a single longitudinal mode.

5.3 Signal detection

An optical powermeter, sensitive to nW levels, is used for spectral measurements. Due to its high sensitivity, its time constant is very slow (1/10s), it thus averages the signal over the duty cycle for pulsed measurements.

A fast detector (BPW 65, silicon) is used for the L-I curve measurements. The signal is measured by monitoring the voltage across a series resistor. Dividing the resulting current by the quantum efficiency (≈ 0.5) yields the output power. Because of the limited aperture of the collimating lens (40x, 0.65), the detected signal is smaller than the real signal, which, however, yields a very practical result, because it represents the power that can be coupled into a multimode fibre.

5.4 Typical results

The following spectra and L-I curves illustrate the difference between cw and pulsed operation of identical devices and indicate the parameters that can be derived. A more detailed analysis of the effects involved is presented in chapter 6.

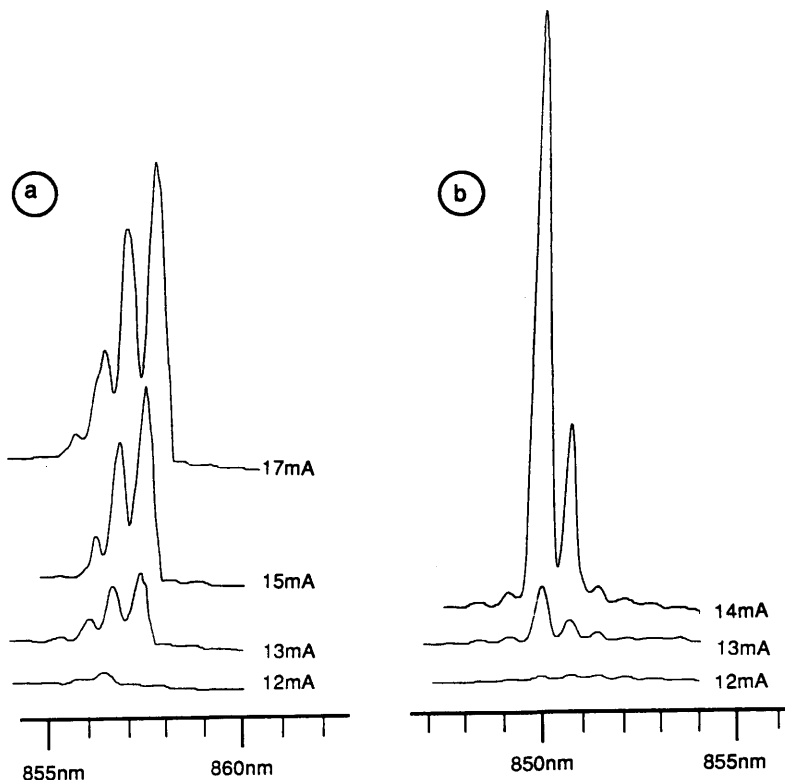


Figure 35. Typical spectra for cw (a) and pulsed (b) operation.

The threshold current is similar in both cases, between 12mA and 13mA. The longitudinal mode spacing is 6\AA , which corresponds to a $300\mu\text{m}$ long cavity. The shift of the gain curve due to temperature is obvious from the difference between the centre wavelengths, and the temperature increase with pumping is apparent from the shift of the modes (section 6.2.7).

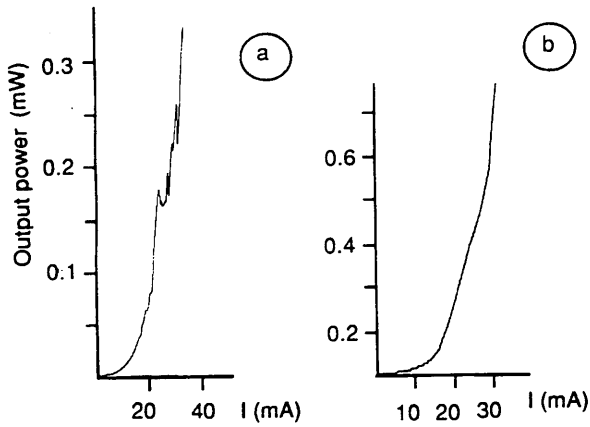


Figure 36. Typical L-I curves for cw and pulsed operation.

The slow turn-on caused by spontaneous emission is apparent, which is more pronounced for cw operation. The output reduction due to heating is also obvious. The kinking phenomenon is due to mode shifts and discussed in detail in section 6.2.6.

6.Devices

Everything you always wanted to know about ring lasers, but never dared to ask

This chapter contains all the information gathered on ring lasers in the past three years. The first part shows results of a strip-loaded stripe laser that was fabricated in the same material to create a reference for the ring laser work. In the second part, various properties of ring lasers are discussed, such as the output characteristics, the loss, the influence of the radius and others. Different device geometries, such as a polygon ring laser, devices with two coupled cavities and experiments on the waveguide geometry are presented in the third part of this chapter. The final part describes the demonstration of strip-loaded, i.e.buried, quarter-ring lasers, which has a tremendous potential for future developments of the device.

6.1 Strip-loaded stripe laser

In order to enable a better assessment of the ring laser work, a strip-loaded stripe laser was fabricated. The results would reveal which of the effects observed on ring lasers are genuinely device dependent, and which are caused by the material design, the fabrication procedure or the measurement apparatus. Usually, when new material is received, a set of broad area stripe lasers is fabricated (section 3.2), to learn about the basic material properties. However, a $600\mu\text{m} \times 50\mu\text{m}$ stripe is quite different from a $4\mu\text{m} \times 300\mu\text{m}$ ring. Therefore, the goal was set to produce a $400\mu\text{m} \times 4\mu\text{m}$ stripe, strip-loaded, to see if textbook-results are obtainable.

The fabrication of this device was chosen to be beneficial to further ring laser development. Stripe lasers, commercially produced, are often of the type depicted below, where an insulator (typically SiO_2) covers the whole of the sample except for a window that provides the top contact. The contact is deposited using angular evaporation or an isotropic technique such as sputtering to provide the step-coverage. The devices are finally separated by cleaving.

This technique makes integration difficult, since the definition of contacts for individual devices by lithography and lift-off becomes a problem; lift-off requires vertically evaporated contacts, which do not connect across the $1.5\mu\text{m}$ deep step between the laser and the substrate, so a bridge between the top and bottom contact is required. Polyimide can be used for that purpose, according to the procedure that has been discussed in section 4.5.

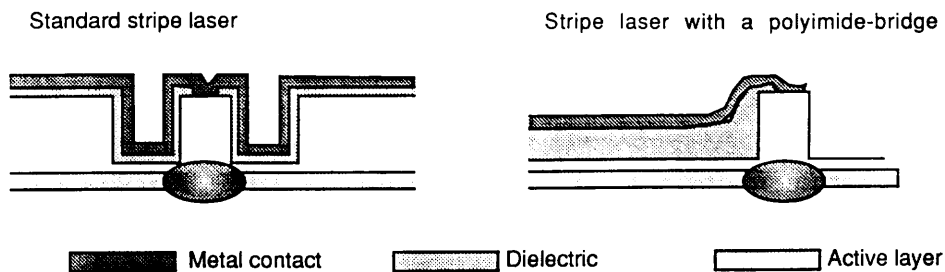


Figure 37. Comparison between a standard and a polyimide-bridge strip-loaded stripe laser.

The following performance-curves were measured:

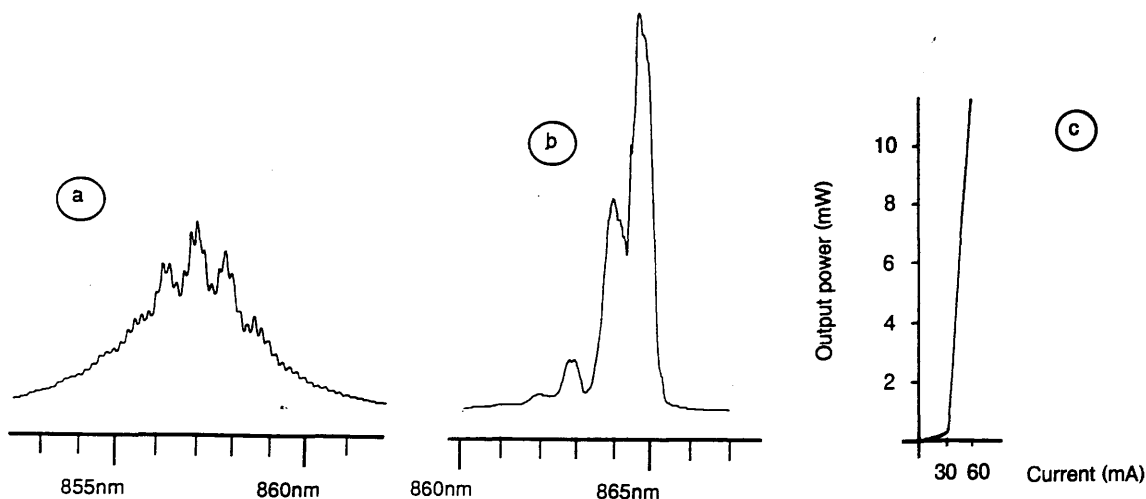


Figure 38. Spectrum of a strip-loaded stripe laser just above (a) and at 1.5x threshold current (b), and L-I curve (c).

The spectrum just above threshold displays multiple longitudinal modes and narrows at higher pumping. However, all devices remained multimode, which shows that single-mode operation is not readily achievable in semiconductor lasers. The (cw) L-I curve is very linear and steep ($\eta_d = 0.3$), which emphasizes one of the problems of ring lasers; their L-I curve has a number of kinks and the differential quantum efficiency very low ($\eta_d = 0.02 - 0.04$).

6.2 Properties of ring lasers

6.2.1 Spectral output - the longitudinal mode spacing

To permit the interpretation of the spectral measurements, a calculation of the expected mode spacing is required. The resonator supports both longitudinal and transverse modes. The spacing of the former is given by the free spectral range of the resonator, i.e. its optical pathlength, whereas the spacing of the latter is determined by the guiding properties of the waveguide, i.e. its 'higher-order' modes.

The free spectral range of a Fabry-Perot resonator is given by⁵⁵

$$\Delta\nu = \frac{c}{n_{eff}l} \quad [6.1]$$

where l is the physical pathlength of one complete roundtrip in the cavity. The parameter n_{eff} is the group index, i.e. it includes the dispersion properties of the material, $n_{eff} = n_0 + \lambda \frac{\delta n}{\delta \lambda}$. Since this value is difficult to calculate for quantum-well material, especially in an active material where it is also gain-dependent, it is easier to measure for a stripe laser that produces a clear spectrum and where all the other parameters of [6.1] are known. A spectrum of a strip-loaded stripe laser similar to the one shown in fig.38a) yields a value of $n_{eff} = 4.0$.

Converting [6.1] into a wavelength difference by using $\Delta\nu = \frac{c\Delta\lambda}{\lambda^2}$ yields

⁵⁵ A.Yariv, "Optical Electronics", 4thed., p.114, HRW Sanders, 1991.

$$\Delta\lambda = \frac{\lambda^2}{n_{eff} l} \quad [6.2]$$

For a ring laser, the physical pathlength is taken as the circumference of the ring, so l in [6.2] changes to $2\pi r$. With $r = 100\mu\text{m}$, $n = 4.0$ and $\lambda = 0.85\mu\text{m}$, the spacing becomes 6\AA , which corresponds to the experimental value shown in figure 35. This result is a clear confirmation of the whispering-gallery mode operation of a pillbox ring laser.

6.2.2 Spectral output - the transverse mode spacing

In order to calculate the transverse mode spacing, it is necessary to model the characteristics of the waveguide first, i.e. to calculate its higher order modes. This is done using a one-dimensional finite difference solution for the scalar wave equation.

This solution usually converges to the lowest-order mode of the system. Since the trial function that initiates the iteration contains components of all waveguide modes, eliminating the zero order mode will make the program converge to the first order mode. The elimination is based on the orthogonality principle. Orthogonality of two modes means that the overlap integral between them is equal to zero. Therefore, to calculate the first order mode, an initial iteration of the program is performed that yields the zero order mode. In a second run, the overlap between the first and the second solution is taken successively and that fraction is subtracted, as shown in the following formalism.

The overlap integral OL is a real number between 0 and 1:

$$OL = \int \left| \frac{E_0 E_1}{E_0 E_0} \right| \quad [6.3]$$

E_0 being the field distribution of the zero order mode and E_1 the field distribution of the current iteration which will finally converge into the first order mode. This fraction is then subtracted from the current solution,

$$E_1 = E_1 - OL E_0 \quad [6.4]$$

to eliminate the components of the zero order mode before re-iteration.

In a one-dimensional program that scans across $5\mu\text{m}$ of waveguide structure with a stepsize of 5nm , about 1000 iterations are required to get to an effective index error of $< 10^{-4}$ if the overlap integral and the index are calculated after every 50^{th} iteration. The overlap OL drops quickly from about 0.8 to values $< 10^{-3}$.

The following graph shows the first two modes of a pillbox resonator as a result of this iteration. The broken line is the refractive index profile at the outside of the pillbox, taking the curvature into account by using conformal mapping. The full lines are the zero and first order modes, respectively.

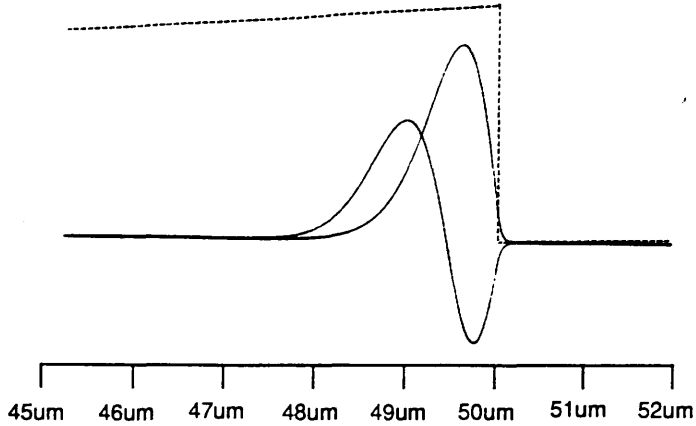


Figure 39. Zero and first order mode in a pillbox resonator, the scale being the radius.

The two propagation constants, $\beta_0 = 3.414$ and $\beta_1 = 3.373$ had been calculated assuming $Al_xGa_{1-x}As$ with $x = 0.2$ in the waveguide region. The radius used in the calculation is $50\mu m$.

Having obtained the effective indices of the first two modes, the next step is to derive the wavelength spacing between them via the spacing of the longitudinal modes.

The longitudinal mode spacing of a cavity was given by [6.2]. This mode spacing can also be seen as a function of the effective index, $\Delta\lambda = f(n_{eff})$. The change in mode spacing with a change in the index, i.e. the transverse mode spacing, can be obtained by taking the derivative of [6.2] in respect to n ,

$$\frac{\delta(\Delta\lambda)}{\delta n_{eff}} = -\frac{\lambda^2}{n_{eff}^2 l} \quad [6.5]$$

solving for the transverse mode spacing and simplifying to differences rather than differentials,

$$\Delta(\Delta\lambda) = \frac{\Delta n_{eff} \lambda^2}{n_{eff}^2 l} \quad [6.6]$$

Typical values of $\Delta n_{eff} = 0.04$ from above, $\lambda = 0.85\mu m$, $l = 300\mu m$ and $n = 4.0$ give a transverse mode spacing of $\Delta(\Delta\lambda) = 0.2\text{\AA}$. This is beyond the resolution of the grating monochromator of $0.5\text{-}1\text{\AA}$ as calculated in section 5.2.

The scanning Fabry-Perot resonator, assuming perfect alignment, is able to resolve this mode spacing given the spectral width of present devices. However, perfect alignment has not been achieved yet, a requirement that will be less stringent once stable single longitudinal mode operation has been established and the spectrum is narrower.

6.2.3 Current spreading in the pillbox resonator

Assuming that the non-radiative recombination current across the laser junction has been suppressed by the silicon nitride treatment, a more detailed analysis of the threshold current can be

performed. Current spreading^{56,57}, i.e. the leakage or fringe current that flows towards the inside of the pillbox beyond the lasing filament, accounts for a significant portion of the overall current consumption. Consider the situation as depicted in the following figure, which shows a contact on top of a p-n junction. The aim is to calculate the fringe current that flows beyond the area of the contact.

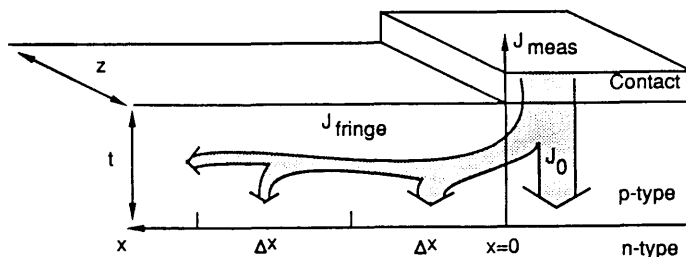


Figure 40. Model of a stripe contact laser to calculate the fringe current.

The following assumptions are made:

1. The top layer is thin compared to the distance over which the current density falls off and has a uniform resistivity, so a simplified one-dimensional model can be used.
2. The junction characteristic is assumed to be exponential below lasing threshold, i.e. Shockley's equation is obeyed.
3. The potential on the n-side of the junction is constant.
4. The edge of the stripe contact is at $x=0$ where the laser is assumed to be at threshold, i.e. the lasing filament does not extend beyond the contact.

The Voltage drop in x-direction is calculated using Ohm's law, expressing the resistance in terms of the resistivity along a section of width Δx , length z and thickness t .

$$\Delta V = I \rho \frac{\Delta x}{t z}, \text{ for } \Delta x \rightarrow 0 \quad \frac{\delta V}{\delta x} = I \frac{\rho}{t z} \quad [6.7]$$

The current density across the p-n junction is (Shockley's equation)

$$J = J_0 \left[\exp\left(\frac{eV}{nkT}\right) - 1 \right] \quad [6.8]$$

Expressing the current density as the current across the area $\Delta x z$ and considering $\Delta x \rightarrow 0$,

$$\frac{\delta I}{\delta x} = J_0 z \left[\exp\left(\frac{eV}{nkT}\right) - 1 \right] \quad [6.9]$$

The current can be eliminated by differentiating [6.7] with respect to x and combining it with [6.9]. Since $\frac{eV}{nkT} \gg 1$, the exponential can also be simplified, giving

$$\frac{\delta^2 V}{\delta x^2} = \frac{\rho}{t} J_0 \exp\left(\frac{eV}{nkT}\right) \quad [6.10]$$

⁵⁶ W.P.Dumke, "Current thresholds in stripe-contact injection lasers", Solid-state Electronics, Vol.16, pp.1279-1281, 1973.

⁵⁷ G.H.B.Thompson, "Physics of semiconductor laser devices", pp.308-310, J.Wiley&Sons, 1980.

6.Devices

Solving this equation shows that the current density J through the active layer drops off with distance x from the edge of the contact according to the relation

$$J(x) = 2 \frac{J_0}{\left(\frac{x}{l_s} + \sqrt{2}\right)^2} \quad [6.11]$$

where l_s is the spreading length given by

$$l_s = \sqrt{\frac{t n k T}{\rho J_0 e}} \quad [6.12]$$

Integrating $J(x)$ with respect to x yields the total fringe current density to one side of the contact,

$$J_{fringe} = \sqrt{2} J_0 l_s \quad [6.13]$$

Hence, in order to calculate J_{fringe} , a knowledge of J_0 is required. For stripe lasers, J_0 is identical to the current density measured for broad area devices, so J_{fringe} can be readily calculated. In the case of ring lasers, J_0 also contains the current that is required to overcome the additional scattering loss, so it is device - specific. However, it can be calculated with an expansion of the above formalism, as shown in the following.

The measured current density, J_{meas} , is the sum of the effective and the fringe current density:

$$J_{meas} w = J_0 w + J_{fringe} \quad [6.14]$$

J_0 and J_{meas} must be multiplied by the stripe width w because J_{fringe} is a current density per unit length. Combining [2] and [3] gives

$$J_0 = J_{fringe}^2 \frac{\rho e}{2 t n k T} \quad [6.15]$$

Substituting $a = \frac{\rho e}{2 t n k T}$ and combining [4] and [5] yields a quadratic equation,

$$J_{fringe}^2 + \frac{J_{fringe}}{a w} - \frac{J_{meas}}{a} = 0 \quad [6.16]$$

with the solution

$$J_{fringe} = \frac{-1 \pm \sqrt{1 + 4 J_{meas} a w^2}}{2 a w} \quad [6.17]$$

Transforming the current densities into currents and discarding the nonphysical negative solution yields

$$I_{fringe} = \frac{-1 + \sqrt{1 + 4 \frac{I_{meas}}{z} a w}}{2 a w} z \quad [6.18]$$

Using the values for a $100\mu\text{m}$ diameter ring laser, i.e. length $z = 300\mu\text{m}$, width of the pumped filament $w = 4\mu\text{m}$, measured threshold current $I_{th} = 15\text{mA}$, average resistivity $\rho = 4 \times 10^{-2} \Omega \text{cm}$, ($\rho = 6 \times 10^{-2} \Omega \text{cm}$ for structure c) in figure 41 because the top contact layer has been etched off), thickness of the contact layer $t = 2\mu\text{m}$, room temperature and an assumed ideality factor of 2 at threshold yields a fringe current of

$$I_{fringe} = 11.5\text{mA}$$

so the fringe current constitutes 75% of the threshold current, and an effective current of only 3.5 mA is required to start laser operation in the ring cavity.

	WIDTH, w	I_{thresh}	I_{fringe}	I_0	J_0
(a)	4 μm	15mA	11.5mA	3.5mA	300A/cm ²
(b)	2 μm	13mA	11.3mA	1.7mA	280A/cm ²
(c)	4 μm	12.5mA	6.2mA	6.3mA	525A/cm ²

Figure 41. Current spreading and effective current density for different device geometries.

Three different structures were analyzed to verify this result. Two devices had a 4 μm wide pumped filament, one of which was etched on the inside (1 μm deep) to reduce the spreading current, and a third laser was fabricated with a 2 μm wide filament. The structures and the resulting spreading currents are displayed in figure 41, which shows that the effective threshold current density of all three structures is reasonably consistent considering the uncertainty of the assumptions made and the measurement accuracy involved. The increase in effective threshold current for structure c) indicates that the spreading current in a) and b) is overestimated, which is due to the model assuming straight rather than circular structures. Therefore, an effective threshold current density of 600 A/cm² is assumed in the further calculation.

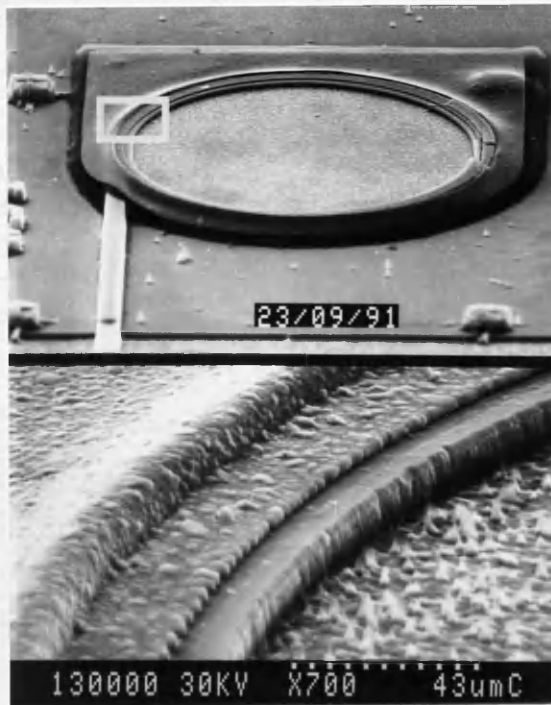


Figure 42. Micrograph of the device that produced a threshold of 12.5mA, displaying the shallow etch in the centre of the pillbox.

6.2.4 Scattering loss

The value of 600A/cm² for the effective current density yields a gain of 2500cm⁻¹ in the well from the gain-current relation (fig.17). The scattering loss is then derived from the threshold condition in a quantum well ring laser, which can be written as

$$\Gamma_w n_w g_w = \alpha_i + \alpha_{coup} + \alpha_{scat} \quad [6.19]$$

where Γ_w is the optical confinement factor, n_w the number of wells, g_w the gain per well, α_i the internal loss of the material, α_{coup} the coupling loss, which corresponds to the mirror loss in a stripe laser, and α_{scat} the scattering loss. The dependence of α_{scat} on the radius of curvature is discussed in the next section.

For the single quantum well material used, $\Gamma_w = 3.4\%$, which leads to a value of 80cm^{-1} for the left side of [6.19]. The internal loss, from stripe laser measurements, is 8cm^{-1} , which leaves 72cm^{-1} for the combined coupling and scattering loss. This translates into 9dB for the interaction length of $300\mu\text{m}$ along the full ring. Assuming a coupling loss of around 6dB leaves 3dB for the scattering loss per 360° , which is a very low value considering the small radius of curvature. The accuracy of this result, however, is limited, because the coupling loss at the Y-junction is not known; the estimate of 6dB assumes that the loss is somewhat higher than for a cleaved mirror.

A review revealed that 3dB/ 360° compares favourably with other published results: A value of 3dB/ 90° has been reported for ion-beam milled waveguides⁵⁸, the difference being probably caused by wall roughness, which is fabrication dependent and difficult to quantify. A loss of 0.6dB/ 90° has been achieved in sapphire waveguides⁵⁹. Taking into account the loss-dependence on the refractive index step as discussed in section 4.4, the combined scattering loss of the GaAs-nitride-air interfaces is 2.5 times higher than the loss at the sapphire-air interface. Hence, the loss reported is in the same order of magnitude as the result shown here. It is also interesting to note that the value of 3dB/ 360° is similar to the loss quoted for square-shaped lasers⁶⁰ of 0.6dB per reflection, i.e. 2.4dB for a complete round trip.

6.2.5 Radius

The radius of curvature is one of the most important parameters of a ring laser. Since the size and the radius are dependent on each other, they cannot be investigated separately in rings. Therefore, half-rings with straight sections (devices in the shape of a "U") were fabricated, the straight sections accounting for the difference in circumference of the different radii, so all devices were equal in length. The radius was varied between $30\mu\text{m}$ and $145\mu\text{m}$ and the resulting threshold currents are shown in fig.43a).

⁵⁸ M.W.Austin, "GaAs/GaAlAs curved rib waveguides", IEEE Journal of Quantum Electronics, Vol.18, pp.795-800, 1982.

⁵⁹ E.C.M.Pennings, J.van Schoonhoven, J.W.M. van Uffelen and M.K.Smit, "Reduced bending and scattering losses in new optical 'double-ridge' waveguide", Electronics Letters, Vol.25, pp.746-748, 1989.

⁶⁰ S.Oku, M.Okayasu and M.Ikeda, "Low-threshold cw operation of square-shaped semiconductor ring lasers (orbiter lasers)", IEEE Photonics Technology Letters, Vol.3, pp.588-590, 1991.

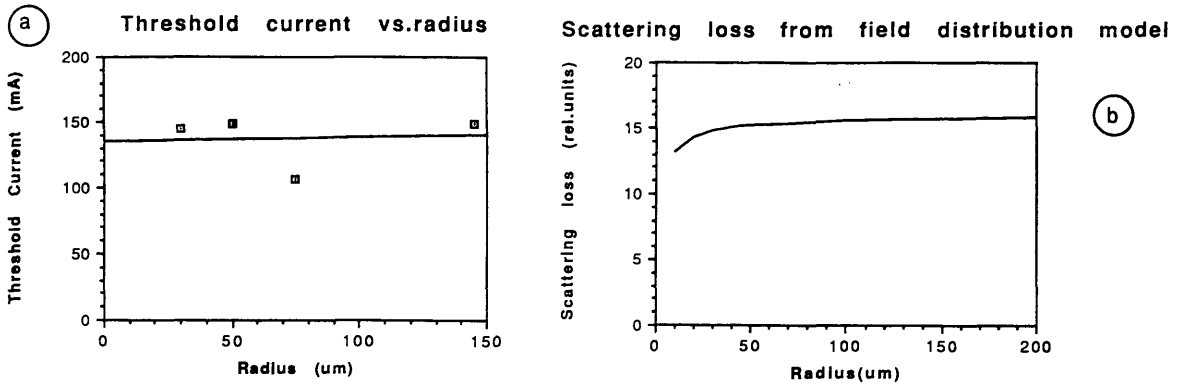


Figure 43. a) Dependence of the threshold current and b) the calculated scattering loss on the radius of curvature.

The curve suggests that the threshold current, i.e. the loss, is independent of the radius in the investigated range. This implies that scattering is the dominant loss mechanism, since the threshold current would increase with decreasing radius if radiation loss, the mechanism for bending loss in buried waveguides, was the limiting factor.

A theoretical analysis based on the model developed in chapter 2 was performed to verify this result. To derive the loss, it is assumed that the fraction of the mode travelling along the sidewall is responsible for the scattering loss⁶¹, so, with R as the radius of the pillbox,

$$\alpha \propto \frac{E^2(R)}{\int E^2(r)dr} \quad [6.20]$$

This is a loss per unit length. The interesting parameter, though, is the loss per angle, which is given by $\alpha_\phi = \alpha \phi R$, so for a fixed angle, it is proportional to the loss - radius product,

$$\alpha_\phi \propto R \frac{E^2(R)}{\int E^2(r)dr} \quad [6.21]$$

The dependence of α_ϕ on the radius is shown in figure 43b). The curve is essentially flat, which agrees well with figure 43a). The drop towards lower radii indicates the limited validity of the model.

Both results clearly support the conclusion that the loss is independent of the radius in the range of $30\mu\text{m}$ to $150\mu\text{m}$., which can be understood considering the position of the optical mode in respect to the sidewall; the loss per unit length is higher for smaller radii, since the interaction is stronger and the field is pushed further into the wall. A smaller radius has a shorter bend, however, so the loss per unit angle remains constant.

⁶¹ M.S.Stern, P.C.Kendal, R.C.Hewson-Browne, P.N.Robson, and D.A.Quinney, "Scattering loss from rough sidewalls in semiconductor rib waveguides", Electronics Letters, Vol.25, pp.1231-1232, 1989.

Earlier work on whispering-gallery lasers⁶² shows a linear dependence of the loss on the inverse radius, so the loss - radius product is also a constant. Results obtained in sapphire waveguides⁶³ show a constant loss for radii bigger than $70\mu\text{m}$; since the confinement of the GaAs-silicon nitride-air interfaces is much stronger than for sapphire-air, the critical radius will be shifted towards shorter radii, which makes the result shown in figure 43 plausible.

However, these findings disagree with recently published data⁶⁴ that show an increase in loss for radii smaller than $100\mu\text{m}$.

6.2.6 Y-junction and L-I curve

The following figure shows the L-I curves of different ring laser devices, displaying the influence of the pumping current and the coupling geometry on the output characteristic.

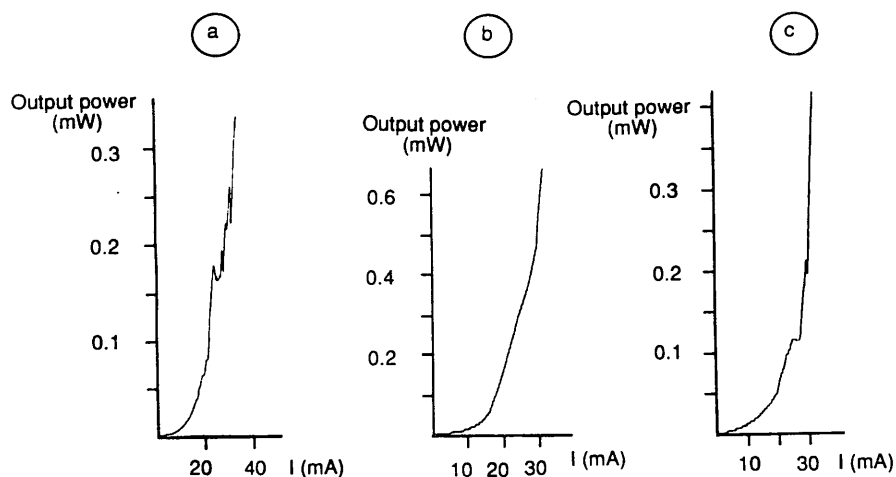


Figure 44. L-I curves of ring lasers, operating a) cw, b) pulsed, $1\mu\text{s}$, 1:10, and c) cw, device with two curved output waveguides.

The cw curves display several kinks that disappear as the pulse length is shortened, which indicates a temperature rather than gain related effect. A detailed investigation of the spectrum of device a) reveals that the kinks are related to mode hopping, i.e. energy transfer from one mode to another, while the overall output intensity remains nearly unchanged.

⁶² I.Ury, S.Margalit, N.Bar-Chaim, M.Yust, D.Wilt, and A.Yariv, "Whispering-gallery lasers on semi-insulating GaAs substrates", Applied Physics Letters, Vol.36, pp.629-631, 1980.

⁶³ E.C.M.Pennings, J.van Schoonhoven, J.W.M. van Uffelen, and M.K.Smit, "Reduced bending and scattering losses in new optical 'double-ridge' waveguide", Electronics Letters, Vol.25, pp.746-748, 1989.

⁶⁴ J.P.Hohimer, D.C.Craft, G.R.Hadley, G.A.Vawter, and M.E.Warren, "Single-frequency continuous-wave operation of ring resonator diode lasers", Applied Physics Letters, Vol.59, pp.3360-3362, 1991.

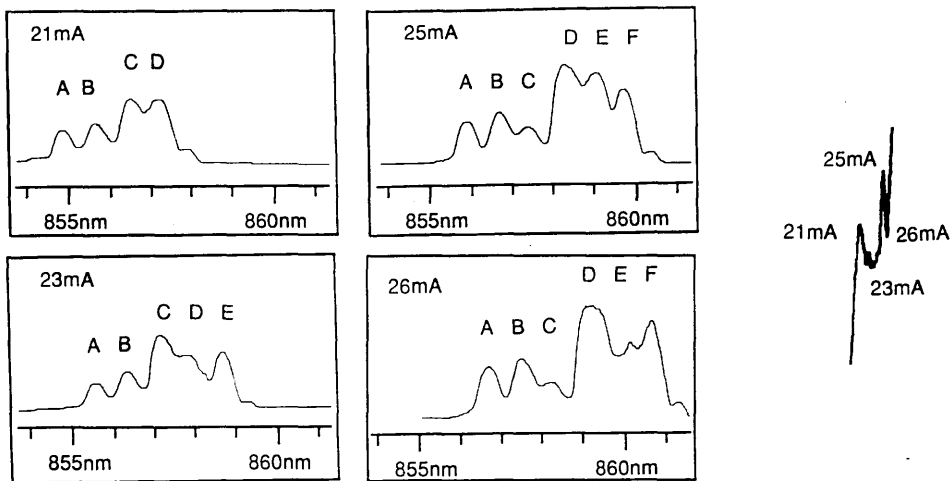


Figure 45. Investigation of a section of figure 44a), showing the spectrum at various kinks of the curve.

At 21mA, the spectrum consists of 4 longitudinal modes. As the current is increased, intensity is transferred from mode "D" to "E", whilst the intensity of all other modes remains constant. A steep rise in output power is registered with a further increase in current, which is related to the appearance of mode "F". The power drops again as the current is increased to 26mA, which is obviously caused by the disappearance of mode "E". This interplay of modal intensities can be explained by lateral shifts of the mode position with increased pumping. The influence of the mode position on the operation of the ring laser is illustrated by the following figure.

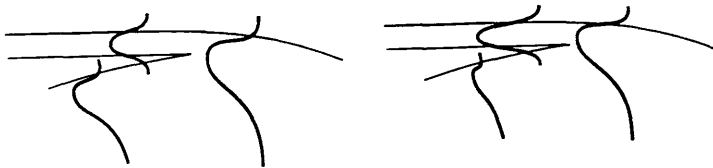


Figure 46. Model for the influence of the mode position on the splitting ratio at the Y-junction and thus the feedback.

As the current is increased, the temperature raises. The higher temperature causes an increase in refractive index according to [6.27]. Since the refractive index change is highest in the lasing filament, the mode is pushed further to the outside of the resonator. This displacement modifies the splitting ratio at the Y-junction, which influences the feedback and thus the amplification of the mode. Therefore, only a small change in temperature, and thus the position of the mode can have a rather drastic effect on the output. The sketch illustrates the situation for the lowest order mode losing feedback; one of the higher-order modes with a different field distribution is likely to benefit from the index change, which leads to the apparent intensity transfer discussed above. It must be noted that the model is based on transverse modes that can not be detected with the monochromator; therefore, the experimental evidence is not entirely conclusive. However, since the transverse and longitudinal modes are interrelated, the model is reasonably justified.

The temperature dependence explains why devices fabricated earlier⁶⁵ (also figure 5) showed straight L-I curves. They were operated pulsed, which yields results as presented in fig.44b). Another con-

⁶⁵ A.S.-H. Liao and S.Wang, "Semiconductor injection lasers with a circular resonator", Applied Physics Letters, Vol.36, pp.801-803, 1980.

firmation of the feedback model is that a straight L-I curve is displayed by another type of ring laser, the square-shaped "Orbiter laser"⁶⁶ where the output coupler connects to a straight waveguide. In a straight waveguide, the mode position is not dependent on the refractive index, so the modes are not displaced laterally. Further evidence is given by the L-I curve of a semicircular laser that also displays kink-free behaviour.

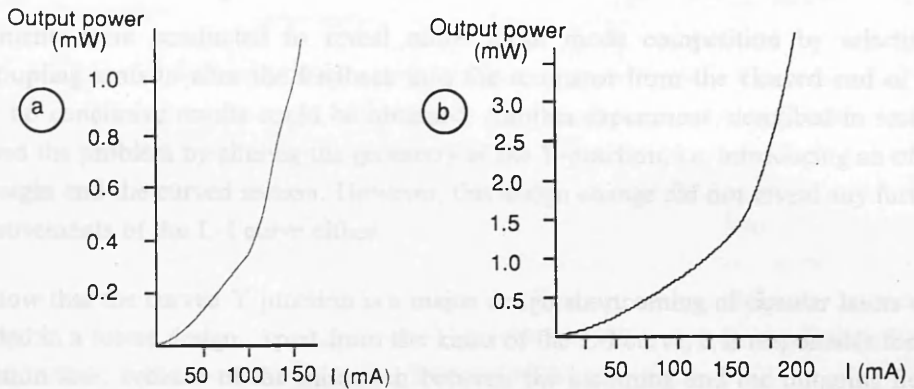


Figure 47. L-I curves of a rectangular ring laser (a) and a semicircular laser (b) displaying no kinking.

Both curves were obtained from a pulsed measurement, using $10\mu\text{s}$ long pulses to cause as much heating as possible without preventing laser action; this is to ensure that the straight curves are not related to the avoidance of the temperature effect.

The model cannot be considered complete without including the competition between the two sets of modes circulating in either direction of the resonator, as illustrated by fig.44c), which shows the L-I curve of a ring resonator with two curved waveguides.

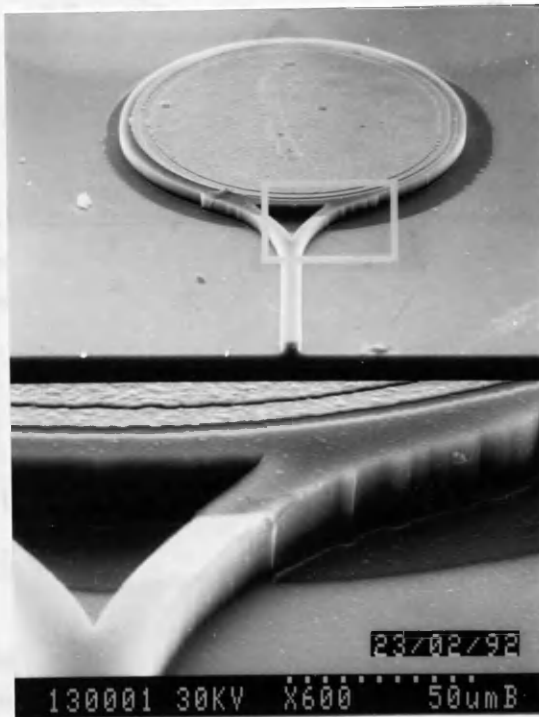


Figure 48. Ring laser with two symmetrically arranged curved waveguides ("tennis-racket" - design).

⁶⁶ S.Oku, M.Okayasu, and M.Ikeda, "Low-threshold cw operation of square-shaped semiconductor ring lasers (orbiter lasers)", IEEE Photonics Technology Letters, Vol.3, pp.588-590, 1991.

The symmetry of this structure is believed to stabilize the laser operation, which shows in a more linear L-I curve. However, the threshold current is increased due to the larger total coupling area, i.e. more discontinuities in the resonator. This phenomenon requires a more detailed investigation before it can be explained completely.

Further experiments were conducted to reveal more about mode competition by selectively pumping the coupling arms to alter the feedback into the resonator from the cleaved end of the waveguide, but no conclusive results could be obtained. Another experiment, described in section 6.3.3, approached the problem by altering the geometry of the Y-junction, i.e. introducing an offset between the straight and the curved section. However, this design change did not reveal any further insights or improvements of the L-I curve either.

These results show that the curved Y-junction is a major design shortcoming of circular lasers and should be avoided in a future design. Apart from the kinks of the L-I curve, it is responsible for an additional radiation loss, because of the mismatch between the incoming and the outgoing fields at the junction.

6.2.7 Temperature in a ring laser

A computer program was developed to simulate the junction temperature of a device under operating conditions. It is capable of including the whole of the structure and replaces an earlier, simplified program⁶⁷ that solved the heat transport equation separately for the laser rib and the substrate. The heat transport equation describes the heat distribution in a given device,

$$\frac{\delta^2 T}{\delta x^2} + \frac{\delta^2 T}{\delta y^2} + \frac{\delta^2 T}{\delta z^2} + \frac{q}{k} = \frac{\rho c}{k} \frac{\delta T}{\delta t} \quad [6.22]$$

q being the heat generation density, k the thermal conductivity, ρ the density of the material and c the specific heat capacity.

Since the steady state situation is considered, the time dependence can be neglected, and the term on the right side of [6.22] equals zero. The structure is circular, so it is useful to transform the equation into cylindrical coordinates. The angular dependence can be ignored for reasons of symmetry.

$$\frac{\delta^2 T}{\delta r^2} + \frac{1}{r} \frac{\delta T}{\delta r} + \frac{\delta^2 T}{\delta z^2} + \frac{q}{k} = 0 \quad [6.23]$$

The finite-difference form of [6.23] is

$$\frac{T_{i+1j} - 2T_{ij} + T_{i-1j}}{\Delta^2} + \frac{1}{i} \frac{T_{i+1j} - T_{i-1j}}{2} \Delta + \frac{T_{ij+1} - 2T_{ij} + T_{ij-1}}{\Delta^2} + \frac{q}{k} = 0 \quad [6.24]$$

where i denotes meshpoints in the radial direction, j in the vertical direction and Δ is the meshsize. Solving the equation for T_{ij} and rearranging gives

$$T_{ij} = \frac{1}{4} \left[\left(1 + \frac{\Delta}{2i}\right) T_{i+1j} + \left(1 - \frac{\Delta}{2i}\right) T_{i-1j} + T_{ij-1} + T_{ij+1} + \frac{q\Delta^2}{k} \right] \quad [6.25]$$

⁶⁷ W.Chen, "Thermal problems in semiconductor ring lasers", M.Sc. thesis, Glasgow University, 1989.

The boundary conditions are such that the temperature at the bottom of the substrate is forced to 20°C, simulating the heatsink. The temperature flow across the other boundaries is put to zero since the heat dissipation into the ambient can be neglected. The same applies to the inner boundary for $r \rightarrow 0$, since there is no heatflow for reasons of symmetry. Thus,

$$\frac{\delta T}{\delta r} \text{ side boundaries} = \frac{\delta T}{\delta y} \text{ top boundary} = 0, \quad \text{numerically } T_{n-1} = T_{n+1} \quad [6.26]$$

The program makes use of an overrelaxation routine to speed up convergence. The computing time for a mesh of 50x50 points is in the order of a minute, the cut-off is a temperature change of less than 0.1°K, so the computed accuracy is in the order of 1°K. The heatsource is a 8μm x 2μm and 300μm long torus, so the program assumes that the voltage drops entirely across the top contact and the active region and that all the current is transformed into heat. The former assumption is sufficiently close to reality, since the resistance of the substrate and the bottom contact are very small, the latter is justified since the differential quantum efficiency of the devices is only a few percent. The width of 8μm is based on the calculation of the spreading current which showed that only half of the injected carriers contribute to the 4μm wide lasing filament.

The output of the program was compared to experimental results that were derived from the change of the spectrum with pumping current. The spectrum changes according to the following two mechanisms:

1. The centre wavelength of the lasing spectrum increases with 3Å/°K, due to the shift of the gain spectrum⁶⁸.
2. Each individual mode shifts due to the refractive index change induced by the temperature difference. The refractive index changes⁶⁹ as follows:

$$\Delta n = 4 \times 10^{-4} \Delta T \quad [6.27]$$

Since the resonant wavelength depends linearly on the refractive index, $k \lambda_0 = n l$, k being an integer and l the physical length of the cavity for a complete round-trip, the wavelength-change is also a linear function of the temperature change:

$$\Delta \lambda_0 = \frac{\lambda_0}{n} \Delta n \quad [6.28a]$$

$$\Delta \lambda_0 = 0.85 \times 10^{-10} \Delta T \quad [6.28b]$$

using $\lambda_0 = 0.85\mu\text{m}$ and $n = 4$, so the wavelength change is in the order of 1Å / °K.

The two spectra shown in figure 35 illustrate these effects. The shift of the centre wavelength at threshold between pulsed and DC measurement has been used to calibrate the temperature scale, and the shift of the modes with increased pumping is used for the additional points.

⁶⁸ T.L.Paoli, "A new technique for measuring the thermal impedance of junction lasers", IEEE Journal of Quantum Electronics, Vol.11, pp.498-503, 1975.

⁶⁹ H.C.Casey, M.B.Panish, "Heterostructure Lasers", Pt.A, p.31, Academic Press, 1978.

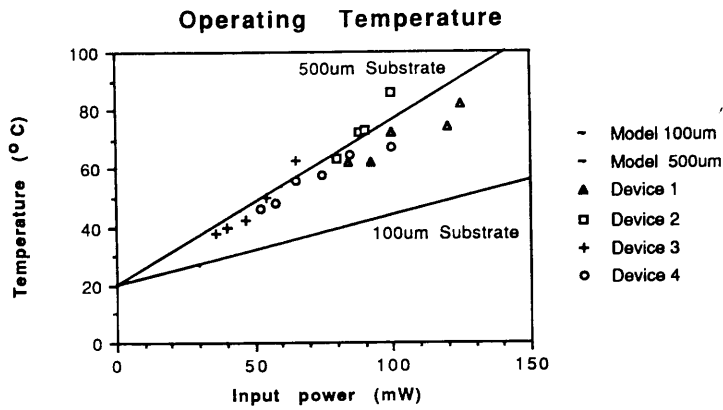


Figure 49. Temperature change with pumping current derived from spectral measurements and comparison with modeled results.

The model represents the real situation fairly accurately, and the scatter of the experimental points is adequate, considering that devices from four different batches were used that had different threshold currents and contact resistances. The lower line represents the modeled results for a substrate thickness of $100\mu\text{m}$, indicating that thinning the substrate would be a very useful measure in reducing the operating temperature. In the current fabrication procedure, the substrate is not thinned for practical reasons.

A confirmation of the superiority of the pillbox over a fully etched rib, the design favoured in earlier work⁷⁰ was obtained by simulating the junction temperature in the latter. The temperature was 94°C at an input power of 60mW , so it increased by about 40°C ; this explains why cw operation is easier to achieve in a pillbox ring laser device.

6.2.8 Degradation and device lifetime

The exposed junction caused by the deep etch is a serious problem. Apart from non-radiative recombination along surface traps, the lifetime of the devices is severely limited: During operation, electron-hole pairs are constantly being created at the pn junction. When recombining, some of them produce phonons that are strong enough to break arsenic bonds, which enables arsenic to migrate away from it_5 lattice site. This is not a problem in an indefinitely large crystal, because there is a dynamic equilibrium between dislocation and recombination. If this process happens close to the surface, though, the equilibrium is disturbed. The arsenic can diffuse to the surface and react with oxygen, impurities, or another arsenic atom to form As_2 ⁷¹. Hence, the arsenic gets bound to the surface, i.e., the crystal slowly depletes of As atoms, which leads to degradation. The arsenic byproducts usually form states within the bandgap, which leads to non-radiative recombination and increased optical absorption.

The common solution to this problem is to overgrow the junction with electrically passive material, so all current-induced processes are restricted to the inside of the crystal and the above effect does not occur. Since one of the key points about a ring laser is its simplicity, overgrowth, an expensive fabrication step, is avoided in this project.

⁷⁰ A.F.Jeziarski, "Semiconductor ring lasers", Ph.D.Thesis, Glasgow University, 1991.

⁷¹ "Detection of a monolayer of As by Raman scattering during photoluminescence degradation of GaAs", J.H Campbell and P.M.Fauchet, CLEO 90, paper CWB7.

The passivation treatment using silicon nitride (section 4.4) was identified as a simple alternative to suppress the non-radiative recombination current on the surface. However, device degradation is still a problem. Uncoated devices degrade in a matter of 1-2 hours (output power dropping to 50% with constant current), whereas coated devices degrade slower, in the order of 12-20 hours. These values are still unpractical, but a thorough study of the passivation process⁷², might lead to further improvement. The high temperature of operation, around 60°C, is another factor that accelerates the degradation of the devices

6.2.9 Polarization

According to a detailed investigation⁷³, the loss in a circular waveguide is different for modes of different polarization. Those with the electric field oscillating in the plane of the active layer (TE) suffer higher losses than the modes oscillating in a plane perpendicular to the active layer (TM). This result implies that the output of a ring laser is TM polarized. However, the quantum well material used exhibits a polarized gain, favouring the TE mode because of the restricted electron motion in such a structure, so quantum well ring lasers operate in the more lossy TE mode.

In order to evaluate the strength of this effect, the polarization (intensity ratio of TE/TM) was measured both in double heterostructure (DH) and in quantum well (QW) materials. DH lasers were only slightly polarized (TE/TM = 8/7), so other loss mechanisms must be predominant. The ratio in QW lasers was TE/TM = 2/1, which shows the influence of the quantum wells. The spectra did not reveal any difference, i.e. they only changed in size rather than in shape, so it is not the case that some modes are of one and others are of the other polarization. However, this could be a clue that the polarization is of a more complex type, such as circular or elliptical. Concluding, the device geometry does not have a significant impact on the polarization, so the use of quantum well material with its preferred TE polarization does not cause a serious problem for a circular laser.

6.3 Different device geometries

The continuing quest for the optimum device geometry led to some rather oddly shaped devices.

6.3.1 Racetrack and polygon

Lasers were designed in the shape of a racetrack to see if the length and the radius could be adjusted independently. The resulting threshold current of a device with 84 μm radius and a 70 μm long straight waveguide section was 50mA, compared to 32mA for a comparable circular laser. The increased threshold current shows that coupling a straight guide into a curved one leads to considerable mode conversion loss.

The same increase in threshold current was measured for a rectangular laser with four 45° mirrors. The reason for that is not clear, but it is assumed that considerable mode conversion loss occurs at each mirror. When designing this resonator shape, the threshold current was expected to decrease, because the scattering loss in a straight waveguide is lower than in a curved one and the mirrors operate on total internal reflection. However, strong luminescence was observed at each mirror,

⁷² S.J.Pearnton, J.W.Corbett, and T.S.Shi, "Hydrogen in crystalline semiconductors", Applied Physics A, Vol.43, pp.153-195, 1987.

⁷³ E.A.J.Marcattii, "Bends in optical dielectric guides", Bell Systems Technical Journal, Vol.48, pp.2103-2132, 1969.

which indicates scattering or mode conversion loss. This increased loss at the mirrors outweighed the reduced loss of the straight sections, so the threshold current was higher altogether. With a better design of the 45°mirrors, this problem can possibly be overcome, as other results^{74, 75} indicate.

Concluding, this experiment showed that any discontinuity in the laser waveguide is a reason for mode conversion and radiation loss, so it should be avoided by any means.

6.3.2 Two coupled ring resonators

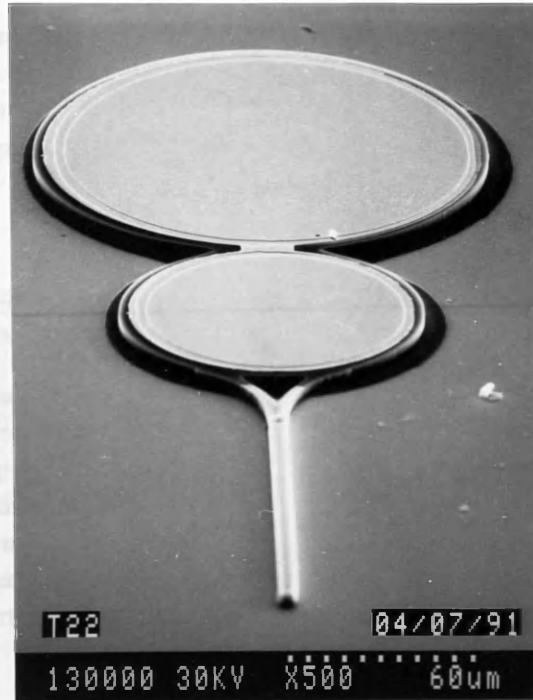


Figure 50. A micrograph of a resonator consisting of two coupled rings.

An attempt was made to achieve single-mode operation in a ring laser by combining two ring resonators of different size. The approach is based on the theory of coupled cavities that predicts the selection of those modes that are resonant in both cavities⁷⁶.

The experiment was designed to couple a ring of 600 pixel radius ($49\mu\text{m}$ at 320x) with a ring of 800 and 900 pixel radius, respectively, expecting that they would only operate on the modes that are resonant in both cavities. The coupling was also varied by changing the overlap between the two from just touching to strongly overlapping. A Y-shape output waveguide was chosen, expecting that the device would benefit from this more symmetrical arrangement.

⁷⁴ S.Oku, M.Okayasu, and M.Ikeda, "Low-threshold cw operation of square-shaped semiconductor ring lasers (orbiter lasers)", IEEE Photonics Technology Letters, Vol.3, pp.588-590, 1991.

⁷⁵ A.Behfar-Rad, S.S.Wong, J.M.Ballantyne, B.A.Soltz, and C.M.Harding, "Rectangular and L-shaped GaAs/AlGaAs lasers with very high quality etched facets", Applied Physics Letters, Vol.54, pp.493-495, 1989.

⁷⁶ W.T.Tsang, N.A.Olsson, and R.A.Logan, "High-speed direct single-frequency excursion in cleaved-coupled-cavity semiconductor lasers", Applied Physics Letters, Vol.42, pp.650-652, 1983.

The devices operated with threshold currents as low as 40mA, which was in the same order as single rings at that stage, i.e. the increased threshold current was mostly due to the increased size. However, the spectra did not stand up to the expectation, neither was single-mode operation achieved, nor could a common denominator between the free spectral width of the individual resonators or an influence of the coupling be observed. For some devices, the contacts of the two rings were not connected, so they offered the possibility of individual tuning within a limited range. However, pumping the two individual ring resonators independently did not show any sign of interaction either.

The overall result was encouraging in that it demonstrated the operation of a device comprising two coupled ring resonators, but further investigation is required to obtain more conclusive results. The operation is expected to be very sensitive to the relative position of the junction between the two rings, similar to the Y-junction between the laser and the waveguide.

6.3.3 Output waveguide

The geometry of the coupling waveguide was varied to study the influence of the Y-junction on the threshold current and the linearity of the L-I curve.

1. Standard semiconductor stripe lasers show an improved performance when the mirrors are coated for higher reflectivity. The threshold current drops and the obtainable output power increases with an optimum value for the reflectivity around 80%⁷⁷, depending on the material structure and the dimensions of the device. The same is expected for ring lasers by changing the distance between the waveguide and the resonator, where the strength of the feedback is expected to increase with increasing separation. The ability to control the feedback by lithography is a particularly appealing prospect, because it is easier than applying reflective coatings.

Lasers were fabricated as illustrated by the insets in figure 51. The separation was varied between 0 μm and 6 μm , which encompasses the two extreme cases of a fully overlapping waveguide (distance = 0 μm) and one that is not touching the ring at all (distance = 6 μm). The waveguide width is 4 μm , and it is still touching the ring at 5 μm separation due to the proximity effect when exposing the pattern. The ring diameter is 100 μm , as usual.

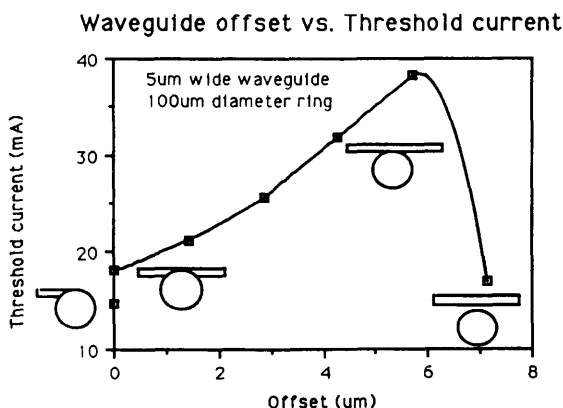


Figure 51. The influence of the waveguide separation on the threshold current.

⁷⁷ A.Yariv, "Optical electronics", 4th ed., pp.603-606, HRW Sanders, 1991.

The result is opposite to what had been expected. Instead of decreasing, the threshold current increased with increasing waveguide offset. The highest threshold current occurred when the waveguide is just touching the ring, so this arrangement is the most lossy one. If the waveguide is removed even further, it leaves the resonator without an output and the threshold is derived from the scattered radiation off the sidewalls. This device, with $x = 6\mu\text{m}$, was expected to have the lowest threshold of all, because the coupling loss had been completely eliminated. However, this assumption could not be verified, which might be caused by the uncertainty related to deriving the threshold from the scattering signal alone. The increased threshold current of the other devices is probably related to the Y-junction, so instead of increasing the feedback, the position change of the waveguide in respect to the ring resonator increases the radiation loss at the Y-junction.

2. The same experiment was used to study the influence of the waveguide extending to either side of the junction, i.e. coupling the modes travelling in both direction. The resulting difference is small and in favour of the single waveguide, as shown by the first point on the graph. This shows that a symmetrical arrangement is not necessarily beneficial to the laser performance, in contrast, the loss is increased due to the larger coupling area.
3. In an attempt to increase the output power, a different design was chosen whereby the modes travelling in both directions are coupled out individually and the waveguides are combined. An example of this geometry is shown in figure 48. The L-I curve (figure 44c) and the output power were marginally better than for devices with a single junction, but the core of the problem remains to be solved.

All of the results described above cannot be explained satisfactorily as yet. The simple, straightforward models derived from intuition seem to ignore vital factors and more complex models are required. It is particularly important to perform an in-depth study of the field distribution at the Y-junction, taking into account the effects arising from gain and loss in the material.

6.3.4 Ring lasers with a reverse-biased section

Ring lasers with a diameter of $130\mu\text{m}$ that incorporated two contacts were built in order to study the possibilities of passive mode-locking. The width of the second contact was varied between $10\mu\text{m}$ and $40\mu\text{m}$ and was separated from the main contact by a $5\mu\text{m}$ wide, $1.5\mu\text{m}$ deep etched trench. Passive mode-locking is initiated by reverse biasing this section, which then acts as an absorber, that, if the device is operated appropriately, saturates if the clockwise and counterclockwise modes collide. Hence, a train of short pulses should establish, the distance between them being determined by the roundtrip time of the cavity. Also, the number of modes should be reduced, because the weaker ones do not have enough intensity to saturate the absorber, so they vanish.

The devices had threshold currents between 19mA ($10\mu\text{m}$ section) and 22mA ($40\mu\text{m}$ section), when only the main contact was pumped, which indicates that a small, but tolerable loss is introduced by the trenches and the unpumped sections. The spectra showed no difference to standard devices. When the second contact was reverse biased, no major change ensued, except for a reduction in the overall output intensity. Hence, the resistance between the two contacts of about 500Ω was too low to transform the second section into a strong absorber, and the reverse bias simply subtracted current from the main contact. Therefore, better isolation between the two contacts, i.e. etching the trenches down to the active layer, is required for successful operation.

6.4 Strip-loaded ring laser

The problem of the exposed active layer of a ring laser has been discussed earlier, where the solution of passivating the sidewalls and coating them with silicon nitride has been suggested. A different approach that avoids the problem in the first place is not to etch through the junction, i.e. to rely completely on the strip-loading effect for guiding around the bend. The modelling of the waveguide properties (section 2.3.2) suggests that this is possible for radii of more than $400\mu\text{m}$, and that a complete removal of the upper cladding is required, since the strip-loading effect is stronger the closer the loading strip is to the waveguide layer. In order to verify this prediction and to see if strip-loading combined with gain-guiding can be utilized, quarter-ring lasers with radii between $300\mu\text{m}$ and $600\mu\text{m}$ were fabricated in double quantum well GaAs/AlGaAs material. Buffered HF was used to selectively remove the upper cladding layer after the initial dry etching process. This ensured that the upper cladding was completely removed in order to get the strongest possible guiding.

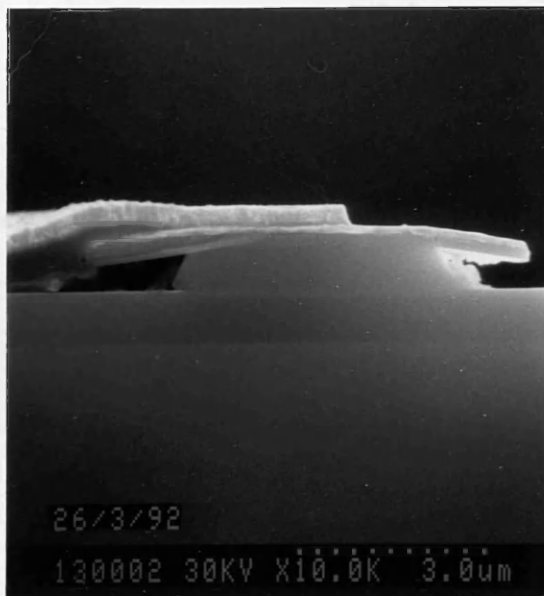


Figure 52. Cross-section of a strip-loaded quarter-ring laser, showing selective HF-etching and the polyimide-bridge.

The roughness incurred by the wet etching process is not as critical as for the pillbox ring lasers, because the active layer, i.e. most of the optical mode is buried and the dominant loss mechanism of strip-loaded devices is radiation rather than scattering. The resulting threshold currents ranged from 38mA ($950\text{A}/\text{cm}^2$, $600\mu\text{m}$ radius) to 47mA ($1100\text{A}/\text{cm}^2$, $300\mu\text{m}$ radius) with around 1mW output power per facet at $1.5\times$ threshold current.

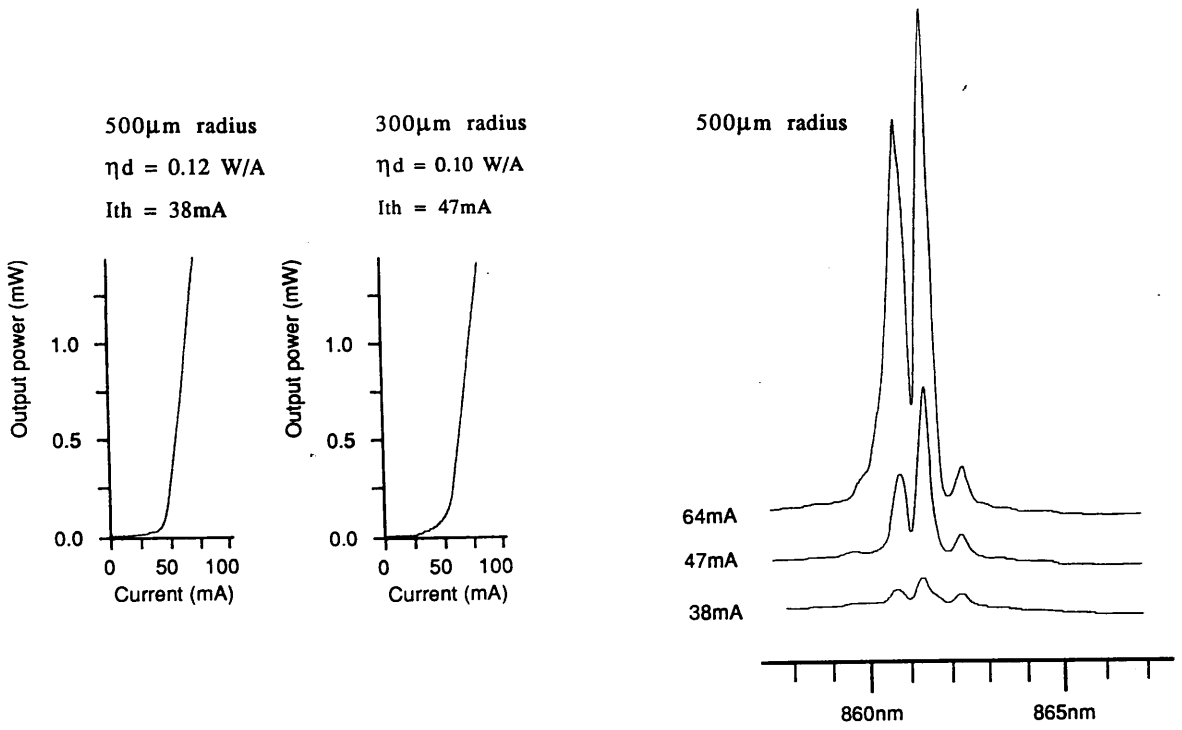


Figure 53. L-I curves and spectrum of strip-loaded quarter-ring lasers.

These surprisingly good results indicate that strip-loading is a viable guiding mechanism even for curved lasers. The fabrication simplicity makes the structure very attractive.

7. Integration

This chapter is divided into two parts: First, it describes the efforts made towards integration of optical and optoelectronic devices, such as lasers, waveguides, modulators and detectors. This type of circuit is referred to as a photonic integrated circuit, PIC, because it has mainly optical functions. A particular emphasis has been put on the theoretical analysis and numerical modelling of the more complicated material structure that is required therefore. The second part presents the work conducted towards integrating optoelectronic and electronic devices, i.e. combining a laser and a transistor in an OEIC.

7.1 Photonic Integrated Circuit (PIC)

The material structure and its operating principle⁷⁸ is sketched in the following figure.

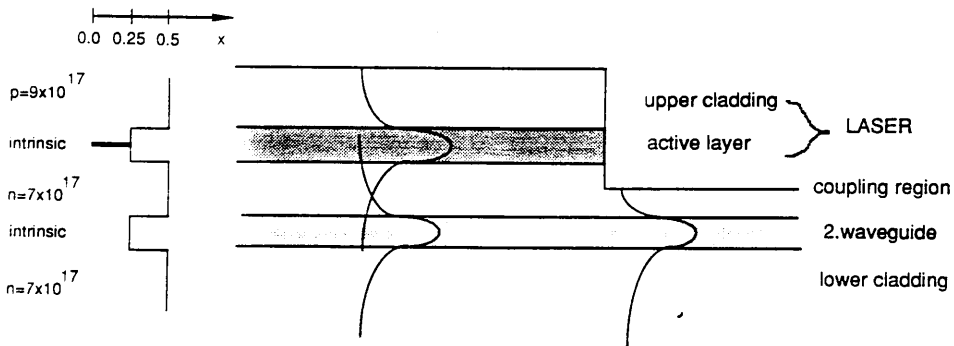


Figure 54. Material structure and the principle of directionally coupling between the laser and the waveguide.

Light is directionally coupled into a second waveguide below the laser guiding layer. The second waveguide does not incorporate a quantum well, so it is transparent for the radiation generated. Beyond the laser area, the interaction discontinues and the light travels with low loss to the next element of the circuit.

The material design was based on the simplest possible approach. Naturally, it was not optimized, but it provided a good base for studying the effects involved. Discrimination between the laser and the waveguide is performed by dry etching. Initially, etching was assumed to be a major problem, because an accuracy of 4% is required ($\pm 100\text{nm}$ in $2.5\mu\text{m}$). Therefore, about $1.5\mu\text{m}$ were etched in a first and the remaining $1.0\mu\text{m}$ in a second step, which reduced the required accuracy to 10%. Later, it was possible to control the process well enough to obtain the etch depth accurately in a single step.

Broad stripe lasers were built where the coupling into the underlying waveguide was observed. The threshold current of these lasers with one dry-etched and one cleaved facet was comparable to ones with both facets cleaved in the same material, in the order of $300\text{-}400\text{ A/cm}^2$. The intensity measured at the output of the $200\mu\text{m}$ long waveguide was about the same as measured on the back facet, which shows that the waveguide is not very lossy. A more detailed investigation of the waveguide loss gave the following data.

⁷⁸ H.Ribot, P.Sansonetti, J.Brandon, M.Carre, L.Menigaux, R.Azouldy, and N.Bouadma, "Monolithic integration of GaAs/GaAlAs buried heterostructure orthogonal facet laser and optical waveguide", Applied Physics Letters, Vol.54, pp.475-477, 1989.

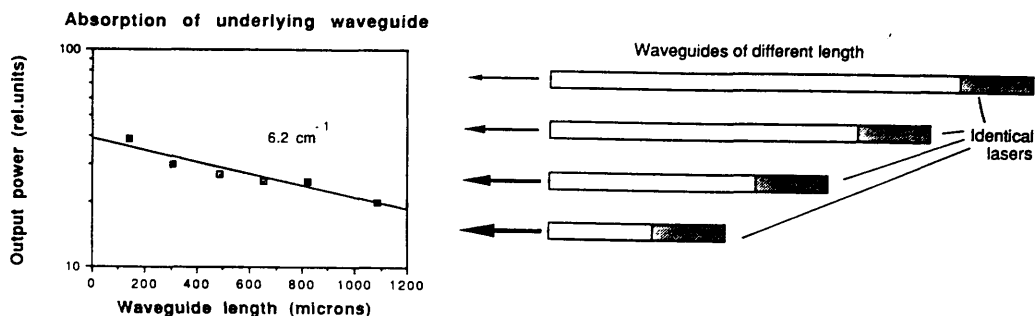


Figure 55. The loss of the underlying waveguide and the principle of measurement.

Identical stripe lasers were fabricated that couple into waveguides of various lengths. The output is projected onto a small detector to minimize the influence of the scattered radiation off the laser facet. The resulting value of 6.2 cm^{-1} is relatively high and is partially caused by the fact that the waveguides had been etched as ribs rather than using strip-loaded guiding. The rib-geometry is necessary to ensure sufficient confinement in the curved section when the waveguide is used in conjunction with a ring laser. However, the loss is sufficiently low for circuits in a 100's of μm -scale, the $1/e$ -distance being 1.6mm.

Having demonstrated the basic principles of the material, a model was developed to evaluate its suitability for an integrated ring laser circuit.

7.1.1 Modelling the passive properties of the PIC-material

This first part (7.1.1) deals with the basic properties of the PIC material, i.e. it treats the two waveguides as a passive directional coupler. Section 7.1.2 discusses the problem of finding the change of refractive index in an active medium in order to account for the alteration of the propagation constant caused by the gain. The third part, 7.1.3, presents a complete solution of the coupled-mode equations, incorporating the effects of injected carriers, gain and loss.

Firstly, the phenomenon of directional coupling is discussed. In optics books⁷⁹, directional couplers are usually treated by perturbation theory. The two waveguides are assumed to interact weakly, so the field in each waveguide is calculated ignoring the presence of the other one, an additional term accounting for the perturbation. Since it is an approximation, this technique is only of limited use and accuracy.

Another technique, more commonly used for microwaves,⁸⁰ is the 'supermode' approach. It is very straightforward, more general than the perturbation method and is based on the following idea: A two-waveguide configuration with two identical single-mode waveguides is able to support two modes, a symmetric ('even') and an antisymmetric ('odd') one, with the propagation constants β_a and β_b ; the resulting field distribution being the sum of the two supermodes. In the situation sketched in figure 56a), the two fields add up in the guide on the left and subtract in the guide on

⁷⁹ For example: D.L.Lee, "Electromagnetic principles of Integrated Optics", pp.220-224, J.Wiley&Sons, 1986.

⁸⁰ K.C.Gupta, R.Garg, and I.J.Bahl, "Microstrip lines and slotlines", Artech 1979; also in the 4th edition of A.Yariv, "Optical Electronics", pp.524-529, HRW Sanders, 1991.

the right, so the resulting field is concentrated in the left guide. Since both modes have different propagation constants, the situation as in figure 56b) occurs after they have travelled the length L down the line; the antisymmetric mode has gone 180° out of phase in respect to the symmetric one. The fields now add up in the guide on the right and subtract in the one on the left, so the energy has been transferred across.

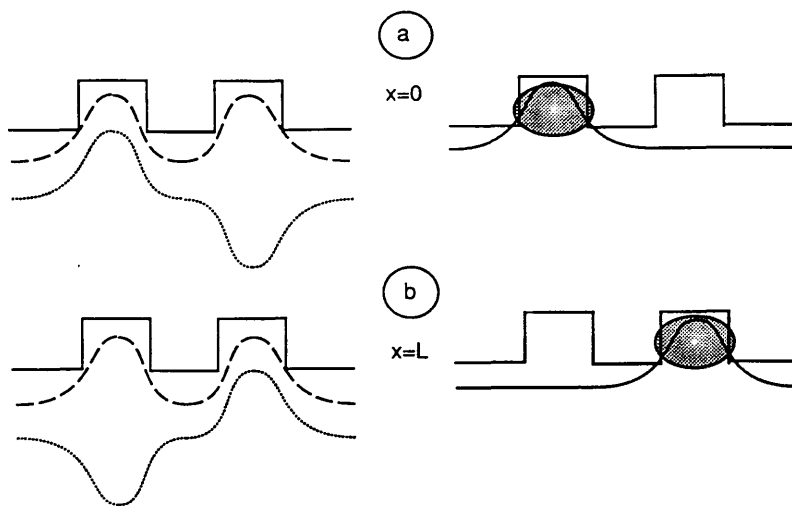


Figure 56. The superposition of the two supermodes in a directional coupler.

Thus, the condition for coupling is

$$(\beta_1 - \beta_2)L = \pi \quad [7.1]$$

And the coupling length is

$$L = \frac{\pi}{\Delta\beta} = \frac{\lambda}{2 \Delta n_{eff}} \quad [7.2]$$

If the waveguides are not identical, the power transfer is not complete, but the same principle still applies.

It is important to keep in mind that the two modes are orthogonal, i.e. they do not interfere; they travel down the line independently and the sum of two fields is observed rather than an interference pattern. The program used to find the propagation constants of the two supermodes has been described earlier (section 6.2.3) in the context of higher-order waveguide modes. The same principle applies here, because the two supermodes are the fundamental and the first order mode of the system.

The first test of the program was to compare the result for a completely symmetrical arrangement to the analytical solution given by [7.3].⁸¹

$$\kappa = \frac{2k_0(n_w^2 - n_c^2)q \cos^2 \frac{hd}{2}}{n_{eff}(d + \frac{2}{q})(q^2 + h^2)} \quad [7.3]$$

with

$$h = \sqrt{n_w^2 k_0^2 - \beta^2} \quad q = \sqrt{\beta^2 - n_c^2 k_0^2} \quad [7.4]$$

⁸¹ D.L.Lee, "Electromagnetic principles of Integrated Optics", p.231, J.Wiley&Sons, 1986.

7.Integration

where κ is the coupling coefficient, n_w and n_c are the waveguide and the cladding index, respectively, d is the waveguide depth and k_0 the wavenumber, $2\pi/\lambda_0$. The structure analyzed was the same as shown in fig.54 except for the quantum well in the top layer, so the result is comparable to the real arrangement. The resulting coupling coefficient using [7.3] is $\kappa = 485\text{cm}^{-1}$ ($L = 32\mu\text{m}$), compared to $\kappa = 536\text{cm}^{-1}$ ($L = 29\mu\text{m}$) using the finite-difference program.

This discrepancy is mainly caused by the numerical error related to the calculation of the second order mode which shows what accuracies one can expect in this sort of modelling. Applying the program to the real material gave only a small change to $\kappa = 560\text{cm}^{-1}$ and $L = 28\mu\text{m}$ with the propagation constants of $\beta_1 = 3.352k_0$ and $\beta_2 = 3.337k_0$ for the two supermodes.

7.1.2 Refractive index in an active medium

So far, the treatment only considered passive properties of the waveguides. In order to get a more accurate representation of the device under operation, the influence of the injected carriers must also be considered. The injected carriers in a semiconductor have two major effects on the refractive index, the direct interaction, "plasma effect", and the gain. Assuming $N = 2 \times 10^{18}/\text{cm}^3$ carriers at threshold, the refractive index change due to the plasma effect alone is in the order of $\Delta n = -0.01$ ⁸², which is neglected in this treatment, because the change occurs in both sections of the double-waveguide material, so it does not contribute to the difference between the two. The gain, however, is concentrated on the laser waveguide and must be considered.

The most rigorous approach to estimate the index change with gain would be to calculate the gain spectrum dependence on the injected carriers for the quantum well material and to perform a Kramers-Kronig analysis of that expression. The Kramers-Kronig integral relates changes in absorption, i.e. gain, to changes in refractive index. It would be beyond the scope of this work to perform the rather tedious calculation, especially since it involves many parameters that are not accurately known. Another method is to measure the shift of the superluminescent modes with increasing current, a measurement that can only be performed below lasing threshold, because carrier injection above threshold does not increase the gain. The reported result for this measurement⁸³, performed on multiple quantum well material, is $\Delta n = -0.01 \times 10^{-20} N$. Using the same value for the carrier concentration N at threshold as above, yields $\Delta n = -0.02$. Subtracting the change for the plasma effect results in a refractive index change due to gain at threshold of

$$\Delta n = -0.01 \tag{7.5}$$

$\Delta n = -0.02$ has been reported for double heterostructure (DH) material⁸⁴. Since a DH structure has a lower gain per injected carrier, assuming $\Delta n = -0.01$ in quantum well material seems plausible. However, this value only represents the order of magnitude of the effect, because it depends on the specific laser structure.

⁸² J.G.Mendoza-Alvarez, F.D.Nunes, and N.B.Patel, "Refractive index dependence on free carriers for GaAs", Applied Physics Letters, Vol.51, pp.4365-4367, 1980.

⁸³ N.Ogasawara, R.Ito, and R.Morita, "Linewidth enhancement factor in GaAs/AlGaAs multi-quantum well lasers", Japanese Journal of Applied Physics, Vol.24, pp.L519-L521, 1985.

⁸⁴ C.H.Henry, R.A.Logan, and K.A.Bertness, "Spectral dependence of the change in refractive index due to carrier injection in GaAs lasers", Journal of Applied Physics, Vol.52, pp.4457-4461, 1981.

7.1.3 The solution of the coupled-mode equation for the PIC material

Having developed a numerical representation of the passive properties of the double-waveguide material and found a correction factor for the influence of gain on the refractive index, the structure could be modeled more precisely. The treatment is based on previous work on waveguides in $LiNbO_3$ ⁸⁵.

The coupled-mode equations for waves propagating in z-direction in a directional coupler can be expressed as follows:

$$\begin{aligned}\frac{\delta E_1}{\delta z} &= \kappa E_2 - \gamma_1 E_1 \\ \frac{\delta E_2}{\delta z} &= \kappa E_1 - \gamma_2 E_2\end{aligned}\quad [7.6]$$

where κ is the coupling coefficient which is assumed to be identical for coupling in both directions. The coefficient γ is the sum of the absorption coefficient α and the propagation constant β , so $\gamma_i = \alpha_i + j\beta_i$. Applying the Laplace-Transformation yields

$$\begin{bmatrix} sE_1(s) - E_1(0) \\ sE_2(s) - E_2(0) \end{bmatrix} = \begin{bmatrix} -\gamma_1 & \kappa \\ \kappa & -\gamma_2 \end{bmatrix} \begin{bmatrix} E_1(s) \\ E_2(s) \end{bmatrix}\quad [7.7]$$

Solving for $E_1(s)$ and $E_2(s)$

$$(s - s_1)(s - s_2) \begin{bmatrix} E_1(s) \\ E_2(s) \end{bmatrix} = \begin{bmatrix} s + \gamma_2 & \kappa \\ \kappa & s + \gamma_1 \end{bmatrix} \begin{bmatrix} E_1(0) \\ E_2(0) \end{bmatrix}\quad [7.8]$$

where

$$s_{1/2} = -\frac{1}{2}(\gamma_1 + \gamma_2) \pm \frac{1}{2}\sqrt{(\gamma_1 - \gamma_2)^2 + 4\kappa^2}\quad [7.9]$$

Finally, taking the inverse Laplace transformation of this equation gives

$$\begin{bmatrix} E_1(z) \\ E_2(z) \end{bmatrix} = \frac{1}{s_1 - s_2} \begin{bmatrix} (\gamma_2 + s_1)e^{s_1 z} - (\gamma_2 + s_2)e^{s_2 z} & \kappa(e_1 z - e_2 z) \\ \kappa(e_1 z - e_2 z) & (\gamma_1 + s_1)e^{s_1 z} - (\gamma_1 + s_2)e^{s_2 z} \end{bmatrix} \begin{bmatrix} E_1(0) \\ E_2(0) \end{bmatrix}\quad [7.10]$$

Equation [7.10] represents the most general solution of the coupled wave equations for reciprocal coupling. The standard procedure would be to assume equal absorption coefficients and/or propagation constants in order to simplify the above equation and to find an analytical expression. This is not possible here, because both the absorption and the propagation coefficients are different in the two waveguides, so only a graphic solution is possible.

The boundary conditions are another problem specific to the ring laser device. The upper waveguide has no discontinuity, so both the phase and the amplitude must be continuous at all points, so

$$E_1(0) = E_1(L)\quad [7.11]$$

L being the length of the optical path in the circular cavity. The lower waveguide suffers loss at the Y-junction, where a fraction of the field, say $1-p$, is coupled out, so that

$$E_2(0) = p E_2(L)\quad [7.12]$$

⁸⁵ C.Millar, "Evanescent field coupling of thin film and fibre optical waveguides", Ph.D. thesis, Glasgow University, 1976.

7. Integration

$p = 0$ and $p = 1$ being the limiting cases of no feedback and no coupling loss, respectively. Substituting and rewriting [7.10] as

$$\begin{bmatrix} E_1(z) \\ E_2(z) \end{bmatrix} = \begin{bmatrix} a(z) & b(z) \\ b(z) & c(z) \end{bmatrix} \begin{bmatrix} E_1(0) \\ E_2(0) \end{bmatrix} \quad [7.10a]$$

and using [7.11] and [7.12] at $z = L$ yields

$$\begin{aligned} E_1(0) &= a(L) E_1(0) + b(L) E_2(0) \\ \frac{1}{p} E_2(0) &= b(L) E_1(0) + c(L) E_2(0) \end{aligned} \quad [7.13]$$

$$\begin{aligned} E_1(0) &= \frac{b(L)}{1 - a(L)} E_2(0) \\ E_1(0) &= \frac{\frac{1}{p} - c(L)}{b(L)} E_2(0) \end{aligned} \quad [7.14]$$

and

$$\frac{b(L)^2}{1 - a(L)} + c(L) = \frac{1}{p} \quad [7.15]$$

This expression determines the phase and the amplitude in the two coupled ring resonators as a function of the coupling loss, because the coefficients a , b and c represent the loss and propagation constants of the two respective waveguides. Since the coupling at the Y-junction does not introduce a phase change, p only has a real component, so the imaginary part of [7.15] must be equal to zero. This condition is only fulfilled if both β_1 and β_2 represent resonant cavity modes, a rather obvious result. The real part of [7.15] yields a relation between the gain in the laser, the loss in the waveguide and the coupling coefficient. Assuming a loss of 25cm^{-1} in the lower waveguide yields the following dependence of the gain in the laser, α_1 , on the coupling coefficient, p .

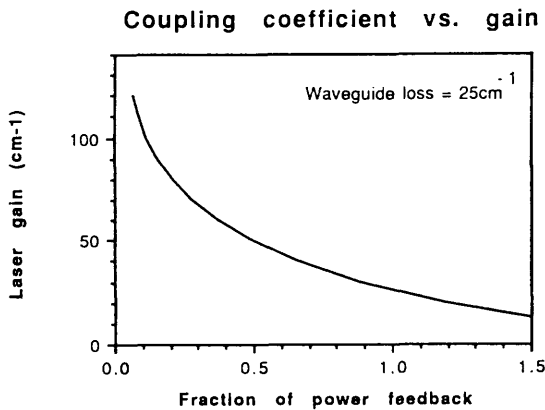


Figure 57. Gain in the laser waveguide vs. coupling coefficient at the Y-junction to fulfill the boundary conditions of equation 7.10.

The result is consistent, because the coupling coefficient is unity when the laser gain equals the waveguide loss, $-\alpha_1 = \alpha_2$. The value of 25cm^{-1} has been chosen since it represents the sum of the scattering loss due to the curvature ($3\text{dB}/360^\circ\text{C}$, section 6.2.4) and the internal loss (6cm^{-1} , section 7.1) of the passive waveguide. Assuming a power coupling coefficient of 20-30% at the Y-junction, similar to the value for a cleaved facet, yields $-\alpha_1 = 70 - 80\text{cm}^{-1}$ for the gain in the laser. This value is the additional gain that the laser has to provide to overcome the losses incurred by the lower

7.Integration

waveguide, so internal and scattering loss in the laser waveguide pushes the total gain requirement up to 100cm^{-1} . The practical implications of this high loss are discussed in the next section.

Having thus solved the boundary conditions enables the calculation of the field distribution in the coupled structure.

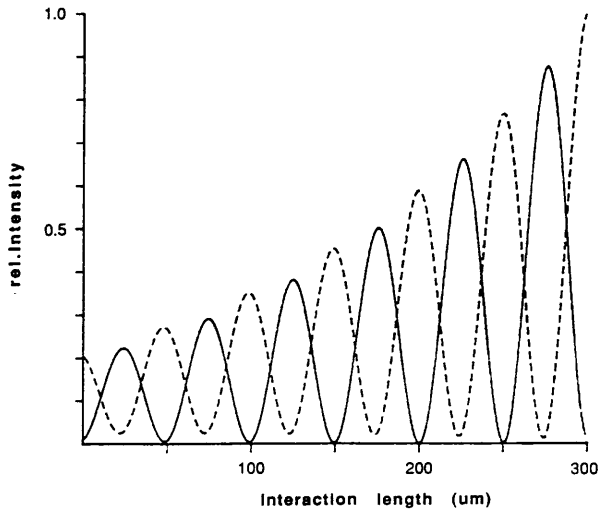


Figure 58. Field distribution in the laser (solid curve) and the underlying waveguide (broken curve).

Accounting for the refractive index reduction due to gain and using the material parameters shown in figure 54 yields propagation constants of $\beta_1 = 3.3490 k_0$ and $\beta_2 = 3.3518 k_0$ and a coupling coefficient $\kappa = 615\text{cm}^{-1}$. The graph shows that the present structure is very strongly coupled, which enforces the mode selection and is a manifestation of the low optical confinement factor (section 3.3.3) in the quantum well. It is also interesting to note that the lower field reaches a maximum at the junction, which leads to a maximum of outcoupled power.

7.1.4 Ring lasers in double-waveguide material

Ring lasers fabricated in this structure had threshold currents of 40mA and higher, most devices operating both at around 840nm and 790nm, which corresponds to lasing in the first and second quantized state. Second quantized state operation of single quantum well lasers⁸⁶ is associated with a loss higher than 100cm^{-1} , which matches the value estimated in the previous section. In order to improve this threshold current, a future structure needs to incorporate more quantum wells to provide more gain, and to have the passive waveguide only weakly coupled to the laser to improve the optical confinement factor Γ_w , which is only 1.4% in the present structure. Despite this relatively bad result, further experiments were conducted to investigate the integration potential of the double-waveguide concept.

7.1.5 Integrated modulator

An integrated circuit consisting of a ring laser, a waveguide and a modulator was designed. The modulator operates on electroabsorption, using the same pn junction as the laser, so the function of the circuit is as follows: Light is generated in the laser, couples into the waveguide, travels to the modulator, and couples back into the active region. The modulator is pumped to transparency in the on-state and highly absorbing in the off-state.

⁸⁶ M.Mittelstein, Y.Arakawa, A.Larsson, and A.Yariv, "Second quantized state lasing of a current pumped single quantum well laser", Applied Physics Letters, Vol.49, pp.1689-1691, 1986.

The following figure shows the device thus fabricated.

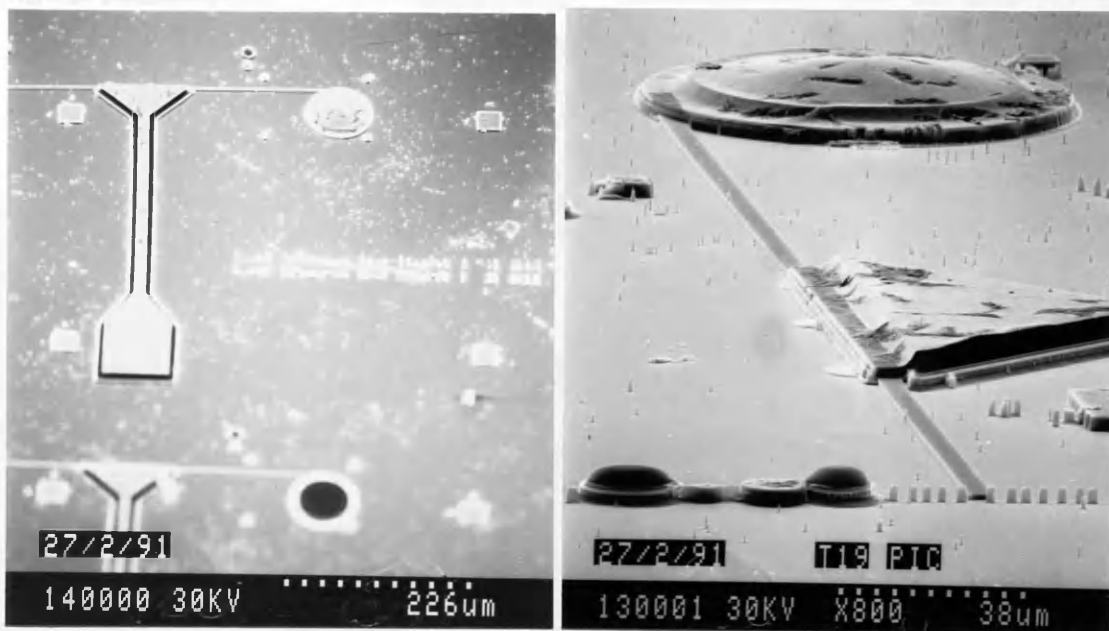


Figure 59. Two views of the integrated laser, waveguide and modulator circuit.

The modulator feed-in represents a microstrip line and was designed⁸⁷ for high speed operation.

Two major design shortcomings prevented successful operation.

1. The high-speed properties of the microstrip line could only be measured approximately, because polyimide had been used to isolate the contacts, which made wire-bonding impossible. The devices were thus microprobed, which limited the frequency range that could be evaluated to 1GHz, lower than the specified design frequency.
2. It was not possible to operate the modulator in its designated mode, because of electrical cross-talk with the laser: If the modulator is forward biased beyond I-V threshold, the potential on the n-side of the junction increases. Since the modulator and the laser are within a short distance of each other (300-500 μ m) and connected via the n^- -substrate, the potential on the n-side of the laser junction increases as well. Since the potential on the p-side of the laser is constant, the voltage across the laser junction is reduced and the output decreases. Instead of modulating the laser output, the laser current is modulated.

The second problem could have been overcome by using a constant current source, but a better solution would be to isolate the two devices using semi-insulating substrate.

7.1.6 Integrated detector

In state-of-the-art laser packaging, a photodiode is usually mounted behind the rear facet of a stripe laser to monitor the degradation of the laser performance with time. Integrating the two components on the same substrate simplifies and reduces the cost of the package significantly, another challenge that can be met by the double-waveguide structure. Most of the alternatives proposed by

⁸⁷ S.Tedjini, Laboratoire pour Electronique et Microondes (LEMO), Grenoble, France.

7.Integration

other workers in the field^{88,89} require elaborate fabrication techniques that are just as costly as the hybrid package.

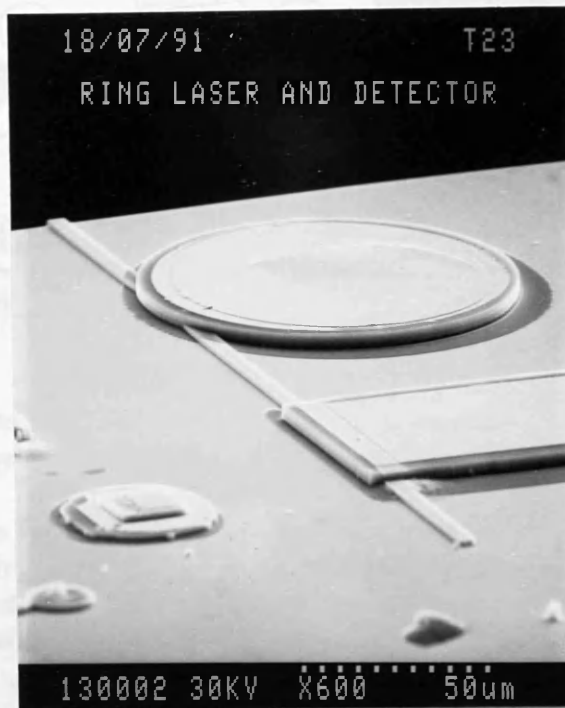


Figure 60. Micrograph of the integrated ring laser - waveguide - detector circuit.

The solution proposed here involves a design similar to the one developed in the previous section. If the modulator is subjected to a reverse bias, it acts as a photodiode. Light is coupled into the upper waveguide and is absorbed, which creates a photocurrent that can be used to monitor the laser output. When the device is used in this mode, it is critical to have no or negligible leakage current, which is illustrated by the electrical representation in figure 61a). To investigate the leakage current, the reverse I-V characteristic was examined.

7.2 Optoelectronic integrated circuit (OEIC)

The motivation for fabricating a monolithic integrated circuit (OEIC) derives from the following advantages: (1) the device is fabricated on a single substrate and is therefore more compact and easier to handle; (2) the device is fabricated on a single substrate and is therefore more compact and easier to handle; (3) the device is fabricated on a single substrate and is therefore more compact and easier to handle; (4) the device is fabricated on a single substrate and is therefore more compact and easier to handle; (5) the device is fabricated on a single substrate and is therefore more compact and easier to handle; (6) the device is fabricated on a single substrate and is therefore more compact and easier to handle; (7) the device is fabricated on a single substrate and is therefore more compact and easier to handle; (8) the device is fabricated on a single substrate and is therefore more compact and easier to handle; (9) the device is fabricated on a single substrate and is therefore more compact and easier to handle; (10) the device is fabricated on a single substrate and is therefore more compact and easier to handle; (11) the device is fabricated on a single substrate and is therefore more compact and easier to handle; (12) the device is fabricated on a single substrate and is therefore more compact and easier to handle; (13) the device is fabricated on a single substrate and is therefore more compact and easier to handle; (14) the device is fabricated on a single substrate and is therefore more compact and easier to handle; (15) the device is fabricated on a single substrate and is therefore more compact and easier to handle; (16) the device is fabricated on a single substrate and is therefore more compact and easier to handle; (17) the device is fabricated on a single substrate and is therefore more compact and easier to handle; (18) the device is fabricated on a single substrate and is therefore more compact and easier to handle; (19) the device is fabricated on a single substrate and is therefore more compact and easier to handle; (20) the device is fabricated on a single substrate and is therefore more compact and easier to handle; (21) the device is fabricated on a single substrate and is therefore more compact and easier to handle; (22) the device is fabricated on a single substrate and is therefore more compact and easier to handle; (23) the device is fabricated on a single substrate and is therefore more compact and easier to handle; (24) the device is fabricated on a single substrate and is therefore more compact and easier to handle; (25) the device is fabricated on a single substrate and is therefore more compact and easier to handle; (26) the device is fabricated on a single substrate and is therefore more compact and easier to handle; (27) the device is fabricated on a single substrate and is therefore more compact and easier to handle; (28) the device is fabricated on a single substrate and is therefore more compact and easier to handle; (29) the device is fabricated on a single substrate and is therefore more compact and easier to handle; (30) the device is fabricated on a single substrate and is therefore more compact and easier to handle; (31) the device is fabricated on a single substrate and is therefore more compact and easier to handle; (32) the device is fabricated on a single substrate and is therefore more compact and easier to handle; (33) the device is fabricated on a single substrate and is therefore more compact and easier to handle; (34) the device is fabricated on a single substrate and is therefore more compact and easier to handle; (35) the device is fabricated on a single substrate and is therefore more compact and easier to handle; (36) the device is fabricated on a single substrate and is therefore more compact and easier to handle; (37) the device is fabricated on a single substrate and is therefore more compact and easier to handle; (38) the device is fabricated on a single substrate and is therefore more compact and easier to handle; (39) the device is fabricated on a single substrate and is therefore more compact and easier to handle; (40) the device is fabricated on a single substrate and is therefore more compact and easier to handle; (41) the device is fabricated on a single substrate and is therefore more compact and easier to handle; (42) the device is fabricated on a single substrate and is therefore more compact and easier to handle; (43) the device is fabricated on a single substrate and is therefore more compact and easier to handle; (44) the device is fabricated on a single substrate and is therefore more compact and easier to handle; (45) the device is fabricated on a single substrate and is therefore more compact and easier to handle; (46) the device is fabricated on a single substrate and is therefore more compact and easier to handle; (47) the device is fabricated on a single substrate and is therefore more compact and easier to handle; (48) the device is fabricated on a single substrate and is therefore more compact and easier to handle; (49) the device is fabricated on a single substrate and is therefore more compact and easier to handle; (50) the device is fabricated on a single substrate and is therefore more compact and easier to handle; (51) the device is fabricated on a single substrate and is therefore more compact and easier to handle; (52) the device is fabricated on a single substrate and is therefore more compact and easier to handle; (53) the device is fabricated on a single substrate and is therefore more compact and easier to handle; (54) the device is fabricated on a single substrate and is therefore more compact and easier to handle; (55) the device is fabricated on a single substrate and is therefore more compact and easier to handle; (56) the device is fabricated on a single substrate and is therefore more compact and easier to handle; (57) the device is fabricated on a single substrate and is therefore more compact and easier to handle; (58) the device is fabricated on a single substrate and is therefore more compact and easier to handle; (59) the device is fabricated on a single substrate and is therefore more compact and easier to handle; (60) the device is fabricated on a single substrate and is therefore more compact and easier to handle; (61) the device is fabricated on a single substrate and is therefore more compact and easier to handle; (62) the device is fabricated on a single substrate and is therefore more compact and easier to handle; (63) the device is fabricated on a single substrate and is therefore more compact and easier to handle; (64) the device is fabricated on a single substrate and is therefore more compact and easier to handle; (65) the device is fabricated on a single substrate and is therefore more compact and easier to handle; (66) the device is fabricated on a single substrate and is therefore more compact and easier to handle; (67) the device is fabricated on a single substrate and is therefore more compact and easier to handle; (68) the device is fabricated on a single substrate and is therefore more compact and easier to handle; (69) the device is fabricated on a single substrate and is therefore more compact and easier to handle; (70) the device is fabricated on a single substrate and is therefore more compact and easier to handle; (71) the device is fabricated on a single substrate and is therefore more compact and easier to handle; (72) the device is fabricated on a single substrate and is therefore more compact and easier to handle; (73) the device is fabricated on a single substrate and is therefore more compact and easier to handle; (74) the device is fabricated on a single substrate and is therefore more compact and easier to handle; (75) the device is fabricated on a single substrate and is therefore more compact and easier to handle; (76) the device is fabricated on a single substrate and is therefore more compact and easier to handle; (77) the device is fabricated on a single substrate and is therefore more compact and easier to handle; (78) the device is fabricated on a single substrate and is therefore more compact and easier to handle; (79) the device is fabricated on a single substrate and is therefore more compact and easier to handle; (80) the device is fabricated on a single substrate and is therefore more compact and easier to handle; (81) the device is fabricated on a single substrate and is therefore more compact and easier to handle; (82) the device is fabricated on a single substrate and is therefore more compact and easier to handle; (83) the device is fabricated on a single substrate and is therefore more compact and easier to handle; (84) the device is fabricated on a single substrate and is therefore more compact and easier to handle; (85) the device is fabricated on a single substrate and is therefore more compact and easier to handle; (86) the device is fabricated on a single substrate and is therefore more compact and easier to handle; (87) the device is fabricated on a single substrate and is therefore more compact and easier to handle; (88) the device is fabricated on a single substrate and is therefore more compact and easier to handle; (89) the device is fabricated on a single substrate and is therefore more compact and easier to handle; (90) the device is fabricated on a single substrate and is therefore more compact and easier to handle; (91) the device is fabricated on a single substrate and is therefore more compact and easier to handle; (92) the device is fabricated on a single substrate and is therefore more compact and easier to handle; (93) the device is fabricated on a single substrate and is therefore more compact and easier to handle; (94) the device is fabricated on a single substrate and is therefore more compact and easier to handle; (95) the device is fabricated on a single substrate and is therefore more compact and easier to handle; (96) the device is fabricated on a single substrate and is therefore more compact and easier to handle; (97) the device is fabricated on a single substrate and is therefore more compact and easier to handle; (98) the device is fabricated on a single substrate and is therefore more compact and easier to handle; (99) the device is fabricated on a single substrate and is therefore more compact and easier to handle; (100) the device is fabricated on a single substrate and is therefore more compact and easier to handle.

⁸⁸ O.Wada, T.Sakurai and T.Nakagami, "Recent progress in Optoelectronic Integrated Circuits (OEIC's)", IEEE Journal of Quantum Electronics, Vol.22, pp.805-821, 1985.

⁸⁹ Y. Liou, U.Koren, S.Chandrasekhar, T.L.Koch, A.Shahar, C.A.Burrus, and R.P.Gnall, "Monolithic integrated InGaAsP/InP distributed feedback laser with Y-branching waveguide and a monitoring photodetector grown by metalorganic chemical vapor deposition", Applied Physics Letters, Vol.54, pp.114-116, 1989.

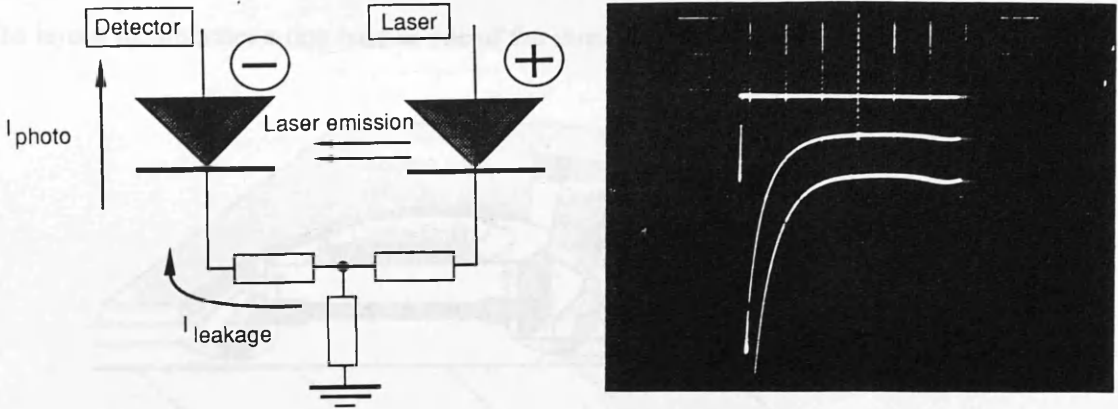


Figure 61. a) The electrical representation of the circuit and b) The I-V characteristic of the detector under reverse bias.

The horizontal scale in figure 61b) is 2V/div., the vertical scale is 0.05mA/div. and the parameter is a laser injection current of 0mA, 20mA and 40mA for the top, middle and bottom curve, respectively. The vertical shift between the curves and the decrease in breakdown voltage is due to the photocurrent created in the detector. This shows that the detector current is independent of the laser injection current and only depends on the laser emission, which makes it suitable for monitoring purposes. In order to verify this observation, one of the lasers was subjected to a high current pulse to destroy the laser junction and allow injection of current without emission of radiation. With this alteration, the vertical shift between the curves did not occur, which confirms that the coupling between the two devices is entirely optical.

Since the ring laser is symmetrical in respect to light travelling either clockwise or counterclockwise, modes in both directions are assumed to be identical. Therefore, one can be used to monitor the other, i.e. the mode travelling to the left in figures 9 and 60 is coupled into a fibre, whereas the one travelling to the right is used to monitor the device.

7.2 Optoelectronic integrated circuit (OEIC)

The motivation for fabricating a circuit containing both an optoelectronic and an electronic device derives from the underlying philosophy of the project, i.e. to demonstrate an integratable laser source and to combine it with other elements in a circuit. The long-term aim is to design a system consisting of a ring laser that feeds into a modulator which is driven by on-chip electronics. The problems arising from the optical part of such a circuit have already been discussed in the previous section; the present section aims to address the problem of combining optoelectronic and electronic components. Vertically integrating both devices and directly modulating the laser with a field-effect transistor was chosen as the simplest solution, a principle which is rather old⁹⁰ and serves primarily to getting familiar with the problems involved. The emphasis was placed on identifying a suitable design and a compatible fabrication procedure, since the two individual devices differ in size and layout and there is only a small overlap of processing steps.

⁹⁰ O.Wada, T.Sakurai, and T.Nakagami, "Recent progress in Optoelectronic Integrated Circuits (OEIC's)", IEEE Journal of Quantum Electronics, Vol.22, pp.805-821, 1986.

7.2.1 Circuit design

The layout incorporates a ring laser as one of the three ports of the FET, the drain.

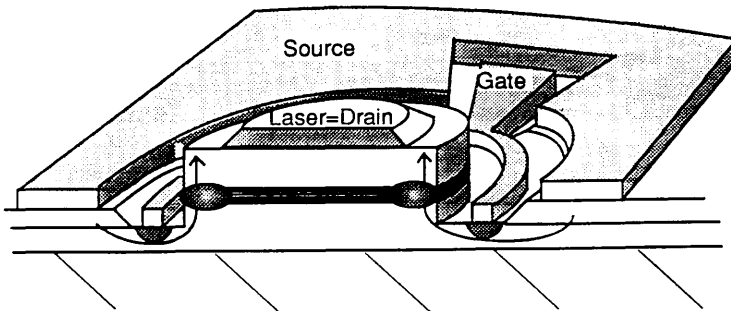


Figure 62. Ring laser OEIC, comprising the laser as the drain of the field-effect transistor.

The gate forms a Schottky-contact with the underlying n-type material (metal-semiconductor field effect transistor, MESFET), a structure that has a very low gate capacitance, which is one of the prerequisites for high-speed operation. The gate is placed around the circular drain (drain = laser) and a negative gate bias with respect to the source controls the current flow from the source to the drain by modulating the depletion region under the gate. Incorporating the laser into the FET, rather than having the two separate on adjacent sites on the chip, has the advantage of reducing the parasitic resistance and capacitance of the circuit thus ensuring high frequency performance. The device is "normally-on", i.e. the channel is conducting if no signal is on the gate. A gatelength of around $1\mu\text{m}$ was chosen to ensure an operating bandwidth of beyond 10GHz, so that the relaxation oscillations of the laser⁹¹ are limiting the high-speed operation.

The FET is operated in drain-source current saturation, so the electric field between source and drain is strong enough to accelerate the carriers in the channel up to their saturation velocity and the current only depends on the gate bias. This mode of operation determines the size of the source-drain gap. The gap has to be small enough to establish a sufficiently strong field for saturation at a low voltage, and big enough to ensure a successful gate alignment. A gap of, say $5\mu\text{m}$, requires a voltage of 2-3 V for the carriers to saturate. Assuming that the gate is centred between source and drain, and that a negative bias of -2V is necessary to pinch off the conducting channel, a voltage of around -4V is established between gate and drain. This value leads to a negligible leakage current of the gate Schottky contact, since a reverse voltage of 5-10V can be tolerated before the gate breaks down. A source-drain gap of $5\mu\text{m}$ is thus a realistic value that should also allow reliable gate alignment considering the size and proximity of the laser mesa.

7.2.2. Material design

Since the requirements for an integrated ring laser are similar to a standard device, the material design developed in section 3.2 was chosen for the laser structure.

⁹¹ A.Yariv, "Optical Electronics", 4th ed., p.578, HRW Sanders, 1991.

7.Integration

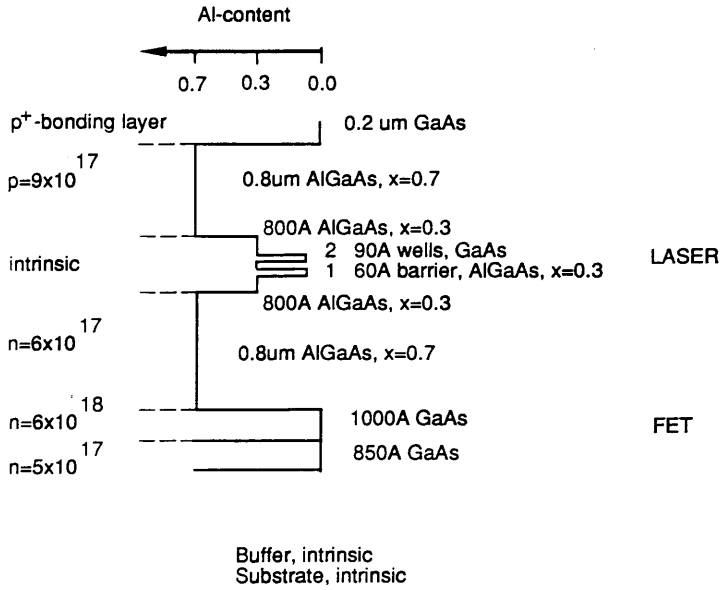


Figure 63. The material design for vertically integrating a ring laser and an FET.

The thin cladding of the structure ($1\mu\text{m}$) is advantageous for the fabrication of the field-effect transistor, because the lithography for the gate is performed in close proximity to the laser mesa. This leads to a total mesa height of less than $2\mu\text{m}$.

The substrate is semi-insulating, which is required for the operation of the FET, so placing it below the laser is the most logical approach; if the FET would have been placed on top and isolated with a buffer layer, a capacitance between the two active layers would have been created that limits high-frequency operation. It is also important to have a distinct composition step at the interface between the two devices, so selective etches that do not attack the FET-layer can be used to remove the laser cladding.

The FET consists of two layers, the highly doped ($2 \times 10^{18}/\text{cm}^3$) contact layer and the lower doped ($5 \times 10^{17}/\text{cm}^3$) active layer. Devices fabricated on an identical structure previously operated successfully up to a frequency of beyond 50GHz for $0.2\mu\text{m}$ gate length. Thus, a known design was used to ensure that successful fabrication would be achieved. In order that the laser operated above threshold and that a minimal gate bias was required to pinch off the current, the FET saturation current at zero volts gate bias was chosen around 150mA per millimeter device width, i.e. 12mA for the $75\mu\text{m}$ trimming contacts and 50mA for the $300\mu\text{m}$ circumference of the laser. The contact layer and part of the active layer were removed by wet etching until this saturation current was achieved. I_{sat} is given by the amount of available carriers and the dimensions of the conducting channel,

$$I_{sat} = e N w h v_{sat} \quad [7.16]$$

e being the fundamental charge, N the doping concentration, w and h the width and height of the channel, respectively, and v_{sat} the saturation velocity. Using the parameters of the material design as shown above, $300\mu\text{m}$ for the width of the channel and a saturation velocity of 10^7cm/s ⁹², yield a value of $I_{sat} = 240\text{mA}$, so 75% of the thickness of the active layer must be removed for the target saturation current.

⁹² S.M.Sze, "Semiconductor Devices - Physics and Technology", p.63, John Wiley&Sons, 1985.

7.2.3.Fabrication

The fabrication of a field-effect transistor encircling the ring laser is shown in the following sketch.

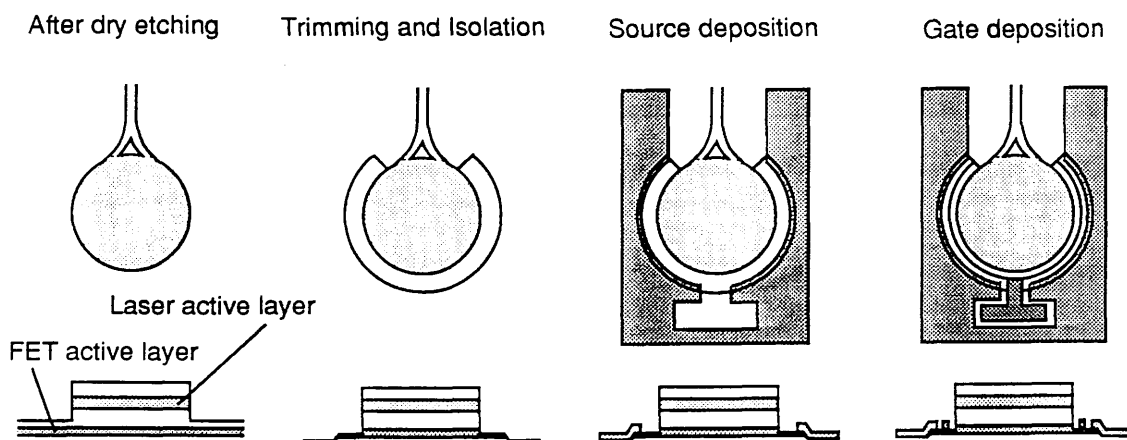


Figure 64. Turning an ordinary ring laser into an integrated ring laser - field-effect transistor circuit.

1. The etch depth of the laser must be carefully controlled so that a thin layer of AlGaAs cladding remains. Removing this layer with a selective wet etch of $HF:H_2O$, 1:10 is expected to remove any residual dry-etch damage.
2. A set of two $75\mu\text{m} \times 75\mu\text{m}$ contacts is deposited elsewhere on the sample to monitor the saturation current in the following trimming operation. These contacts are isolated by trenches to avoid distortion of the results by fringe currents.
3. The thickness of the active layer is trimmed by wet etching to a target saturation current using 4:1:20 $H_2SO_4:H_2O_2:H_2O$ at 6°C . The saturation current, according to [7.16], depends on the length of the contacts, so it is four times higher for the laser ($300\mu\text{m}$ circumference) than for the trimming contacts ($75\mu\text{m}$ length).
4. The active layer is isolated by another wet etching step, so the only path for the current between the source and the drain is underneath the gate.
5. The source contact, AuGeNi, is deposited and annealed to form a ohmic contact.
6. Finally, the Ti-Au gate Schottky diode contact is deposited. Because of the small gate length ($\leq 1\mu\text{m}$) an exposure test on identical devices is required beforehand to determine the necessary exposure dose.

A finished device is shown in the following micrograph, emphasizing the position and size of the gate between the laser and the source contact. The gate is widened at the end to improve its adhesion.

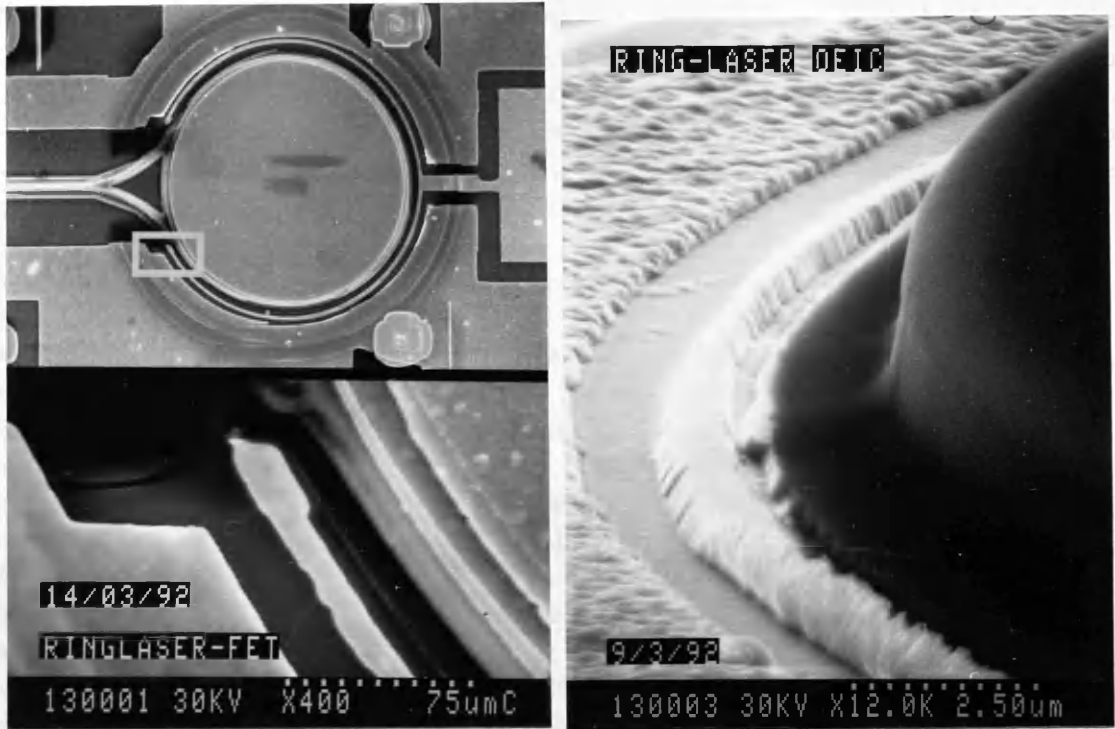


Figure 65. Finished ring laser - field-effect transistor OEIC with a $1\mu\text{m}$ gate length.

The state of the alignment marks is noteworthy: Due to partial exposure and subsequent deposition or etching during 7 levels of lithography, they have been substantially transformed and barely resemble their original shape. This turns the alignment of the gate into a very skillful operation.

Several problems were encountered that mostly derived from prior processing of the laser:

1. The HF-based wet etch to remove the remaining AlGaAs cladding layer also attacks the silicon nitride passivating film of the laser. Therefore, it was necessary to coat the sidewalls with a layer of polyimide, which can be identified as the dark ring on the outer annulus of the laser in the above micrograph.
2. Any dry etching that is performed on the exposed active layer of the FET, such as oxygen-ashing to clear off polyimide, alters the wet etching properties of the material, so that weak etches such as the standard 4:1:100 solution of the $\text{H}_2\text{SO}_4:\text{H}_2\text{O}_2:\text{H}_2\text{O}$ etch can not be used. Stronger concentrations, such as 4:1:20, require cooling to $5\text{-}6^\circ\text{C}$ to remain controllable, but still etch much faster than the standard solution, so reliable etching to the target saturation current is more difficult.
3. Another problem occurred during the second step shown in figure 64, trimming. For a reason not yet understood, the saturation current between the separate $75\mu\text{m} \times 75\mu\text{m}$ contacts was much lower than on the real devices. 15mA was measured on the trimming contact and well above 100mA on the rings, which cannot be explained by the geometrical difference only. Further etching was necessary after the source contact had been deposited, to reduce the saturation current to below 100mA . The strong etching solution that was necessary to penetrate the damaged material caused a significant amount of undercut, so material was removed underneath the source contact. This led to a complete disconnection of the source for some devices and to a very high source resistance for others, which is the main cause for the poor performance seen so far.

4. A problem that is independent of the FET-process occurred in this particular batch early in the fabrication procedure: the HCl solution (1:1, $HCl:H_2O$) that is used to remove the Ni-Cr etch mask also attacked the laser cladding and exposed the outside of the active layer of the laser. This substantially increased the loss of the structure precluding laser action. The fabrication was continued at that stage, because the devices still operated as luminescent diodes and the influence of the gate could still be demonstrated.

7.2.4 Broad area lasers

In order to assess the material and to create a reference for the results of the ring laser-FET circuit, both individual lasers and FET's were fabricated. Broad area lasers were fabricated on two different material types comprising the same laser structure, one on n^+ substrate and the other on semi-insulating substrate including the two FET-layers. The lasers on n^+ substrate had threshold current densities in the range of $200-300 A/cm^2$ for $400-800 \mu m$ long devices. The figures of merit derived from these results are $\alpha_i \leq 10 cm^{-1}$ for the internal loss and $\eta_i \geq 0.9$ for the internal quantum efficiency, both of which are very good values. The lasers on semi-insulating substrate had threshold current densities in the order of $100 A/cm^2$, which is due to the carrier crowding effect⁹³ caused by the contact configuration. The bottom contact is on one side of the laser, and the field between the two contacts leads to a carrier accumulation on that side, so lasing starts in a thin filament rather than across the whole device. Therefore, the results are distorted and it is very difficult to derive the figures of merit. However, it is justified to expect that the performance of the two materials is similar.

7.2.5 Field effect transistors

The FET's were fabricated using a standard layout with a source-drain gap of $3.5 \mu m$ and a gate length of $0.5 \mu m$. To expose the FET - layers, the laser material had been removed by dry etching followed by diluted HF, which terminates on GaAs. The devices thus fabricated display textbook-like behaviour as shown in the following graphs.

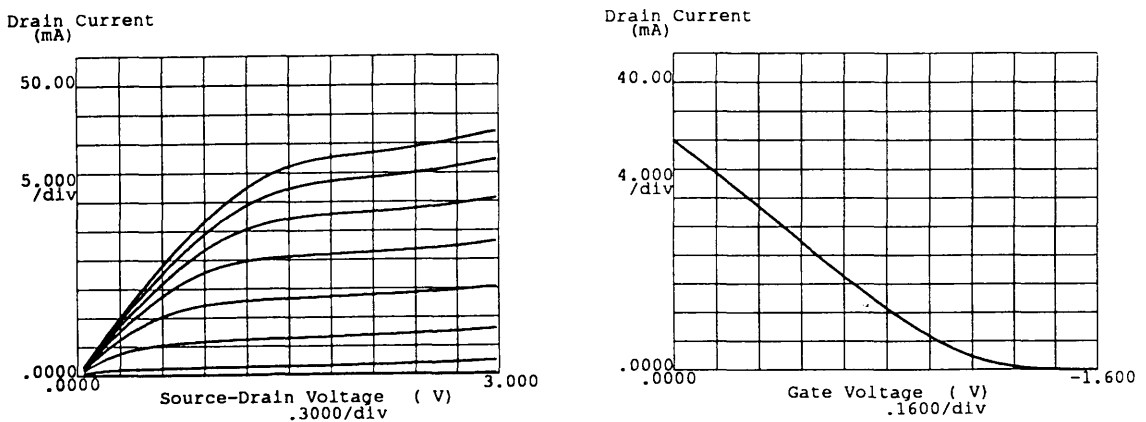


Figure 66. Source-drain current characteristic (left) and its dependence on the gate bias (right).

The source-drain current saturates at around 40mA with a source-drain voltage of 1.5-1.8V. A gate bias of 1.3V is sufficient to pinch off this current, so the device operates as expected. The fact that the current can be pinched off completely with a relatively low gate bias indicates that the dopants are well confined within the active layer of the FET and have not diffused into the underlying

⁹³ C.P.Lee, S.Margalit, and A.Yariv, "Double-heterostructure GaAs-GaAlAs injection lasers on semi-insulating substrates using carrier crowding", Applied Physics Letters, Vol.31, pp.281-282, 1977.

7. Integration

substrate. Interdiffusion is a problem that can occur during the growth of this particular material design where the FET layers are grown first. During the subsequent growth of the laser, the substrate is held at high temperature for an extended period of time (the laser is more than ten times thicker than the FET), so it is likely that carriers diffuse into the substrate and increase the width of the conducting channel. This increases the gate bias that is required for pinch-off, which, as shown above, is not the case in the present material.

The preliminary measurements thus showed that both the laser and the FET had been designed properly and that the material is suitable for the integrated ring laser -FET circuit.

7.2.6 Ring laser OEIC

Due to the problems described in the previous section, the integrated circuit did not repeat the good results that were achieved with the individual devices. This is demonstrated in the following graphs, where the modulation of the laser current and the power output is shown to be rather poor, only 10% modulation on the gate bias was achieved.

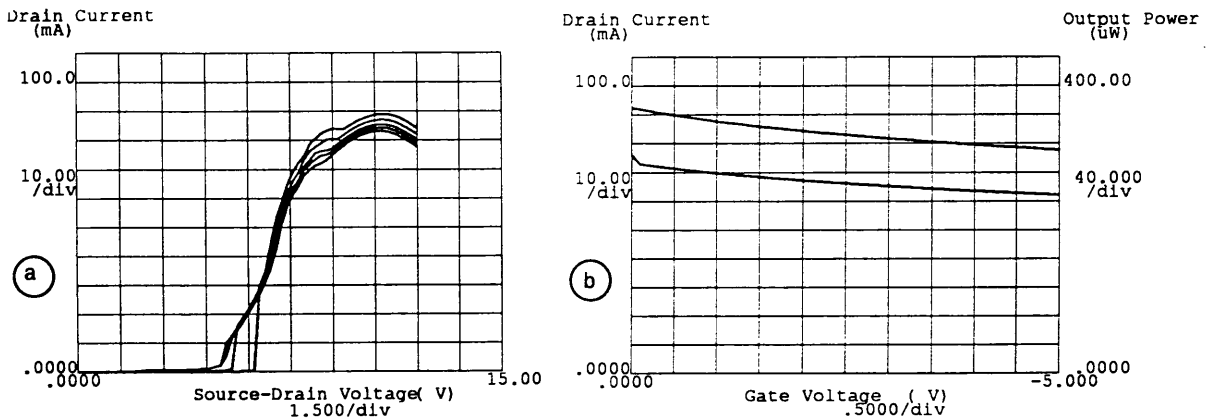


Figure 67. Source-drain current (a) and laser current and output vs. gate bias (b), the upper curve referring to the left scale.

The source-drain current, i.e. the current through the laser, saturates at 10-12V, although the source-drain gap is only 50% larger than for the devices of figure 66. This observation indicates a high source resistance. A sketch of the equivalent circuit illustrates the problem:

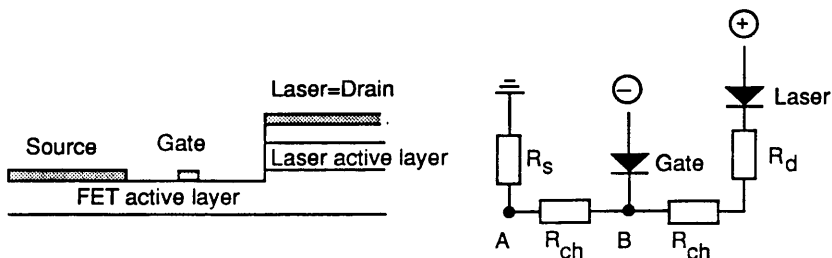


Figure 68. Sketch of the FET - arrangement and the equivalent circuit.

If the source resistance R_s is high compared to the channel resistance $2xR_{ch}$ and the drain resistance R_d , most of the source-drain voltage drops across R_s and a high positive potential is established at point A. Since R_{ch} is small compared to R_s , most of that potential is also present at point B. This leads to a high voltage across the negatively biased gate, which is beyond the breakdown of the Schottky contact and causes leakage. The gate leakage prevents the build-up of a sufficient gate

7.Integration

depletion region which causes the poor modulation displayed in figure 67b). The following figure shows the gate diode characteristic to illustrate the reverse leakage beyond -4V.

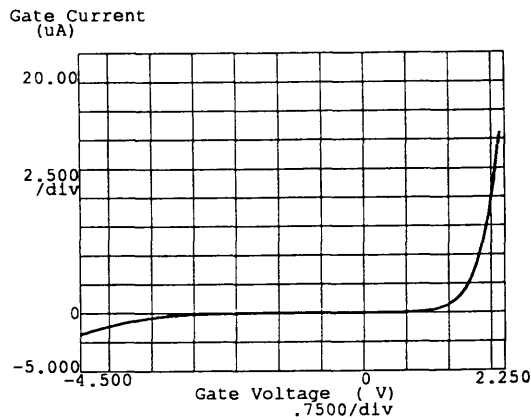


Figure 69. I-V characteristic of the gate diode, indicating the reverse breakdown at 4-5V.

Overall, the results demonstrate that the material has been properly designed, although there is space for improvement, and the fabrication is feasible. The problems that occurred are not seen as insurmountable hurdles to the successful completion of the circuit and are expected to be resolved in a subsequent batch.

8. Conclusion

8.1 Ring laser

Semiconductor ring lasers have conclusively shown that they offer an alternative to straight lasers and that they can be seriously considered for future applications in optoelectronic integrated circuits. The lowest threshold current that was achieved for a $100\mu\text{m}$ diameter ring laser structure is 12.5mA , which is owing to very smooth sidewalls with low scattering loss, a silicon nitride coating to suppress the non-radiative recombination current and to further reduce the scattering loss, and shallow etching on the inside of the pillbox to enhance the current confinement. The fringe current, i.e. the current that flows beyond the laser filament without pumping the laser mode, was calculated and found to constitute 50-80% of the current consumption at threshold, so a large potential of further threshold current reduction has been identified. This result has already been implemented in the latest material design where the cladding thickness was reduced from $2\mu\text{m}$ to $1\mu\text{m}$, and initial tests have shown excellent figures of merit ($\alpha_i < 10\text{cm}^{-1}$, $\eta_i > 0.9$) for this material. A further improvement of the ring laser performance can thus be expected.

Analyzing the threshold current density yielded a value of $3\text{dB}/360^\circ$ for the excess scattering loss due to the bend, which compares favourably to other results available in the literature. The radius-dependence of the scattering loss was investigated by threshold current measurements and compared to a theoretical model based on scattering of the wavefraction that interacts with the resonator sidewall. It was found that the loss is independent of the radius in the investigated range of $30\text{-}150\mu\text{m}$, an effect which can be understood considering the position of the optical mode with respect to the sidewall; the loss per unit length is higher for smaller radii, since the interaction is stronger and the field is pushed further into the wall. A smaller radius has a shorter bend, however, so the loss per unit angle remains constant. This result clearly indicates that scattering is the dominant loss mechanism, since radiation loss would show a much stronger radius-dependence.

8.1.1 Fabrication issues

The low loss was only possible by optimizing the electron-beam lithography process, where the problem of the step-like exposure, "pixelation", has been solved, and smooth curvatures have been obtained. Although electron-beam lithography is a very useful tool for research purposes, optical methods are preferable if the devices are to be exploited commercially. Therefore, compatibility with optical lithography was maintained as much as possible, which is shown in the smallest feature of the 12.5mA threshold current device, which is $4\mu\text{m}$ wide.

The improvements presented have the drawback of incorporating a number of processing steps into the fabrication sequence. For example, the very first pillbox ring laser had been built using a single mask level, the most sophisticated version needs five, and the integrated laser - FET circuit requires nine levels of lithography. The degree of complexity is obviously a disadvantage, because every fabrication step can introduce defects that lower the yield of the batch. Simplicity is one of the assets of the ring laser geometry, because very sophisticated and costly processes such as overgrowth and ion implantation have been successfully avoided so far. However, further simplification is desirable to keep the ring laser attractive.

A very promising concept in that respect is to use strip-loaded guiding. Cw operation of quarter-ring lasers with radii as small as $300\mu\text{m}$ was demonstrated using this guiding mechanism, requiring only three levels of lithography. Since a strip-loaded structure supports very few transverse modes, true single-mode operation is possible. A further advantage of such a structure is that it avoids the problems that arise from etching through the active layer, particularly device degradation. This problem has been addressed in a standard ring laser by applying a passivation coating of silicon

nitride. Further investigation of this process and lowering of the operating temperature might result in stable long-term operation of the devices. However, it is questionable if the stringent lifetime requirements of commercial systems can ever be met by an etched ring laser. Therefore, leaving the active layer buried, as in the case of strip-loaded devices, or overgrowing the junction altogether, might be the only answer in the long run.

8.1.2 Output coupling

Other aspects of ring lasers have been identified that require further investigation, such as the Y-junction between the ring resonator and the coupling waveguide. Measurements have shown that the temperature increase during operation leads to a lateral mode displacement that causes kinks in the L-I curve. Consequently, reducing the operating temperature by thinning the substrate and introducing thermoelectric cooling would improve the operation characteristic. However, this would not solve the inherent problem of the curved Y-junction, i.e. the dependence of the coupling ratio and the feedback on the mode position. Also, mode competition between the forward and the counterpropagating modes in the resonator have to be taken into account. This is underlined by the low differential quantum efficiency ($\eta_d = 0.02-0.04$), which is caused by the current consumption of modes that are not coupled out at all or only inefficiently, because the resonator scattering loss of about 3dB is too small to explain such a low value. These considerations show that the curved Y-junction is a major problem of ring lasers which, in order to be better understood, requires an in-depth study taking into account all effects involved. The operation of other devices, such as two coupled ring resonators, would also benefit from an improved coupling geometry.

A racetrack-type design, i.e. two semicircles joined by a straight section, could solve the problem by avoiding the curved Y-junction altogether. Using a strip-loaded geometry and a directional coupler along the straight waveguide would enable more controlled coupling. Racetrack-type devices have already been fabricated, but the coupling loss between the straight and curved sections prevented low threshold current operation. However, the loss can be reduced by introducing an offset and joining the respective waveguide sections so that the overlap between the field distributions is maximized.

8.1.3 The next generation

Strip-loaded ring lasers have been proposed to solve the problems of fabrication complexity, device degradation and output coupling. The disadvantage of strip-loaded devices is their size; they operate down to radii as low as $300\mu\text{m}$, and possibly lower, but the diameter of a prospective device is still impractical, particularly if an array is envisaged. The size can be reduced by lowering the refractive index at the outside of the ring, using a process such as capped annealing to disorder the material, a technique which has recently been developed in the department. Capped annealing involves rapid thermal processing, and leads to localized disordering of the material in places where it has not been protected by a dielectric film such as silicon nitride. The disordered section has a lower refractive index and a higher bandgap than the original quantum well material. The latter effect can also be used to produce low loss waveguides as an alternative to the double-waveguide approach described here.

8.1.4 Conclusion on ring lasers

Most of the remaining problems are likely to be solved, or viable alternatives have been proposed; ring lasers have thus been demonstrated as integratable laser sources, the first task that was raised in the introduction. The second and third task, the integration of multiple components in a photonic and optoelectronic circuit, has also been achieved.

8.2 Integration

Despite the problems that ensue from the complicated material structure and fabrication sequence, both a photonic integrated circuit, consisting of a ring laser, a low loss waveguide and a monitoring photodetector, and an optoelectronic integrated circuit, consisting of a ring laser controlled by a field-effect transistor, were demonstrated. Vertical integration was used in both cases.

8.2.1 Photonic integration

The incorporation of a low-loss waveguide was achieved by placing it underneath the laser waveguide, using directional coupling to transfer the power between the two. This simple principle allows one to generate the whole structure in a single epitaxial growth, which is a considerable advantage over other schemes for photonic integration. However, the present design is not ideal, because the waveguide extracts too much power from the laser, as shown by the low optical confinement factor of $\Gamma_w = 1.4\%$. Also, the laser has to compensate for the loss of the additional waveguide, which leads to a total gain requirement of $g > 100\text{cm}^{-1}$ and causes a high threshold current and second quantized state operation. The laser section in future double-waveguide designs will have to provide more gain by including further quantum wells, and the waveguide section has to be less strongly coupled to increase the Γ_w of the laser.

The detector uses the same pn-junction as the laser and operates under reverse bias, the two being separated by an unpumped waveguide section. The detector current was found to be independent of the laser current and to respond only to the laser emission, i.e. the reverse leakage of the pn junction was very low.

Using the detector as a modulator by forward biasing the junction and changing its transparency with current injection was not successful. Since the resistance of the pn-junction under forward bias is very low, cross-talk on the common n^+ -conducting substrate was significant and the two devices influenced each other electrically. This shows the importance of electrical isolation between the components of such a circuit, which can be improved in a future design by using semi-insulating substrate.

A different concept would use an electric field-induced effect for modulation, since it is inherently faster than carrier injection. This would involve incorporating quantum wells into the waveguide and locally creating a pn-junction that would be reverse biased to generate an electric field across the waveguide. The electric field would change the absorption edge of the quantum wells and thus modulate the laser emission. Zinc-diffusion, which can be performed at low temperatures (600° , 15min) could be used to locally transform the n-type material into p-type, thus creating a pn-junction. The material requirements for this circuit would not prevent any of the other functions, i.e. the absorption edge of the quantum wells would be chosen such that low loss was ensured at the laser wavelength and the laser could still be operated as a detector under reverse bias. Thus, the next generation of double-waveguide material can potentially include all important functions of a photonic integrated circuit. However, the material design will be a challenge, since predicting all material properties accurately with numerical models might prove difficult.

8.2.2 Optoelectronic integration

An optoelectronic integrated circuit was realized by positioning the FET below the laser, on semi-insulating substrate, and using the laser as one of the three ports of the FET. This structure is ideally suited to study the degree of process and design compatibility between the two devices, such as the limitations on the source-drain gap of the FET imposed by the dimensions of the laser mesa. The poor performance seen so far has been traced down to the fabrication and is not seen as a

8. Conclusion

principle problem of the whole concept. However, it is worthwhile to consider alternatives, such as separating the two devices rather than having the ring laser as an integral part of the transistor; also, using lower doping for the active layer of the FET would result in more fabrication tolerance and less leakage of the gate contact.

Ideally, a design should be devised that consists of multifunctional layers shared between the laser and the transistor to yield a planar circuit, which is a prerequisite for mass-production using optical lithography. However, such an approach is very demanding and only very few attempts have been reported in the literature so far.

8.3 Outlook

Most of the problems towards building a fully integrated optoelectronic circuit, i.e. one with a laser feeding through a low-loss waveguide into a modulator that is driven by on-chip electronics, including a detector that stabilizes the laser via a feedback-loop, have been discussed, and solutions have been demonstrated or proposed. The successful completion of such a circuit involving a ring laser would be a milestone towards more widespread use of optoelectronic circuitry, because unlike currently existing technology, it would be relatively simple to build and thus be more attractive to manufacture.

9. References

9.1 Publications and conference contributions arising from this work

1. T.Krauss and P.J.R.Laybourn, "Semiconductor ring lasers without an inner boundary", Conference on Lasers and electro-optics (CLEO), Paper CTh11, 1990.
2. T.Krauss, P.J.R.Laybourn, and J.Roberts "Cw operation of semiconductor ring lasers", Electronics Letters, Vol.26, pp.2094-2096, 1990.
3. T.Krauss and P.J.R.Laybourn, "Monolithic integration of a semiconductor ring laser and a monitoring photodetector", Proceedings SPIE on Integrated Optical Circuits, Vol.1583-47, 1991.
4. T.Krauss and P.J.R.Laybourn, "Strip-loaded GaAs/AlGaAs quarter-ring lasers", presented on Semiconductor and Integrated Optoelectronics (SIOE), Cardiff, 1992.
5. T.Krauss and P.J.R.Laybourn, "Very low threshold current operation of semiconductor ring lasers", submitted to IEE Proceedings, Pt.J (Optoelectronics), 1992.

9.2 Alphabetical list of references

The numbers in brackets refer to the footnotes in the text.

- M.W.Austin, "GaAs/GaAlAs curved rib waveguides", IEEE Journal of Quantum Electronics, Vol.18, pp.795-800, 1982. (58)
- N.Bar-Chaim, K.Y.Lau, M.A.Mazed, M.Mittelstein, Se Oh, J.E.Ungar, and I.Ury, "Half-ring geometry quantum well GaAlAs lasers", Applied Physics Letters, Vol.57, pp.966-967, 1990. (14)
- A.Behfar-Rad, S.S.Wong, J.M.Ballantyne, B.A.Soltz, and C.M.Harding, "Rectangular and L-shaped GaAs/AlGaAs lasers with very high quality etched facets", Applied Physics Letters, Vol.54, pp.493-495, 1989. (1, 75)
- A.Behfar-Rad, J.R.Shealy, S.R.Chinn, and S.S.Wong, "Effect of cladding layer thickness on the performance of GaAs-AlGaAs graded index separate confinement heterostructure single quantum-well lasers", IEEE Journal of Quantum Electronics, Vol.26, pp.1476-1480, 1990. (42)
- H.Blauvelt, N.Bar-Chaim, D.Fekete, S.Margalit, and A.Yariv, "AlGaAs lasers with micro-cleaved mirrors suitable for monolithic integration", Applied Physics Letters, Vol.40, pp.289-291, 1982. (2)
- P.W.M.Blom, J.E.M.Haverkort, and J.H.Wolter, "Optimization of barrier thickness for efficient carrier capture in graded-index and separate-confinement multiple quantum well lasers", Applied Physics Letters, Vol. 58, pp.2767-2769, 1991. (38)
- D.Botez, L.Figueroa, and S.Wang, "Optically pumped GaAs - Ga_{1-x}Al_xAs half-ring laser fabricated by liquid-phase epitaxy over chemically etched channels", Applied Physics Letters, Vol.29, pp.502-504, 1976. (8)
- J.A.Carra, L.A.D'Asaro, J.C.Dyment, G.J.Herskowitz. "GaAs Lasers utilizing light propagation along curved junctions", IEEE Journal of Quantum Electronics, Vol.6, pp.367-371, 1970. (7)
- H.C.Casey, M.B.Panish, "Heterostructure Lasers", Pt.A, p.31, Academic Press, 1978. (69)
- J.H.Campbell and P.M.Fauchett, "Detection of a monolayer of As by Raman scattering during photoluminescence degradation of GaAs", CLEO 90, paper CWB7. (71)
- C.C.Chang, P.H.Citrin, and B.Schwartz, "Chemical preparation of GaAs surfaces and their characterization by Auger electron and x-ray photoemission spectroscopies", Journal of Vacuum Science and Technology, Vol.14, pp.943-952, 1977. (51)

9. References

- W.Chen, "Thermal problems in semiconductor ring lasers", M.Sc. thesis, Glasgow University, 1989. (23, 67)
- S.P.Cheng, F.Brillouet, and P.Correc, "Design of quantum well AlGaAs-GaAs stripe lasers for minimization of threshold current-application to ridge structures, IEEE Journal of Quantum Electronics, Vol.24, pp.2433-2440, 1988. (37)
- D.G.Deppe and N.Holonyak,Jr., "Atom diffusion and impurity induced layer disordering in quantum-well semiconductor heterostructures", Journal of Applied Physics, Vol.64, pp.R93-R113, 1988. (17)
- W.P.Dumke, "Current thresholds in stripe-contact injection lasers", Solid-state Electronics, Vol.16, pp.1279-1281, 1973. (56)
- W.J.Gibbs,"Conformal transformations", The British Thomson-Houston Co. Ltd, 1958. (26)
- K.C.Gupta, R.Garg, and I.J.Bahl, "Microstrip lines and slotlines", Artech 1979. (80)
- R.N.Hall, G.E.Fenner, J.D.Kingsley, T.J.Soltys, and R.O.Carlson, "Coherent light emission from GaAs p-n junctions", Physical Review Letters, Vol.9, pp.366-368, 1962. (4, 32)
- M.Heiblum and J.H.Harris, "Analysis of Curved Optical Waveguides by Conformal Transformation", IEEE Journal of Quantum Electronics, Vol.11, pp.75-83, 1975. (25)
- C.H.Henry, R.A.Logan, and K.A.Bertness, "Spectral dependence of the change in refractive index due to carrier injection in GaAs lasers", Journal of Applied Physics, Vol.52, pp.4457-4461, 1981. (84)
- J.P.Hohimer, D.C.Craft, G.R.Hadley, G.A.Vawter, and M.E.Warren, "Single-frequency continuous-wave operation of ring resonator diode lasers", Applied Physics Letters, Vol.59, pp.3360-3362, 1991. (64)
- J.P.Hohimer, D.C.Craft, G.R.Hadley, and G.A.Vawter, "Cw room-temperature operation of Y-junction semiconductor ring lasers", Electronics Letters, Vol.28, pp.374-375, 1992. (28)
- R.G.Hunsperger, "Integrated Optics: Theory and Technology", 2nded., Series in Optical Sciences 33, p.61, Springer 1984. (41)
- A.F.Jeziarski and P.J.R.Laybourn, "Integrated semiconductor ring lasers", IEE Proceedings, Vol.135, Pt.J, pp.17-24, 1988. (12, 21)
- A.F.Jeziarski and P.J.R.Laybourn, "Polyimide embedded semiconductor ring lasers", Proceedings SPIE No. 1141, pp.7-11, 1989. (22, 49)
- A.F.Jeziarski, "Semiconductor ring lasers", Ph.D. Thesis, Glasgow University, 1990. (16, 20, 70)
- T.Krauss, P.J.R.Laybourn, and J.Roberts, "Cw operation of semiconductor ring lasers", Electronics Letters, Vol.26, pp.2095-2097, 1990. (13)
- A.Kurobe, H.Furuyama, S.Naritsuka, N.Sugiyama, Y.Kokubun, and N.Nakamura, "Effects of well number, cavity length, and facet reflectivity on the reduction of threshold current of GaAs/AlGaAs multiquantum well lasers", IEEE Journal of Quantum Electronics, Vol.24, pp.635-639, 1988. (35)
- C.P.Lee, S.Margalit, and A.Yariv, "Double-heterostructure GaAs-GaAlAs injection lasers on semi-insulating substrates using carrier crowding", Applied Physics Letters, Vol.31, pp.281-282, 1977. (93)
- D.L.Lee, "Electromagnetic principles of Integrated Optics", pp.220-224, J.Wiley&Sons, 1986. (79, 81)
- A.S.-H. Liao and S.Wang, "Semiconductor injection lasers with a circular resonator", Applied Physics Letters, Vol.36, pp.801-803, 1980. (10, 65)

9. References

- Y.Liou, U.Koren, S.Chandrasekhar, T.L.Koch, A.Shahar, C.A.Burrus, and R.P.Gnall, "Monolithic integrated InGaAsP/InP distributed feedback laser with Y-branching waveguide and a monitoring photodetector grown by metalorganic chemical vapor deposition", *Applied Physics Letters*, Vol.54, pp.114-116, 1989. (89)
- Y.H.Lo, P.Grabbe, R.Bhat, J.L.Gimlett, P.S.D.Lin, A.S.Grozd, M.A. Koza, and T.P.Lee, Bellcore, "Very high speed 1.5 μ m DFB OEIC transmitter", *CLEO 90*, Paper WWM1. (19)
- E.A.J.Marcatili, "Bends in optical dielectric guides", *Bell Systems Technical Journal*, Vol.48, pp.2103-2132, 1969. (6, 73)
- N.Matsumoto and K.Kumabe, *Japanese Journal of Applied Physics*, Vol.16, p.1395, 1977. (9)
- P.McIlroy, A.Kurobe, and Y.Uematsu, "Analysis and application of theoretical gain curves to the design of multi-quantum-well lasers", *IEEE Journal of Quantum Electronics*, Vol.21, pp.1958-1963, 1985. (36)
- J.G.Mendoza-Alvarez, F.D.Nunes, and N.B.Patel, "Refractive index dependence on free carriers for GaAs", *Applied Physics Letters*, Vol.51, pp.4365-4367, 1980. (82)
- C.Millar, "Evanescent field coupling of thin film and fibre optical waveguides", Ph.D. thesis, Glasgow University, 1976. (85)
- M.Mittelstein, Y.Arakawa, A.Larsson, and A.Yariv, "Second quantized state lasing of a current pumped single quantum well laser", *Applied Physics Letters*, Vol.49, pp.1689-1691, 1986. (86)
- M.I.Nathan, W.P.Dumke, G.Burns, F.H.Dill, and G.J.Lasher, "Stimulated emission of radiation from GaAs p-n junctions", *Applied Physics Letters*, Vol.1, pp.62-64, 1962. (5, 33)
- E.G.Neumann, "Curved dielectric optical waveguides with reduced transition losses", *IEE Proceedings*, Vol.129, Pt.H, pp.278-280, 1982. (29)
- N.Ogasawara, R.Ito, and R.Morita, "Linewidth enhancement factor in GaAs/AlGaAs multi-quantum well lasers", *Japanese Journal of Applied Physics*, Vol.24, pp.L519-L521, 1985. (83)
- S.Oku, M.Okayasu, and M.Ikeda, "Low-threshold cw operation of square-shaped semiconductor ring lasers (orbiter lasers)", *IEEE Photonics Technology Letters*, Vol.3, pp.588-590, 1991. (15, 60, 66, 74)
- T.L.Paoli, "A new technique for measuring the thermal impedance of junction lasers", *IEEE Journal of Quantum Electronics*, Vol.11, pp.498-503, 1975. (68)
- W.Patrick, W.S.Mackie, S.P.Beaumont, and C.D.W.Wilkinson, "Polyimide as a negative electron resist and its application in crossovers and metal on Polymer mask fabrication", *Journal of Vacuum Science and Technology B*, Vol.4, pp.390-393, 1986. (50)
- S.J.Pearson, J.W.Corbett, and T.S.Shi, "Hydrogen in crystalline semiconductors", *Applied Physics A*, Vol.43, pp.153-195, 1987. (47, 72)
- E.C.M.Pennings, J.van Schoonhoven, J.W.M. van Uffelen, and M.K.Smit, "Reduced bending and scattering losses in new optical 'double-ridge' waveguide", *Electronics Letters*, Vol.25, pp.746-748, 1989. (59, 63)
- Lord Rayleigh, "The problem of the whispering gallery", *Scientific Papers*, Cambridge University, Vol.5, pp.617-620, 1912. (3)
- H.Ribot, P.Sansonetti, J.Brandon, M.Carre, L.Menigaux, R.Azouldy, and N.Bouadma, "Monolithic integration of GaAs/GaAlAs buried heterostructure orthogonal facet laser and optical waveguide", *Applied Physics Letters*, Vol.54, pp.475-477, 1989. (78)
- S.Sheem and J.R.Whinnery, "Guiding by single curved boundaries in integrated optics", *Wave Electronics*, Vol.1, pp.61-68, 1974. (24)

9.References

- M.S.Stern, P.C.Kendal, R.C.Hewson-Browne, P.N.Robson, and D.A.Quinney, "Scattering loss from rough sidewalls in semiconductor rib waveguides", *Electronics Letters*, Vol.25, pp.1231-1232, 1989. (48, 61)
- S.M.Sze, "Semiconductor Devices - Physics and Technology", p.63, John Wiley&Sons, 1985. (92)
- S.M.Sze, "VLSI Technology", 2nd ed., p.263, McGraw-Hill, 1988. (46)
- G.H.B.Thompson and P.A.Kirkby, "(GaAl)As lasers with a heterostructure for optical confinement and additional heterojunctions for extreme carrier confinement". *IEEE Journal of Quantum Electronics*, Vol.9, pp.311-318, 1973. (31)
- G.H.B.Thompson, "Physics of semiconductor laser devices", pp.308-310, J.Wiley&Sons, 1980. (57)
- W.T.Tsang, "Extremely low threshold AlGaAs modified multi-quantum well heterostructure lasers grown by molecular beam epitaxy", *Applied Physics Letters*, Vol.39, pp.786-788, 1981. (39)
- W.T.Tsang, "Extremely low threshold (AlGa)As graded-index separate-confinement heterostructure lasers grown by molecular beam epitaxy", *Applied Physics Letters*, Vol.40, pp.217-219, 1982. (43)
- W.T.Tsang, N.A.Olsson, and R.A.Logan, "High-speed direct single-frequency excursion in cleaved-coupled-cavity semiconductor lasers", *Applied Physics Letters*, Vol.42, pp.650-652, 1983. (76)
- H.G.Unger, "Optische Nachrichtentechnik 2", Course of the FernUni Hagen (equivalent to the Open University), p.372, 1984. (30)
- I.K.Uomi, Hitachi Ltd, "Ultrahigh speed DFB lasers", *CLEO 90*, Paper CThA1. (19)
- I.Ury, S.Margalit, N.Bar-Chaim, M.Yust, D.Wilt, and A.Yariv, "Whispering-gallery lasers on semi-insulating GaAs substrates", *Applied Physics Letters*, Vol.36, pp.629-631, 1980. (11, 62)
- O.Wada, T.Sakurai and T.Nakagami, "Recent progress in Optoelectronic Integrated Circuits (OEIC's)", *IEEE Journal of Quantum Electronics*, Vol.22, pp.805-821, 1985. (88, 90)
- A.Yariv, "Optical Electronics" 4th ed., HRW Sanders, 1991. (18, 34, 55, 77, 91)

